THIS REPORT HAS BEEN DELIMITED
AND CLEARED FOR PUBLIC RELEASE
UNDER DOD DIRECTIVE 5200.20 AND
NO RESTRICTIONS ARE IMPOSED UPON
ITS USE AND DISCLOSURE.

DISTRIBUTION STATEMENT A

APPROVED FOR PUBLIC RELEASE;
DISTRIBUTION UNLIMITED.

Armed Services Technical Information Agency

AD

43910

NOTICE: WHEN GOVERNMENT OR OTHER DRAWINGS, SPECIFICATIONS OR OTHER DATA ARE USED FOR ANY PURPOSE OTHER THAN IN CONNECTION WITH A DEFINITELY RELATED GOVERNMENT PROCUREMENT OPERATION, THE U. S. GOVERNMENT THEREBY INCURS NO RESPONSIBILITY, NOR ANY OBLIGATION WHATSOEVER; AND THE FACT THAT THE GOVERNMENT MAY HAVE FORMULATED, FURNISHED, OR IN ANY WAY SUPPLIED THE SAID DRAWINGS, SPECIFICATIONS, OR OTHER DATA IS NOT TO BE REGARDED BY IMPLICATION OR OTHERWISE AS IN ANY MANNER LICENSING THE HOLDER OR ANY OTHER PERSON OR CORPORATION, OR CONVEYING ANY RIGHTS OR PERMISSION TO MANUFACTURE, USE OR SELL ANY PATENTED INVENTION THAT MAY IN ANY WAY BE RELATED THERETO.

Reproduced by

DOCUMENT SERVICE CENTER

KNOTT BUILDING, DAYTON, 2, OHIO

UNCLASSIFIED

AD No. 42910
ASTIA FILE COPY

TR

Final Report
of the work of the
Bartol Research Foundation of The
Franklin Institute
Performed under Contract Nonr436(00
January 31, 1954

FINAL REPORT

of the Work of the

BARTOL RESEARCH FOUNDATION

OF THE FRANKLIN INSTITUTE

Performed Under Contract Nonr-436(00)

with the

OFFICE OF NAVAL RESEARCH

BEST AVAILABLE COPY

Report submitted: April 26, 1954

C. E. Mandeville

C. E. Mandeville

Assistant Director

TABLE OF CONTENTS

I Introduction and Summaries

II Supplement

Introduction

The neutron studies, of which this report is a final one, commenced in the summer of 1951 and terminated on January 31, 1954. The data collected and results obtained have been summarized in four reports dated

(1) December 31, 1951
(3) January 31, 1953 *
(4) June 30, 1953
(5) December 31, 1953

The contents of these reports have been subsequently published or accepted for publication in the open literature. In all, six papers have been completed.

---

* Report (3) should have been dated December 31, 1952. It is to be noted that no report (2) was issued for the period January 1, 1952--June 30, 1952. Reasons for this omission will be indicated later. Since report (5), above, was issued simultaneously with termination of this contract, and, since it and the three reports preceding it were relatively complete, it has been decided to issue as a final report a brief summary of the activities of each of the above cited 6-month periods.

July 1 -- December 31, 1951

Using a photographic plate technique, fast neutrons of energy 4.3-Mev were scattered from Wolfram. The energy distribution of the scattered neutrons was obtained, and the results were published (Phys. Rev. 86, 861 [1952]). During this same period, the smaller Bartol Van de Graaff was moved from the older building on the Swarthmore Campus to a newer one located at the off-campus nuclear research center of the Foundation. It was necessary to completely rebuild the Van de Graaff in its new location. During this same period, construction of a Cockroft-Walton set, now in operation, was likewise commenced.

January 1 -- June 30, 1952

This period began with continued constructional activity centered about the smaller generator and the C-W set. A radio-frequency ion source was installed in the smaller machine so that bombarding currents in excess of 20 microamperes of magnetically-resolved deuterons were obtained. This amount of bombarding beam constituted an enormous improvement over previous performance. The

measurements of earlier work had been carried out with bombarding beams of about one microampere or less. Preliminary measurements of the total cross sections of gold, chlorine, and phosphorus were made using the newly increased beam of the generator. Currents of as much as 100 microamperes were developed in the Cockroft-Walton set. However, because the neutrons of one machine were found to interfere with the measurements proceeding with the other, it was necessary to cease operation of the Cockroft-Walton set. An additional building at the nuclear research center was readied for the Cockroft-Walton set.

No report was issued for this six-month period, because the constructional activity was very intense and few results of a publishable nature were obtained. The measurements of total cross sections of P, Au, and Cl were considered to be of only a preliminary nature. These measurements of total cross sections were undertaken with the idea of eventually measuring the angular distribution of the elastically-scattered neutrons as well. When the differential elastic scattering cross section is integrated over all angles and subtracted from the total cross section, the inelastic scattering cross section is obtained.

July 1 -- December 31, 1952

Total cross section measurements for gold, chlorine, and phosphorus were completed and published (Phys. Rev. 90, 615 [1953]). The use of photographic plates as neutron detectors was continued, and attempts to measure the energy distribution of the neutrons inelastically scattered from iron and chromium met with some success. A survey of geometries for neutron-scattering measurements was conducted over a period of several months. A novel method of increasing the measurable intensity of inelastically-scattered neutrons was developed and published (Rev. Scient. Inst., 24, 875 [1953]).

January 1 -- June 30, 1953

Many interesting results were obtained during this period. A geometry was devised which allowed detection of gamma rays excited by inelastic scattering of fast neutrons. The energies of the gamma rays excited by fast neutrons inelastically scattered by chromium, lead, bismuth, and iron were measured. These results have been published (Phys. Rev. 93, 796 [1954]).

Angular distributions of fast neutrons scattered from aluminum, iron, and lead were also determined and published (Phys. Rev. 92, 114 [1953]).

July 1 -- December 31, 1953

The gamma ray spectra excited by inelastic scattering of fast neutrons in nickel, copper, zirconium, and tungsten, were studied. The angular distributions of fast neutrons elastically scattered in cadmium, tin, and bismuth were also determined. These data have not as yet been published, though some of them have been submitted and accepted for publication in The Physical Review.

Additional Results

In December of 1953, investigations of the excitation of metastable states by fast neutrons were undertaken. Thus far, metastable states of Ba^{137} and Hg^{199} have been so activated. These levels may be excited by gamma emission from states greater in energy. The excitation is measured as a function of neutron energy. These measurements have been continued since termination of this contract, under sponsorship of the Atomic Energy Commission, and levels have been located in Hg^{199} at 566, 607, 985, 1283, 1771, and 2259 Kev and in Ba^{137} at 665, 1012, and 1767 Kev. The probable error in the energy measurements is thought to be $\pm$ 15 Kev.

These studies of the excitation of metastable states in nuclei are being conducted with the use of the larger Bartol Van de Graaff generator recently completed.

Conclusion

As indicated in the preceding summary, the technical details and interpretations of the accumulated data and results have been adequately dealt with in the aforementioned four reports and six publications. However, in order to present a complete description of what has been accomplished under the contract, copies of the four preceding reports have been appended to this discussion as a supplement.

S U P P L E M E N T

FIRST SEMI-ANNUAL REPORT

of the Work of the

BARTOL RESEARCH FOUNDATION

OF THE FRANKLIN INSTITUTE

Performed Under Contract Nonr-436(00)

with the

OFFICE OF NAVAL RESEARCH

W. F. G. Swann, Director

Swarthmore, Pennsylvania

December 31, 1951

C O N T E N T S

I The Scattering of Fast Neutrons by Wolfram

A: Introduction

B: The Measurements

C: Conclusions

II The Cockroft-Walton Set

III The Van de Graaff Statitron

I THE SCATTERING OF FAST NEUTRONS BY WOLFRAM

A: Introduction

Employing several different primary neutron energies, the maximum of which was 3 Mev, Barshall et al.[1] have investigated the inelastic scattering of fast neutrons in wolfram and other elements. Their measurements have been subsequently interpreted by Feld.[2] The measurements of the present paper were carried out with a geometry and general method which have been previously described[3] in their application to the particular cases of the scattering of fast neutrons by bismuth and lead. In these previously reported measurements,[3] unfavorable conditions of background were encountered, and it was found to be impossible to give an accurate estimate of the cross-section for inelastic scattering. Many months of plate reading and analysis were required to establish the undesirable features of the method, and during that time the exposure for wolfram had been carried out. Consequently, it has been decided to present the results, recognizing that certain difficulties are inherent in the analysis and interpretation.

---

1) Barshall, Battat, Bright, Graves, Jorgensen and Manley, Phys. Rev. 72, 881 (1947)
Barshall, Manley and Weisskopf, Phys. Rev. 72, 875 (1947)

2) B. T. Feld, Phys. Rev. 75, 1115 (1949)

3) C. E. Mandeville and C. P. Swann, Phys. Rev. 84, 214 (1951)

B: The Measurements

Monochromatic fast neutrons of energy 4.5 Mev, produced in the deuteron-deuterium reaction, were scattered in a scatterer of metallic wolfram, having an average length of 4 cm. The bombarding deuterons were supplied by the Bartol Van de Graaff statitron. With no scatterer present, the curve of figure 1A was obtained. With scatterer in position, the curve of figure 1B resulted. These curves have been normalized to take into account bombarding time and plate area scanned. The principal group of particles in figure 1B is composed of primary neutrons, those which passed through the scatterer without suffering a scattering collision of any kind, and neutrons which have been elastically scattered. The broken line of figure 1B is a plot of the principal group using the shape of figure 1A. From figure 1B, it is clear that insertion of the scatterer has shifted the peak of the curve slightly and broadened it somewhat, giving evidence of elastic scattering. As in the previous paper, the energy interval 0.2 Mev$\leq E_n \leq$3.7 Mev, has been designated as the region of inelasticity. A detail of the results of this region is shown in figure 2. The data without scatterer are represented by the open circles, whereas those obtained with scatterer in position are indicated by the closed circles. These data have been plotted in energy intervals of 0.2 Mev. The open circles are not, however, taken tc be the true background. It was

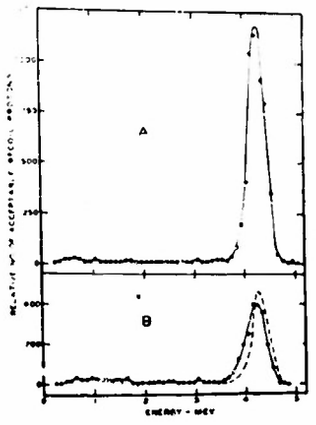


Fig. 1. Curve A is the "background run" or energy distributions of neutrons with no scatterer. Curve B was observed with the wolfram scatterer in position. The two curves were "normalized" to take into account irradiation time and plate area scanned.

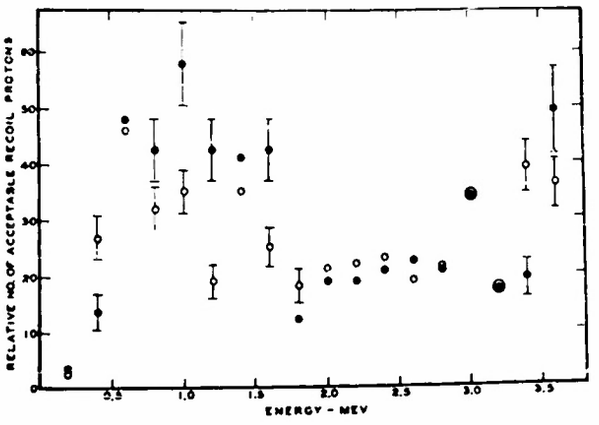


Fig. 2. Distribution of neutron energies less than or equal to 3.7 Mev collected with and without the wolfram scatterer in position. The data are plotted in energy intervals of 0.20 Mev. The open circles refer to the "background run" with no scatterer, and the closed circles to data obtained with scatterer in position.

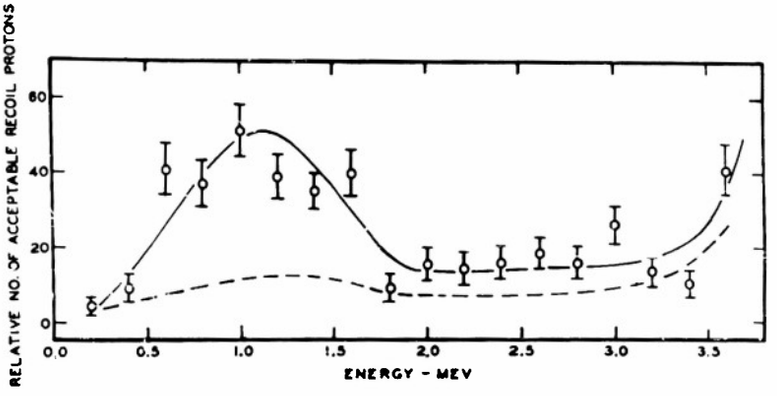


Fig. 3. Distribution in energy of 4.3 Mev neutrons inelastically scattered in wolfram. The broken line is the distribution after correction for variation with energy of n-p scattering cross section and acceptance probability.

demonstrated in the case of neutron scattering by bismuth[3] that the background without scatterer is greatly reduced by scattering of the background neutrons with scatterer in position. To obtain the appropriate background with scatterer in position, the open circles of figure 2 have been reduced by the factor $\exp(-n_W \sigma_W x)$ where n_W is the number of wolfram atoms per cc, σ_W the total scattering cross section for wolfram, and $x = 4$ cm, the average length of the wolfram scatterer. The product $n_W \sigma_W$ was, of course, evaluated as a function of energy, on each energy interval of width 0.2 Mev. Thus, letting I_{oj} be the number of tracks on the j^{th} interval of the "background run", and letting I_j be the background with scatterer in position, I_j can be calculated. The total number of background tracks on the large interval, 0.2 Mev $\leq E_n \leq$ 3.7 Mev, is given by

$$I_o = \sum_1^N I_{oj},$$

and the total number of background tracks in the region of inelasticity with scatterer in position may be calculated from

$$I = \sum_1^N I_j = \sum_1^N I_{oj} \exp(-n_W (\sigma_W)_j x)$$

The observed and calculated values of I and I_o are given in Table I, where it is seen that I calculated is 95 $\pm$ 3 tracks, the actual observed I_o without scatterer being 471 $\pm$ 15 tracks. This calculated value of I is to be compared with an observed value of I of 524 $\pm$ 21 tracks. This great difference between

calculated and observed values of I is taken to be evidence for inelastic scattering of 4.3 Mev neutrons in wolfram.

Table I. Number of tracks calculated and observed in the inelastic region, for W

Observed I_o	Observed I	Calculated I
471 ± 15	524 ± 21	95 ± 3

Considerable debate has centered about the fact that the open circles of figure 2, the observed background tracks with no scatterer present, show an increase in the vicinity of 1 Mev just as do the closed circles of data obtained with scatterer present. These tracks, in the case of the open circles are presumed to arise from neutrons generated in the reaction $C^{12}(D,n)N^{13}$, since carbon may be present as a contaminant on the target of D_2O. If these neutrons originate at the target and proceed to the photographic plates without having been first scattered about the observation room, they will certainly be reduced in intensity when the scatterer is placed in position. From figure 2, it is evident that considerably more neutrons are encountered in the vicinity of 1 Mev with scatterer in position. Most of these are evidently inelastically scattered ones, since those of any carbon contamination would be reduced in each energy interval by the factor $\exp(-n_W \sigma_W x)$.

It has been argued that perhaps the neutrons from $C^{12}(D,n)N^{13}$ are room scattered to give the tracks of the closed circles in the vicinity of 1 Mev with scatterer in position, and that the assumption that the background emanates primarily from the direction of the target is incorrect, contrary to the findings of the bismuth measurements.[3] Further evidence that the background neutrons do emanate from the target area may be cited as follows. Many targets of light nuclei have been irradiated by deuterons supplied by the Bartol Van de Graaff statitron. The neutrons from $C^{12}(D,n)N^{13}$ have often appeared in spectra observed in photographic plates placed at angles of zero and ninety degrees with the incident beam in the laboratory system of coordinate axes. These plates have always given evidence of a sharply defined group from $C^{12}(D,n)N^{13}$, exhibiting the proper energy shift with angle of observation. This would not be the case were "room scattering" of the carbon neutrons an important factor. These irradiations were often of the same length in time as those of the scattering experiments and were carried out in a much less advantageous geometry from the standpoint of the reduction of background. The removal of the target of the scattering experiments to a point at a great distance from scattering materials has been previously described.[3]

C: CONCLUSIONS

As described above, the data of the open circles of figure 2 were reduced in each energy interval by the factor $\exp(-n_W \sigma_W x)$ and subtracted from the appropriate closed circle. After properly combining the statistical probable errors, the curve of figure 3 was obtained. The broken line of figure 3 represents the distribution in energy of fast neutrons inelastically scattered in wolfram, corrected for variation with energy of the n-p scattering cross section and acceptance probability. The distribution appears to be for the most part constant with energy, rising somewhat in the region of lower energies. Using figure 1B and a method of analysis previously described,[3] it is estimated that at 4.3 Mev the inelastic scattering cross section is less than three-fourths as large as the elastic one for W.

II. THE COCKROFT-WALTON SET

A highly efficient r-f ion source has been developed for use in the two Bartol Van de Graaff statitrons. One of these ion sources (first employed as a "test bench" for ion source development) has been incorporated into a Cockroft-Walton set. This C-W set has been constructed for the purpose of furnishing an intense source of neutrons. Yield curves of the reactions $D(D,n)He^3$ and $D(T,n)He^4$ have been consulted, and they indicate that these reactions would supply copious quantities of neutrons, even at very low bombarding energies.

A power supply, variable involtage from zero to 100 Kv and sustaining a maximum load of 1 Ma., has been obtained from the Beta Electronics Corporation of New York.

A photograph of the C-W set is given in figure 4 where the principle components are seen to be supported upon a steel framework. At the present time, it is planned to use a vertical unresolved beam. Very little energy spread would result, since the maximum energy would be 100 Kev. However, a magnet has been constructed for eventual resolution of the beam and for bringing the beam to a horizontal position if necessary.

It is thought that the C-W generator will afford a convenient method for observing gamma rays emitted in the scattering process.

Plans are at present underway to bombard a heavy paraffin target and monitor the neutron yield to ascertain whether sufficient intensity is present for experimentation and to determine what shielding is necessary to satisfy the

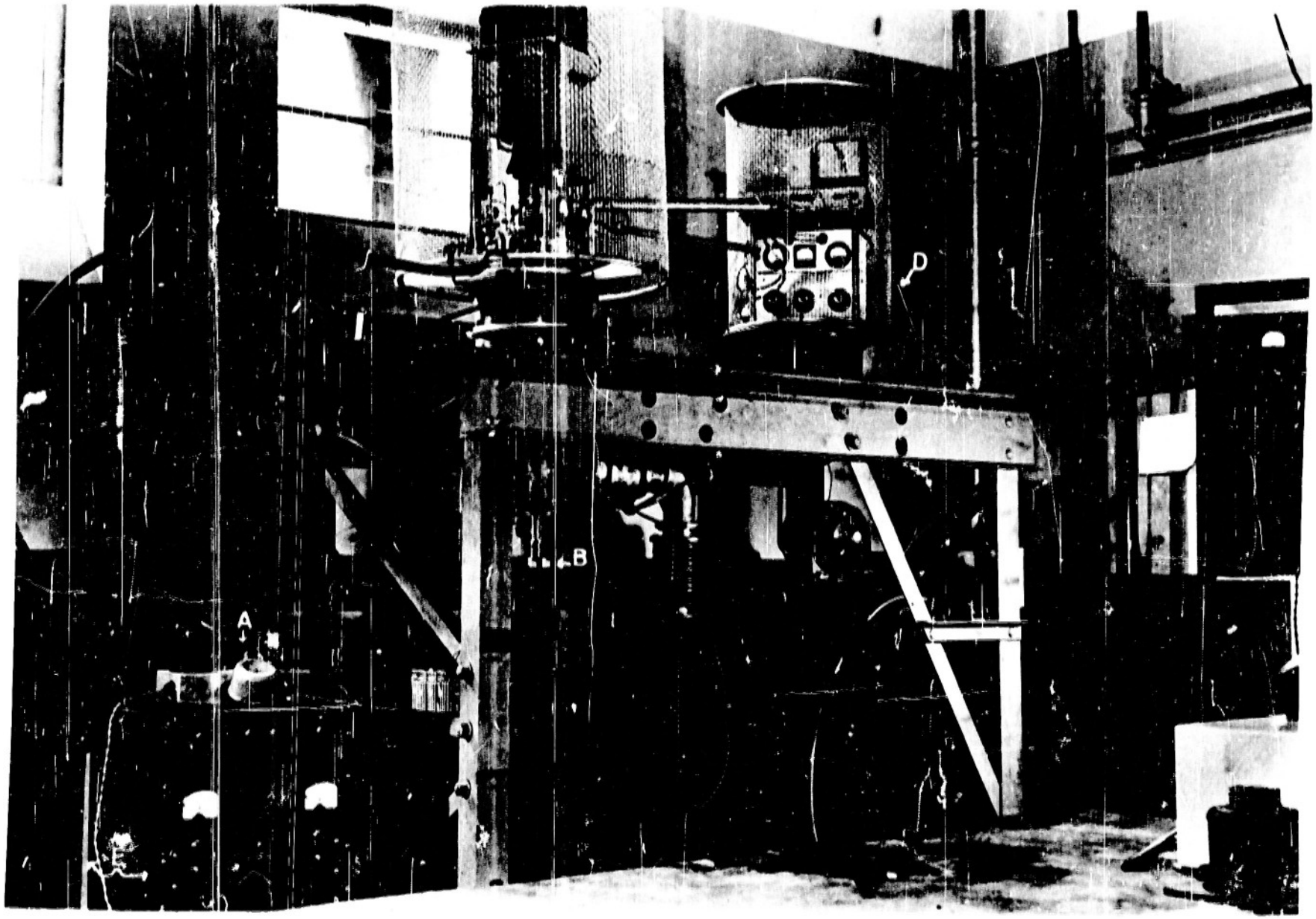


Figure 4. The Cockroft-Walton set. A, current integrator. B, the target. C, the ion source with shield. D, the control panel for the ion source. E, the high voltage power supply.

requirements of health physics.

III: THE VAN de GRAAFF GENERATOR

The small Bartol Van de Graaff statitron has been moved from principal building on the Swarthmore campus to the cite of the more recent nuclear physics installations. The "target end" of the statitron is shown in figure 5. One of the first uses of this generator in its new environment will be the performance of scattering experiments in which the total cross sections of various nuclei will be measured as a function of energy of the monochromatic neutrons from the reaction $T(p,n)He^3$.

Report submitted:
January 21, 1952

Bartol Research Foundation
W. F. G. Swann, Director

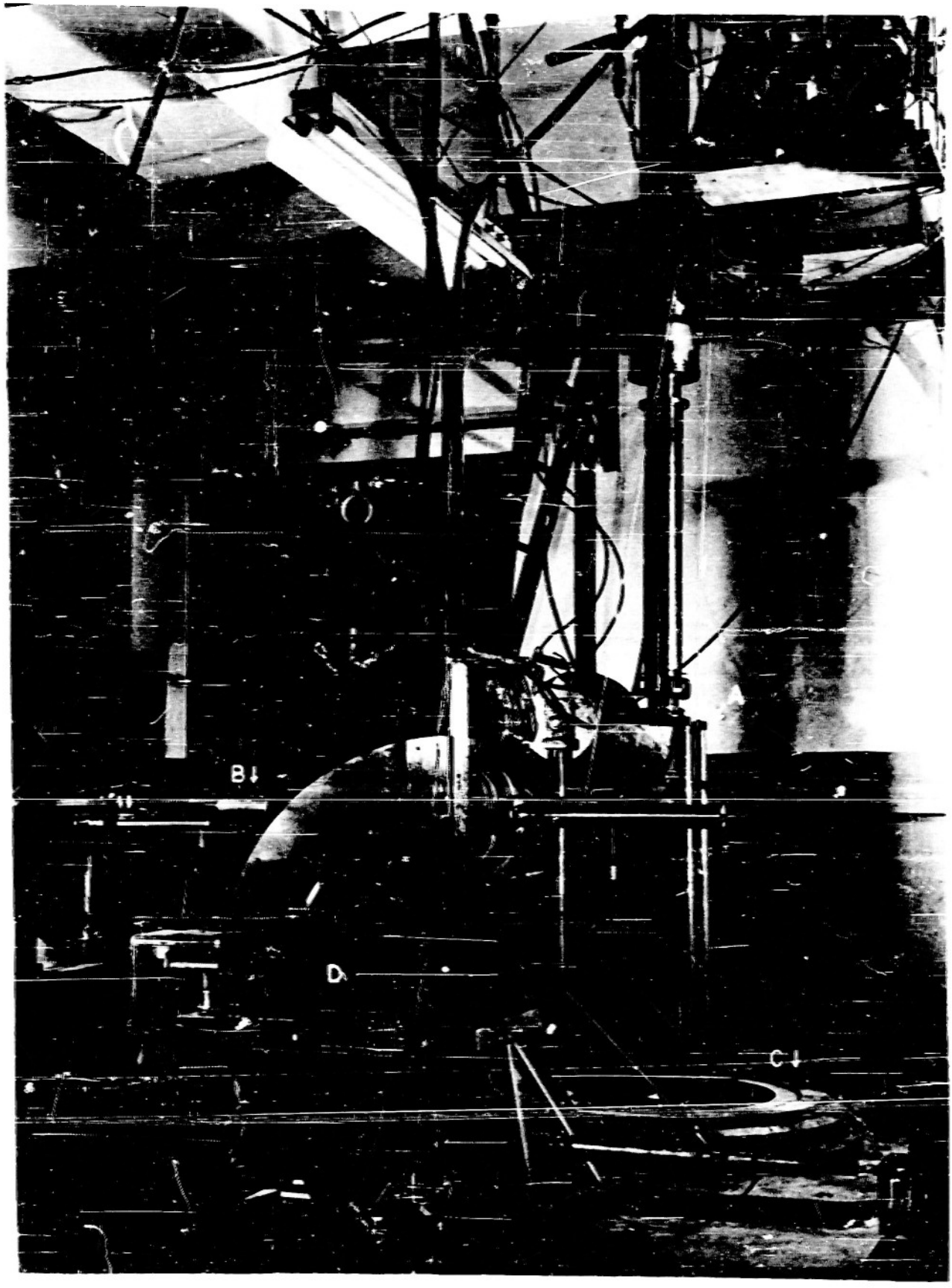


Figure 5. The target end of the small Van de Graaff statitron. A, the beam focusing magnet. B, the neutron counter. C, the rotating gun mount. D, a semi-circular focusing magnetic spectrograph for analysis of charged disintegration products.

SEMI ANNUAL REPORT

of the Work of the

BARTOL RESEARCH FOUNDATION

OF THE FRANKLIN INSTITUTE

(June 30, 1952 -- January 31, 1953)

Performed Under Contract Nonr 436(00)

with the

OFFICE OF NAVAL RESEARCH

W. F. G. Swann, Director

Swarthmore, Pennsylvania

January 31, 1953

TABLE OF CONTENTS

I. Inelastic Scattering.

II. Total Neutron Cross Sections.

III. Instrumentation and Future Measurements.

PERSONNEL

Physicists: (Part-time or full-time)

Stanley Bachkin*

D. W. Kent

C. E. Manderille

P. R. Metzger

M. A. Rothman

S. C. Snowdon

W. D. Whitehead

Technicians: (Half-time)

W. F. Camp

R. W. Gunnett

* Terminated employment

I. INELASTIC SCATTERING.

The progress of inelastic scattering measurements at this laboratory has been outlined previously in several reports and publications[1-4]. The present data constitute

---

1) Interim Technical Report to Project NEPA, released September, 1950, later appearing in part as "The Scattering of Fast Neutrons by Bismuth and Lead". Mandeville and Swann, Phys. Rev. 84, 214 (1951).

2) Final Report of the Work of the Bartol Research Foundation of the Franklin Institute to Project NEPA as Performed under Contract SC-2034, issued April 30, 1951.

3) First Semi-Annual Report of the Work of the Bartol Research Foundation of the Franklin Institute Performed under Contract Nonr-436(00), issued December 31, 1951. Part of this report later was published as "The Scattering of Fast Neutrons by Wolfram", Mandeville, Swann and Seymour, Phys. Rev. 86, 861 (1952).

4) Status Report, Contract Nonr-436(00), January - September, 1952, submitted September 24, 1952.

---

an extension of the earlier efforts. To date, the principal detector has been the photographic plate. Earlier

measurements[1, 3] consisted in obtaining data with and without scatterers before the photographic plates. A disadvantage of the geometry was that primary unscattered neutrons could reach the plates along with the elastically and inelastically scattered neutrons giving rise to a large and undesirable background. This difficulty was summarized in the final report under Contract SC-2034 to project NEPA[2], April 30, 1951. In this same report it was also suggested that a geometry be adopted wherein the photographic plates would not be in the beam of primary neutrons incident upon the scatterer, that they should be located at 90° to the beam to receive neutrons scattered through that angle. Such a geometry was indicated in Figure 2 of Reference 2. A "90-degree" geometry was adopted by Stelson and Preston[5]

---

5) Stelson and Preston, Phys. Rev. 86, 132 (1952).

---

when they studied the neutron groups relating to the inelastic scattering of fast neutrons by iron[5].

Although the data of Stelson and Preston[5] were statistically poor, their results seemed to hold promise. Accordingly the large paraffin collimator of their measurements was constructed as described in Reference 4. In actuality, two collimators were prepared at Bartol, one of length

50 cm as initially built by Stelson and Preston, the other a shorter and more widely flared version of length 20 cm. The shorter collimator was cast to increase the neutron intensity at the scatterer. Objections have been raised in various quarters to the Stelson-Preston experiment. It has been argued that the presence of such large quantities of paraffin as they used, leads to a degradation of the primary neutron energy and to spurious groups of low energy neutrons which might be interpreted as having been inelastically scattered. Consequently, before doing any collimator experiments, it was decided to investigate some different variations of the so-called "wedge" geometry for shielding the photographic plates. A schematic diagram of one form of this geometry was given in Figure 1 of Reference 4. To keep scattering materials at a minimum, it was decided to irradiate a scatterer of iron in the geometry of Figure 1 of the present paper. This arrangement represents the extreme case in which there is no collimation or shielding to give any degradation of the primary neutron beam.

The desirable neutrons which are detected in the plates of Figure 1 are those which have proceeded from the deuterium target to the scatterer and thence through an angle of 90° to the photographic plates. Present also are recoil protons produced by irradiation of the photographic plates by the neutrons arriving directly from the target. In the measurement of the plates, only the upper half of the plates, the

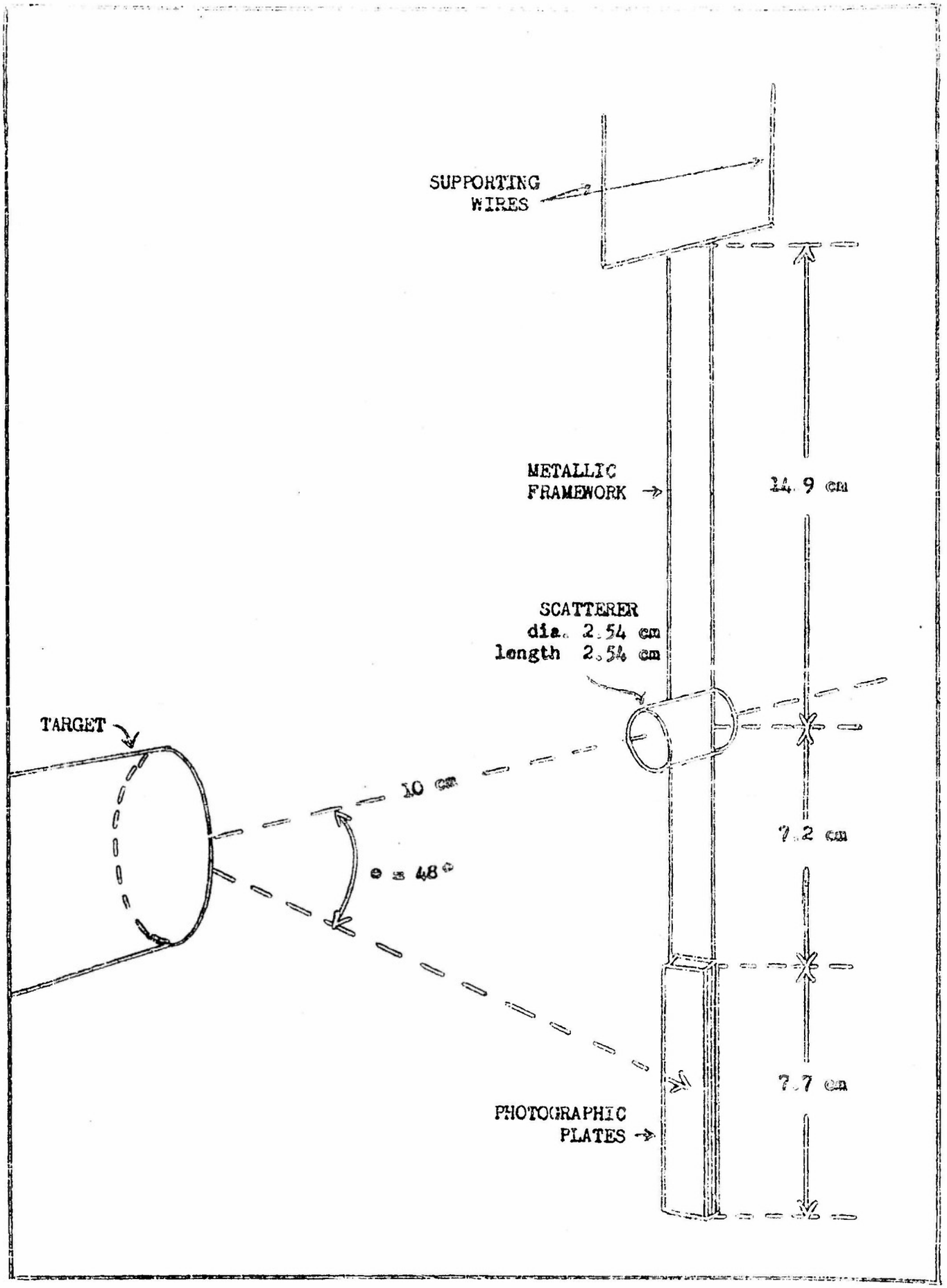


Fig. 1 SCHEMATIC DRAWING OF SCATTERING ARRANGEMENT

half nearer the scatterer, was read. In the geometry of Figure 1, recoil protons can appear which make an angle of as little as thirty degrees with the forward direction. The complement of the angle indicated in the drawing of Figure 1 is 42^{0}. An acceptance angle of twelve degrees of the forward direction was employed in the photographic plates so that at the center of the photographic plate it would be possible to find acceptable recoil protons making an angle as small as thirty degrees with the path of the incident associated neutron coming directly from the target. The energy of the recoil proton would be given by

$$E_p = E_n \cos^2 \theta$$

where as indicated above, θ could be as little as thirty degrees, so that the recoils could have as much as three-fourths of the primary neutron energy. Since only the upper half of the plates were read, the angle was usually greater than 30^{0}. In the measurements of this section of the report, deuterons of energy 1.3 Mev were passed through a nickel foil of thickness $\sim$ 300 Kev into a target of deuterium gas about 200 Kev thick. The resultant neutrons had an energy of $\sim$ 4 Mev as indicated by a control plate placed at the position of the scatterer. Most of the recoil protons resulting from direct irradiation of the plates were removed by choosing only recoil protons of energy in excess of 2.3 Mev. Another

source of recoil protons is neutrons proceeding directly from target to plates to be scattered from the AgBr of the emulsion and from the silicon in the glass backing of the emulsion. Extensive calculations were performed to get an estimate of this effect, and they seemed to indicate that about four or five times as many neutrons are scattered from the Ag, Br, and Si as from the iron scatterer itself. This fact alone places in doubt any results which might be obtained from the unshielded geometry of Figure 1. Nevertheless, to obtain a complete experimental picture, a cylindrical iron scatterer of length one inch and diameter one inch was irradiated in the geometry of Figure 1.

A rotational method of exposure was adopted in which a total of five million integrator counts were recorded at the deuterium target of the Van de Graaff generator, two million with scatterer, two million without scatterer, and one million with a control plate in the position normally occupied by the iron scatterer to determine the homogeneity of the primary incident beam of neutrons at 4-Mev. (The calibration of the integrator is 0.05 coulomb per integrator count.) The data with and without scatterer are plotted in Figures 2 and 3, Figure 2 in energy intervals of 0.1 Mev and Figure 3 in intervals of 0.2 Mev. A continuum of recoils appears to be present below 4 Mev. The two curves are dissimilar between 3.3 and 4 Mev, suggesting the possibility that elastically and inelastically scattered neutrons have been contributed by the iron

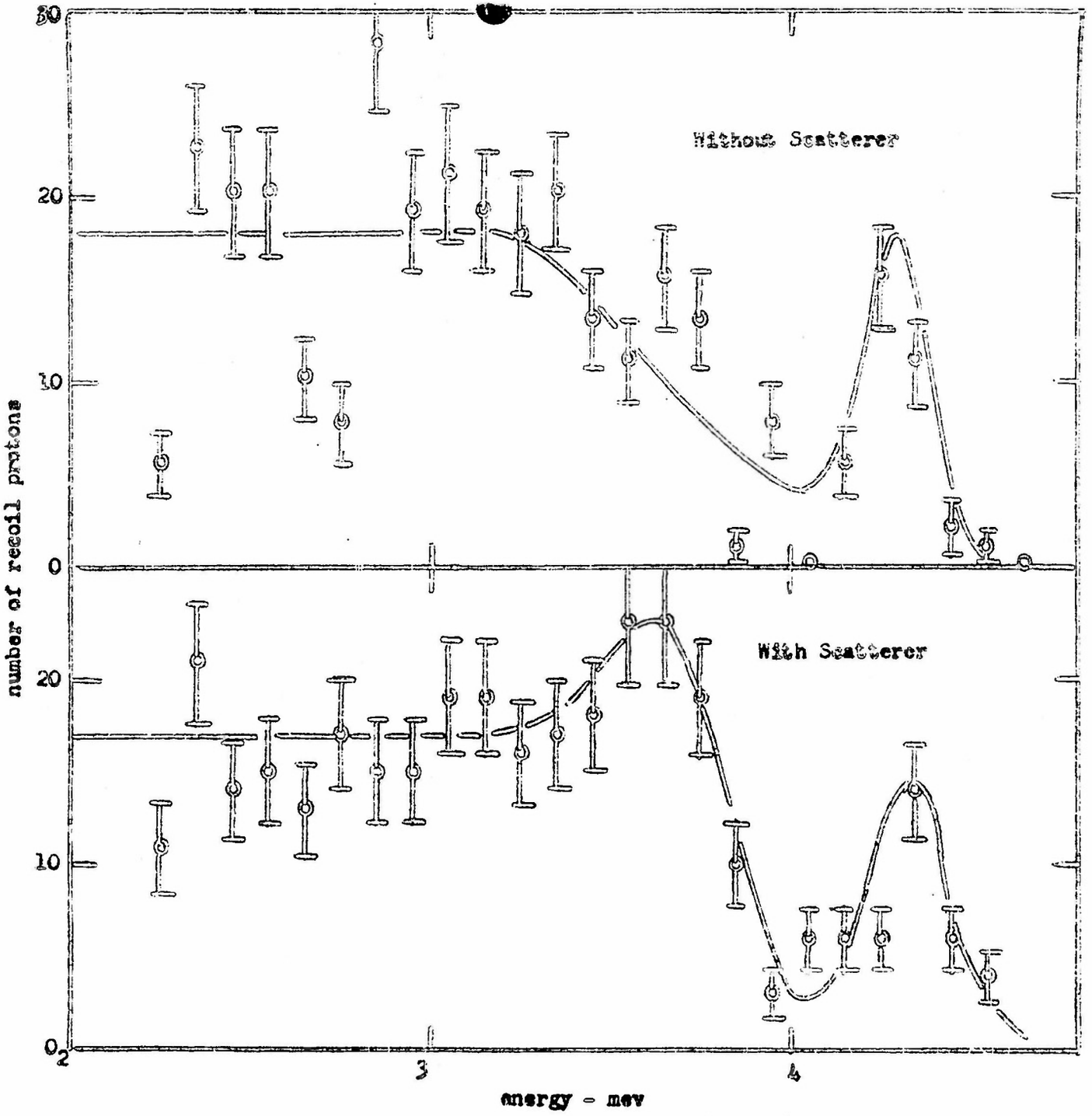

30
20
10
0
Without Scatterer
20
10
0
With Scatterer
number of recoil protons
3
4
energy - mev

Fig. 2

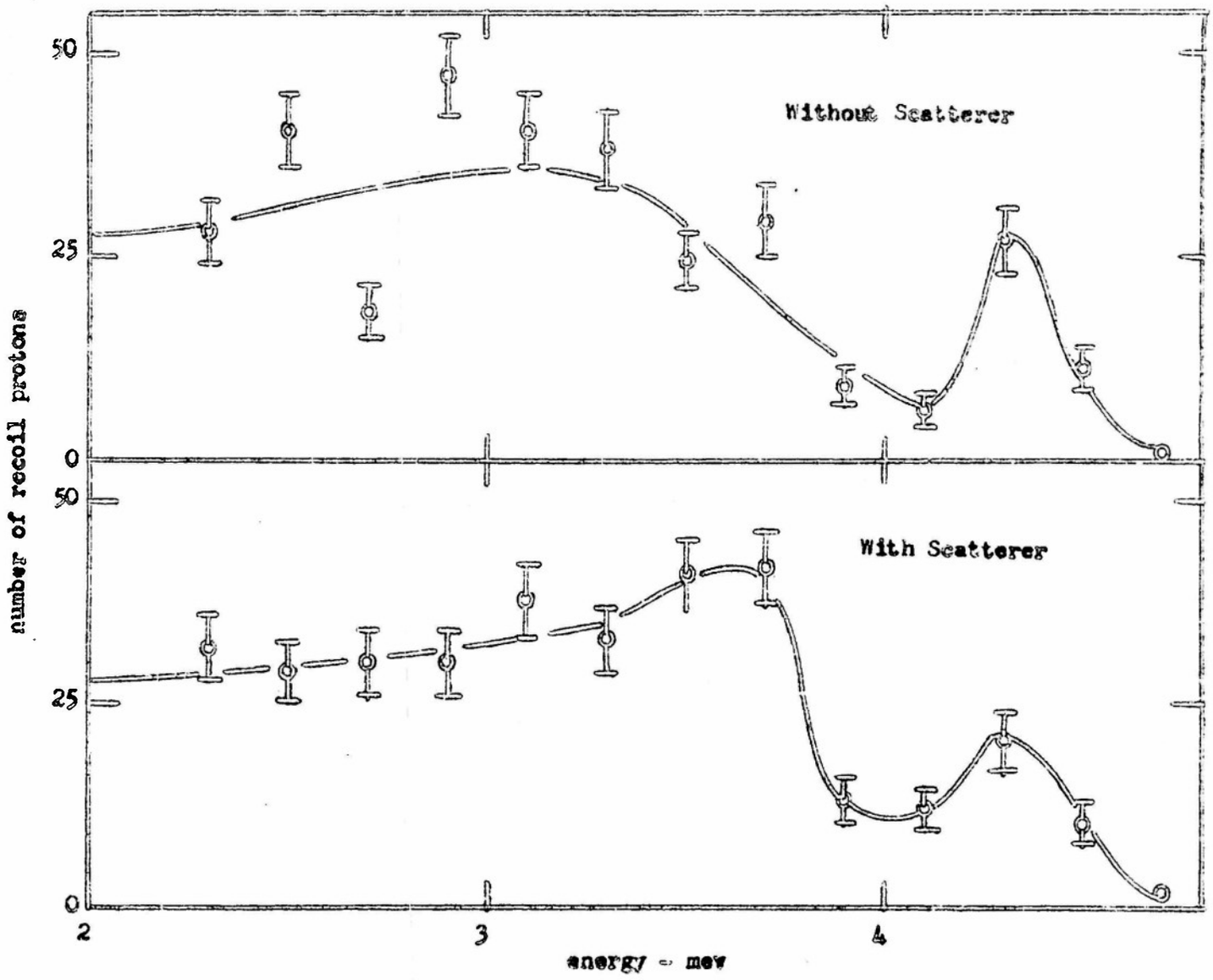

50
25
0
Without Scatterer
50
25
0
With Scatterer
number of recoil protons
2
3
4
energy - mev

Fig. 3

scatterer in this region. At ~4.5 Mev appears a group of neutrons on both sets of plates, beyond the position in energy which is possible according to the kinetics of the deuteron - deuterium reaction. This group of neutrons is assigned to the reaction N^{14} (n,p) C^{14}. When a photographic plate is placed parallel with a neutron beam, the group or neutrons from N^{14} (n,p) C^{14} is not usually noticeable. It is usually completely overshadowed by the neutrons from the D-D reaction. However, when the plates are nearly vertical to neutron beam as are those in Figure 1, the primary neutrons disappear, and the N^{14} (n,p) C^{14} neutrons become apparent.

Since the direct neutrons were so scattered by the AgBr and Si as to partially mask the contribution of the iron scatterer, it became evident that adequate shielding must be interposed between the deuterium target and the photographic plates. The decision as to how much shielding can be employed presents a problem, because if too much is placed between the target and plates, the scatterer will be too far removed from the neutron source, thus reducing the solid angle subtended at the source by the scatterer. Consequently, a survey of possible geometries was carried out with a view to observing the background of scattered neutrons in the plates under various conditions of shielding. By scattered neutrons in this case is meant those scattered from the AgBr and Si. No iron scatterer was present. No directional criteria were applied in measuring the tracks. In fact, they were not actually

measured but merely counted. The number of tracks of all types per field of view was recorded. Any tracks which could be differentiated from the background grains was counted. Thus, the background measurements of the various geometries should be applicable to counter measurements as well as to photographic plates.

The various types of shields are described in Figure 4 (10 cm of paraffin, 10 cm of bismuth), Figure 5 (20 cm of paraffin), and Figure 6 (a Stelson-Preston type collimator of length 20 cm). The results of the shielding measurements are described in Figure 7, where a table of data is presented. From the table it is clear that the paraffin wedge of length 10 cm allows a background only 1.6 times as great as the collimator and that the 20 cm wedge gives rise to a lower background than the scatterer*.

---

* At the bottom of the table is a row of data relating to an unshielded bombardment of a pellicle (an emulsion 300 microns thick without any glass backing). The geometry was that of Figure 1 with no scatterer present. According to the table, 16.8 tracks per field of view were observed. This figure must be divided by three to reduce the pellicle thickness to that of the photographic plates (100 microns), giving 5.6 tracks per field of view, in agreement with 5.5 tracks found in the plates. Thus, the additional 200 microns of emulsion thickness containing AgBr contribute as many

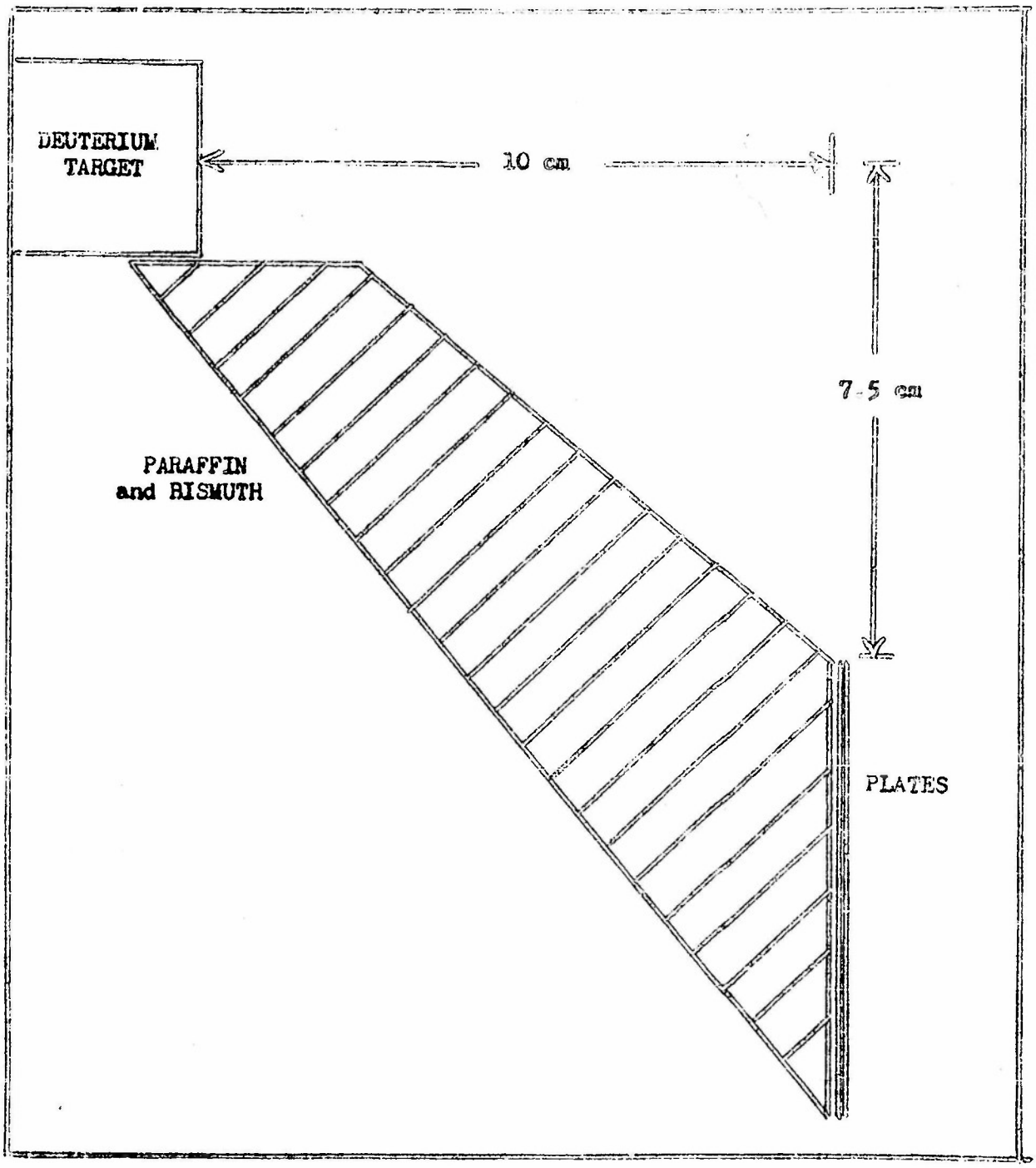


Fig. 4

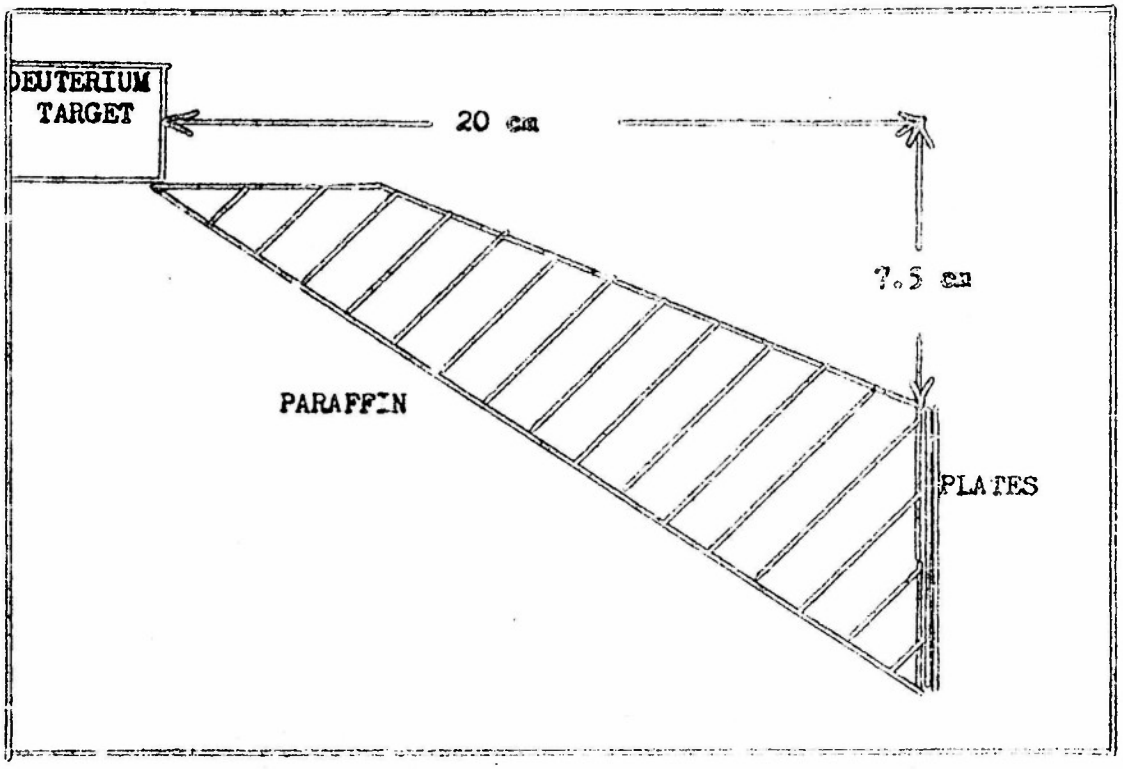


Fig. 5

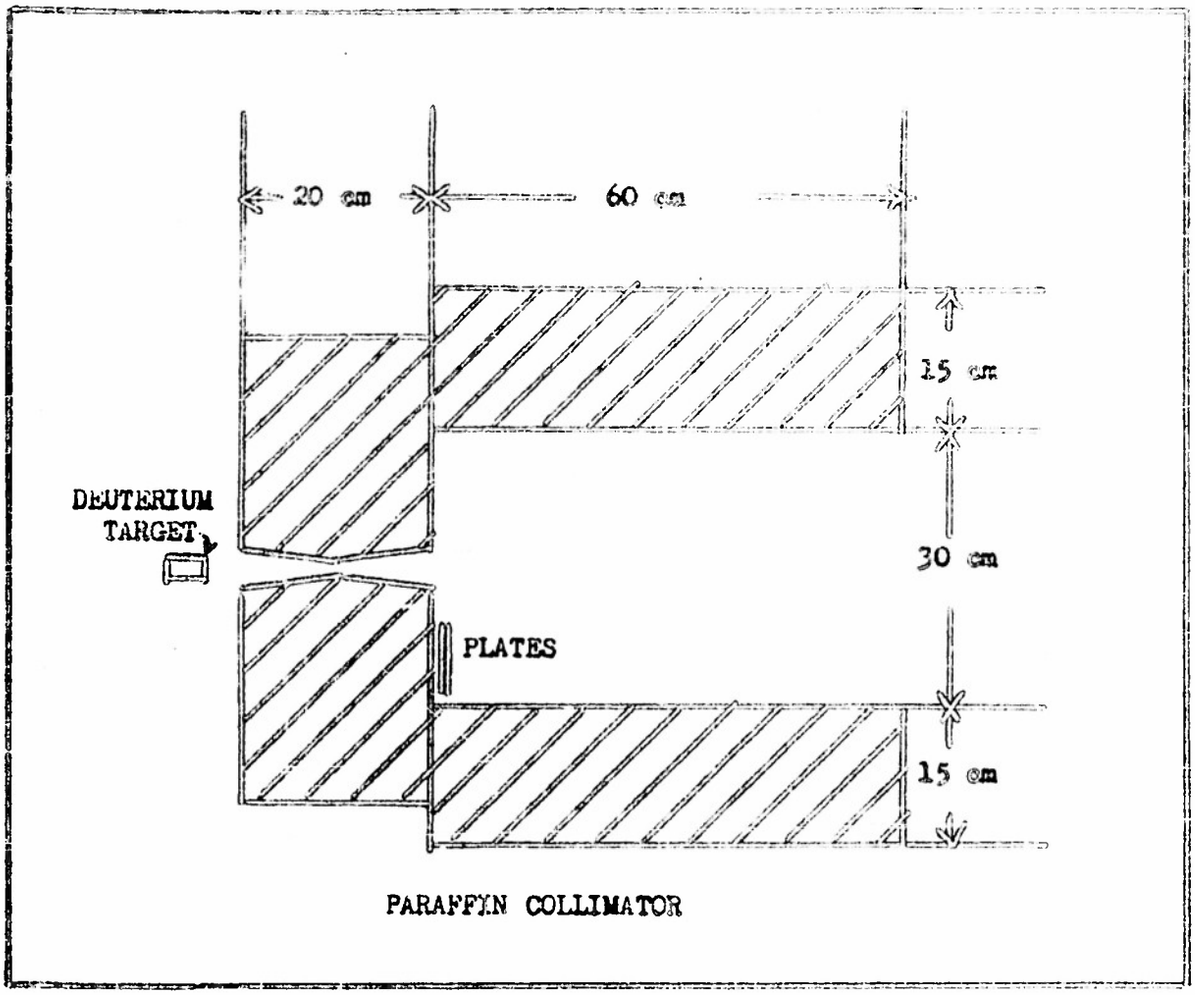

20 cm
60 cm
15 cm
30 cm
15 cm
DEUTERIUM
TARGET
PLATES
PARAFFIN COLLIMATOR

Fig. 6

PLATE NO.	SHIELD	NO. OF TRACKS	NO. OF FIELDS	TRACKS PER FIELD	TRACKS PER FIELD PER 10^5 INT. CNTS.	CORRECTED FOR SOLID ANGLE	NORMALIZED TO 100%
4	None	225	41	5.5	14.3	3710	100
6	Small Paraffin	219	70	3.2	2.77	615	16.6
7	Large Paraffin	75	100	0.75	0.78	403	10.9
9	Bismuth	183	50	3.7	4.23	945	25.5
10	Collimator	75	78	0.96	0.75	563	15.2
Pellicle	None	370	22	16.8			
		CORRECTED FOR THICKNESS		5.6	13.2	3420	92

Figure 7

scattered neutrons to the remaining 100 microns of pellicle thickness as does the glass backing to the 100 micron emulsion of the photographic plate.

In order to obtain a high density of incident neutrons, a decision was made to employ a modification of the 10 cm of paraffin shown in Figure 4. This new form of the 10-cm geometry is shown in Figure 8. The various angles of the momentum relationship are such that only one-fourth of the incident neutron energy can be imparted to a proton in the emulsion. However, only recoils of energy greater than 1.6 Mev were actually accepted. The energy distributions with and without scatterer and the difference curve are plotted in Figure 9. An elastic group is well defined, but the inelastic one is "smeared" over a considerable region and does not exhibit particularly good definition. The broken line of the difference curve represents the energy distribution corrected for variation with n-p scattering cross-section and acceptance probability of the tracks.

To obtain the data of Figure 9, 10,380 fields of view were observed in binocular microscopes to obtain 779 acceptable recoil proton tracks in the case of scatterer present. The background without scatterer was determined by measuring 323 tracks in 5,650 fields of view. As to bombarding time, a total of seven million integrator counts were accumulated with scatterer and seven million without scatterer. A control plate replaced the scatterer for one million integrator counts

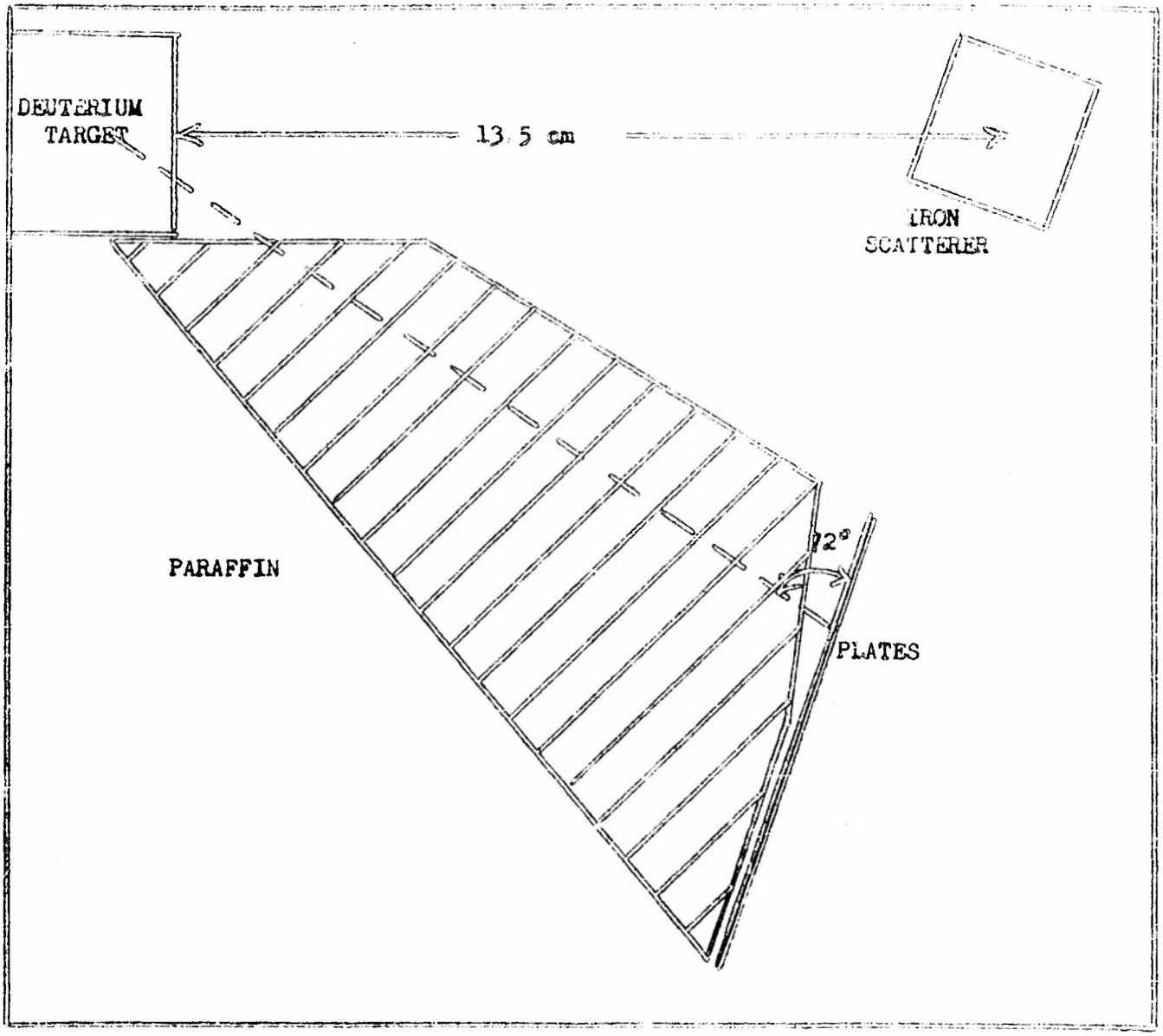


Fig. 8

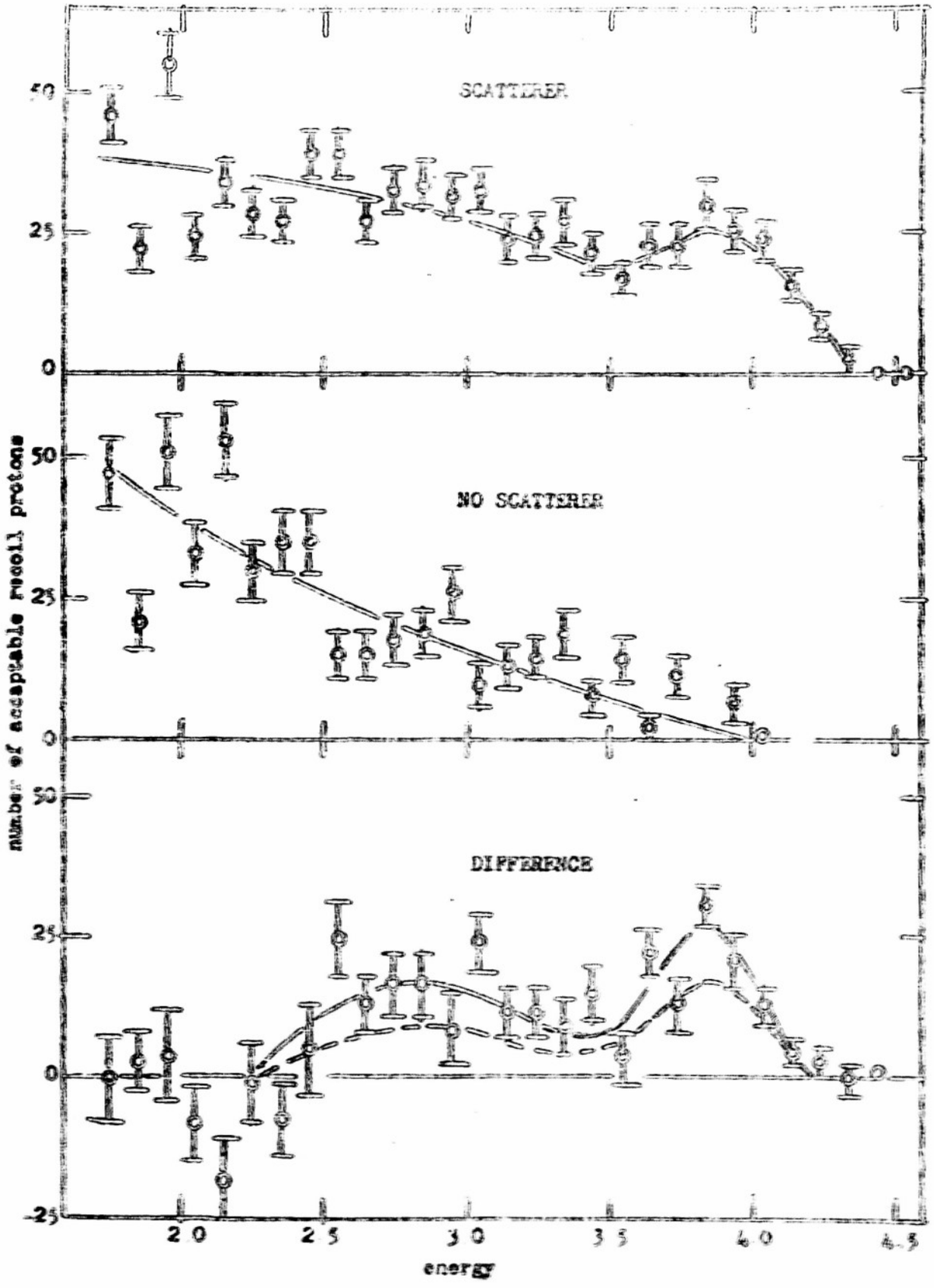

SCATTERER
NO SCATTERER
DIFFERENCE
number of acceptable recoil protons
50
25
0
-25
20
25
30
35
40
45
energy

Fig. 9

to obtain the energy spectrum of the primary beam of neutrons employed in the scattering experiment. It is possible that some of the neutrons from the target could be scattered and degraded in the paraffin, then elastically scattered in the iron to the photographic plates to appear as a low energy group to be confused with inelastically scattered neutrons from the iron scatterer. A background "run" does not take into account neutron groups produced in this manner. The primary neutron spectrum is shown in Figure 10. It is estimated that less than five per cent of the neutrons lie below the principal group. The presence of the smeared inelastic contribution of the difference curve of Figure 9 cannot be explained by such a small percentage of degradation of the primary beam.

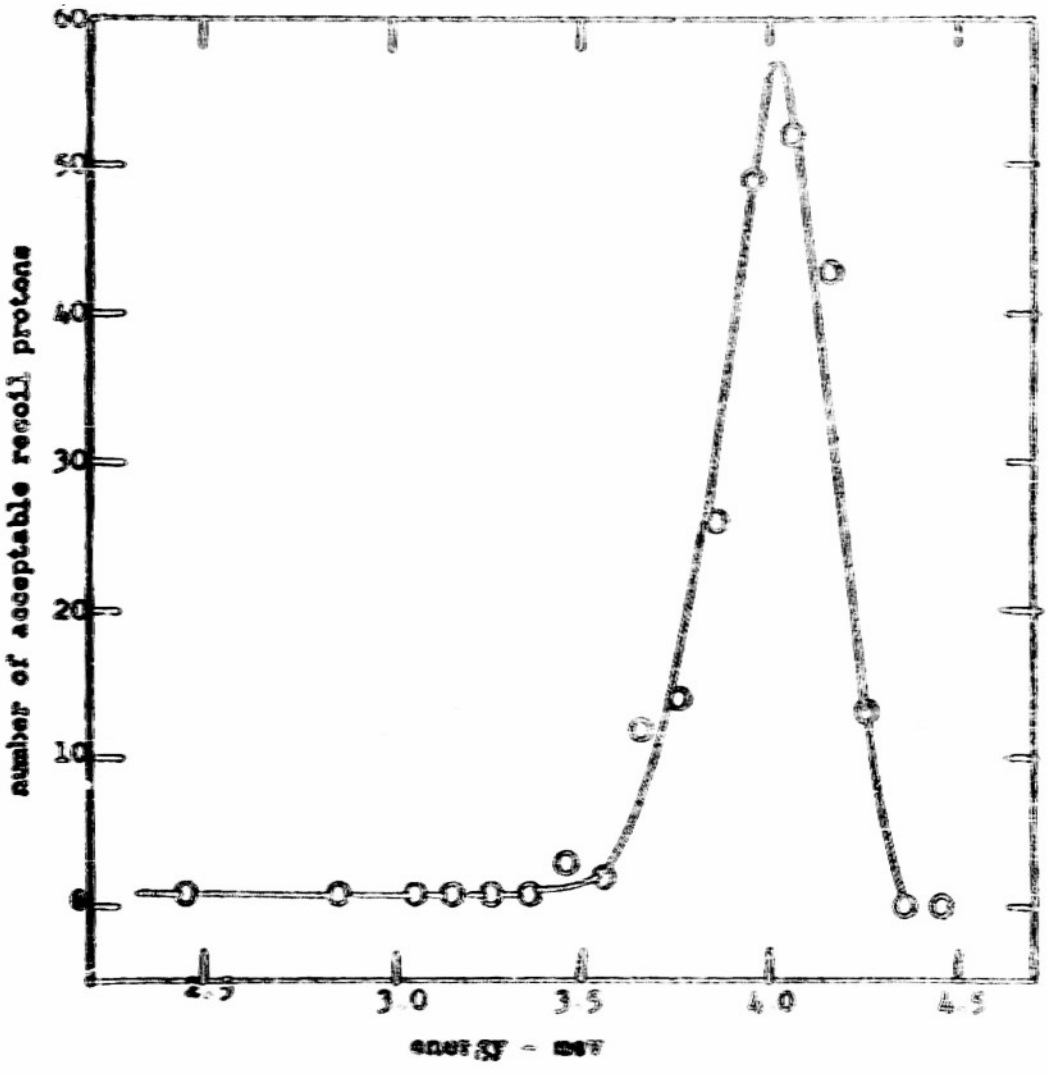

number of acceptable recoil protons
60
50
40
30
20
10
0
3.0
3.5
4.0
4.5
energy - mev

Fig. 10

II. TOTAL NEUTRON CROSS SECTIONS

Introduction

Previous measurements[1] of the total cross section of phosphorus for fast neutrons have yielded only scanty information in the energy range available to us. The total cross section for chlorine has not been reported previously, while that for gold appeared in abstract form[2] during our investigation.

1) R. K. Adair, Rev. Mod. Phys. 22, 249 (1950).

2) R. L. Becker, M. Walt and A. Okazaki, Bull. Amer. Phys. Soc. 27, 19 (1952).

Apparatus

A radio frequency ion source has recently been installed in our small electrostatic generator, which together with suitable auxiliary focusing voltages yields a 15 μ.a. resolved beam of protons in the energy range 500 to 1600 Kev. The generator voltage is kept constant to within 1 to 2 kv by the use of a corona stabilizing circuit whose error signal is derived from a pair of insulated slits located at the output end of the analyzing magnet.

In order to measure the ion beam energy, work was initiated on a torsion balance with which the magnet field of the

analyzing magnet could be measured. Development work was underway at the time of these experiments, and the necessary stability and reproducibility of the torsion balance was achieved. However, since the completion of this work would have required more time than could reasonably be allotted to these experiments, it was decided to rely on the existing generating voltmeter. A careful investigation of the stability and reproducibility of the generating voltmeter revealed that after certain difficulties in the grounding of the rotor were eliminated, the only remaining variable was the temperature expansion of the generator column. When this was reduced as far as possible by the use of water cooling coils on the pressure tank, the reproducibility of the generating voltmeter was generally about 2 Kv. Thus, while the voltmeter left much to be desired, it was adequate for the present experiments, and was then calibrated, using the $F(p;\alpha,\gamma)$ resonance at 873.5 Kev, the $Al(p,\gamma)$ resonance at 993.3 Kev and the $H^3(p,n)$ threshold at 1.019 Mev[3,4]. In addition the $H^3(p,n)$ threshold was checked after each 100 Kev interval throughout the cross section measurements.

3) R. H. Herb, S. C. Snowdon, and O. Sala, Phys. Rev. 75, 246 (1949)

4) R. F. Taschek, G. A. Jarvis, H. V. Argo and A. Hemmendinger, Phys. Rev. 75, 1268 (1949).

The tritium targets were prepared by absorbing tritium gas at 1 mm. Hg pressure into a zirconium film evaporated onto a wolfram backing[5]. Some difficulty was encountered in making

5) A. B. Lillie and J. P. Conner, Rev. Sci. Inst. 22, 210 (1951).

uniform zirconium-tritium targets, as evidenced by the presence of fluctuations in the neutron counting rate of about two or three times the statistical fluctuations. To remove this source of trouble, two pairs of crossed electrostatic deflecting plates were installed just after the output slits of the analyzing magnet. A 60 cycle per second a.c. voltage was applied across one pair of plates, and a 400 cycle per second a.c. voltage was applied across the other pair of plates, in order to spread out the beam over the diaphragms near the target.

The target area was suitably diaphragmed to allow suppression of the secondary electrons from the target and thus, permit the use of a beam current integrator in order to monitor the neutron yield. A conventional condenser and neon-glow tube was used in conjunction with a scale of 256 scaler for measuring the total charge accumulated on the target during each run.

The neutrons were detected by a conventional enriched $B^{10}F_3$ slow neutron counter[6] surrounded by paraffin with an outer

6) Manufactured by N. Wood Counter Laboratory, 5491 Blackstone Avenue, Chicago 15, Ill.

layer of cadmium. The outside dimension of the counter with paraffin was 4 inches and its effective length was 6 inches. Two checks of the stability of the neutron detector and its associated circuitry, using a 10 millicurie Ra-Be source, showed that electronic jitter and voltage drifts did not influence the counting rate more than one per cent.

Finally, there was present in all the measurements a time dependent background of neutrons coming mainly from the region of the analyzing magnet chamber. This was reduced considerably by interposing a stack of five gallon cans filled with a saturated water solution of borax. In addition, the counting rate of these background neutrons was determined at frequent intervals while taking the data, and an attempt was made to correct the desired neutron counting rate for this source of neutrons. Since the amount of these background neutrons was never more than five per cent, it is felt that this source of fluctuation is adequately accounted for.

Experimental

Before measuring the total neutron cross sections, the effect of the exact location of the scatterer was investigated. Figure 11 shows that the location of the scatterer along the target-detector axis is not very critical, and that the scattering-in correction can account for the observed variation of the counting rate. As the scatterer is moved nearer to the neutron source, the counting rate rises sharply,

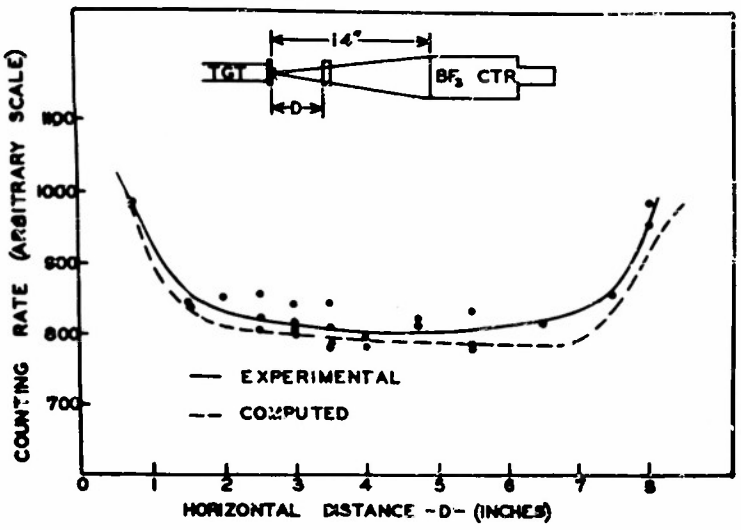


Fig. 11. Counting rate of neutron counter versus the distance of the gold scatterer from the target along the target-detector axis. The solid line is the average of the experimental points. The dashed curve was computed using the following parameters: counting rate without scatterer - 1317, shadow cone background -130, cross section at 1.13 Mev--8.00 barns, counter diameter --4.00 inches, target-detector distance--16 inches.

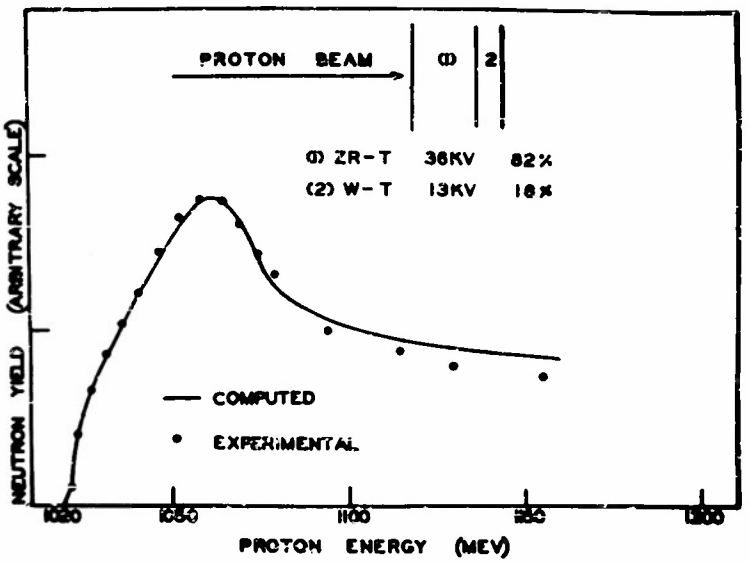


Fig. 12. Yield of neutrons in the forward direction from the $H^3(p,n)He^3$ reaction. The solid curve was computed by adding the yield predicted for a 36Kev thick target containing 82 percent of the tritium to the yield curve predicted for a 13Kev thick target containing 18 percent of the tritium, but displaced in energy by 36 Kev. The algebraic details are given in the appendix.

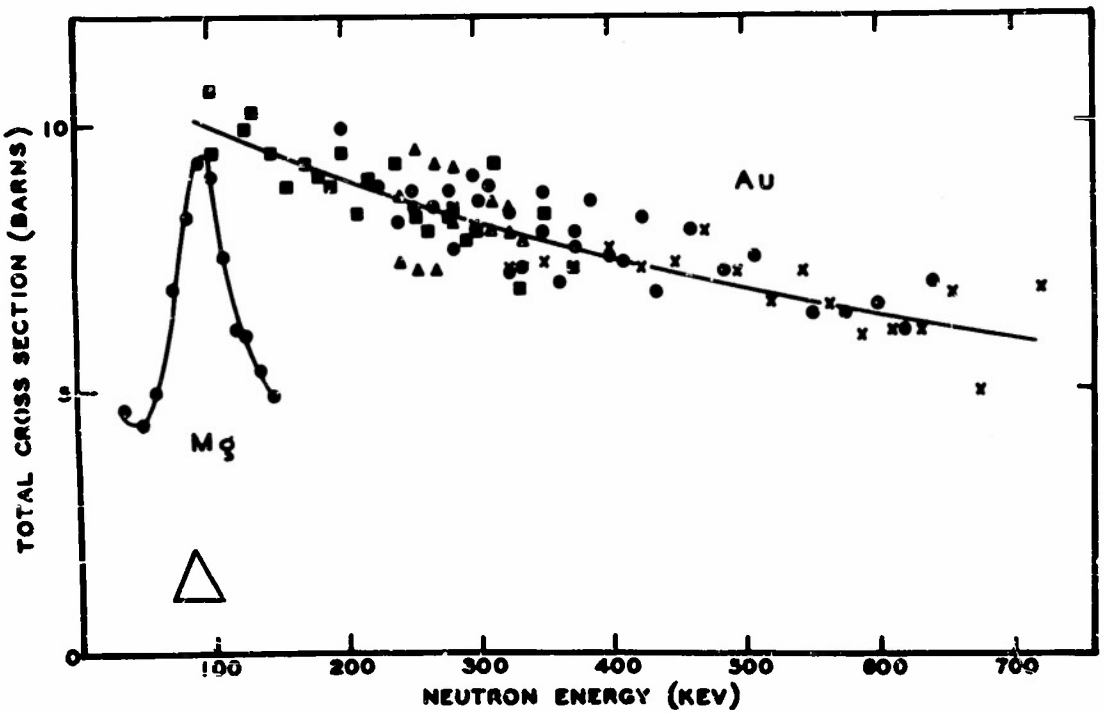


Fig. 13. Total cross section of gold for neutrons in the energy range 100 - 250 Kev was measured with the detector 60° from the direction of the proton beam. The total cross section of magnesium was also measured in the 60° geometry.

and may be accounted for by the rapid increase of the solid angle angle subtended by the scatterer from the target. If the scatterer is moved toward the neutron counter, a sudden increase in counting rate occurs because in our set-up the diameter of the counter is larger than the diameter of the scatterer. As the scatterer passes inside the detector cone, some neutrons pass directly into the detector without passing through the scatterer. The entire effect can be computed from the parameters given in the caption to Figure 11. Hence, it was felt that the correction due to the scattering of neutrons into the detector are adequately accounted for by the following formula:

$$\sigma nd = \ln \left[(1-f/(N/N_0 - f) \right] \qquad (1)$$

where σ is the total cross section, n is the number of scattering nuclei/cm^3, d is the thickness of the scatterer, N is the counting rate with the scatterer in place corrected for the paraffin shadow cone background, N_0 is the counting rate without the scatterer corrected for the shadow cone background, f is a geometrical measure of the scattering-in correction and is given by

$$f = \left[(4\pi/\sigma) (d\sigma/d\omega) \right] \cdot \left[(L/r)^2 \cdot A / 4\pi (L-r)^2 \right] \qquad (2)$$

where $d\sigma/d\omega$ is the differential cross section in the direction of the detector, L is the target-detector distance, r is the

target-scatterer distance, and A is the area of scatterer. The first bracket was taken equal to unity, since it is not exactly calculable but is expected to be near unity in our energy range according to the continuum theory of nuclear reactions[7]. In the geometry used, the scattering-in

---

7) Final Report of the Fast Neutron Data Project, NYO-636.

---

correction, f, usually amounted to four per cent.

The variation of the neutron counting rate as the scatterer was moved in a plane perpendicular to the target-detector axis was also investigated. A misalignment of about one-half inch gave a negligible change in the counting rate provided that the scatterer was aligned initially.

The energy spread of the neutrons was determined almost entirely by the thickness of the zirconium-tritium target. In order to measure this target thickness, careful measurements of the neutron yield in the forward direction were taken (see Figure 12). In the Appendix the shape of the yield curve to be expected was calculated using several reasonable assumptions. If only one uniform target was employed, a departure of the experimental points from the calculated curve was observed in much the same fashion as that described by Bonner and Butler[8]. If,

---

8) T. W. Bonner and J. W. Butler, Phys. Rev. 83, 1091 (1951).

---

however, two different target layers were assumed to constitute

the target, then much of the discrepancy was removed. In particular, if 82 per cent of the tritium was assumed to be present in a 36 Kev layer, and directly in back of this, 18 per cent of the tritium was assumed to be present in a 13 Kev layer, then a unique fit was obtained within the accuracy of the assumptions involved. The second layer is thought to be due to an absorption of the tritium in the wolfram backing onto which the zirconium was evaporated. In any case, the neutron energy spread is seen to be due to a 40-45 Kev thick target.

As a check on this, the narrow resonance in the total neutron cross section of magnesium at 85 Kev reported by Fields and Walt[9] was measured with our source of neutrons.

---

9) R. E. Fields and M. Walt, Phys. Rev. 83, 479 (1951).

Figure 13 shows the observed neutron energy width to be 45-50 Kev in agreement with the target thickness prediction.

Data

The gold scatterer consisted of a one-half inch thick cylinder of pure gold 1 3/4 inches in diameter. Figure 13 gives the results for gold, and it is to be noted that these data were taken before installing the beam-spreaders and the water-can absorbers. A comparison of the gold data with either the chlorine or phosphorus data shows the extent of the reduction

in the fluctuations affected by the use of the beam spreaders and the water cans. Several check points were made on gold after the spreaders and the water cans were installed, and these repeat points fell right along the average line drawn through the points. From these results, it is felt that the total cross section for gold does not have resonances in the energy range 100 to 700 Kev. Furthermore, the magnitude of the cross section agrees well with those of neighboring atomic weight elements.

The total cross section for chlorine was measured using $C Cl_4$ in a 1 3/4 inch diameter cylinder, 2 inches in length. The effect of the carbon was subsequently subtracted, using the carbon cross section given by Adair[1]. Indications of resonances occur at several neutron energies and are separated by about 100 Kev.

The total cross section for phosphorus was measured, using white phosphorus cast into a 1 3/4 inch diameter cylinder, 1 1/2 inches in length. There are several prominent resonances in this energy range, but higher resolution experiments which we hope to be able to carry out probably are needed to give any details concerning the nature of the resonances. The average value agrees well with that reported by Adair[1].

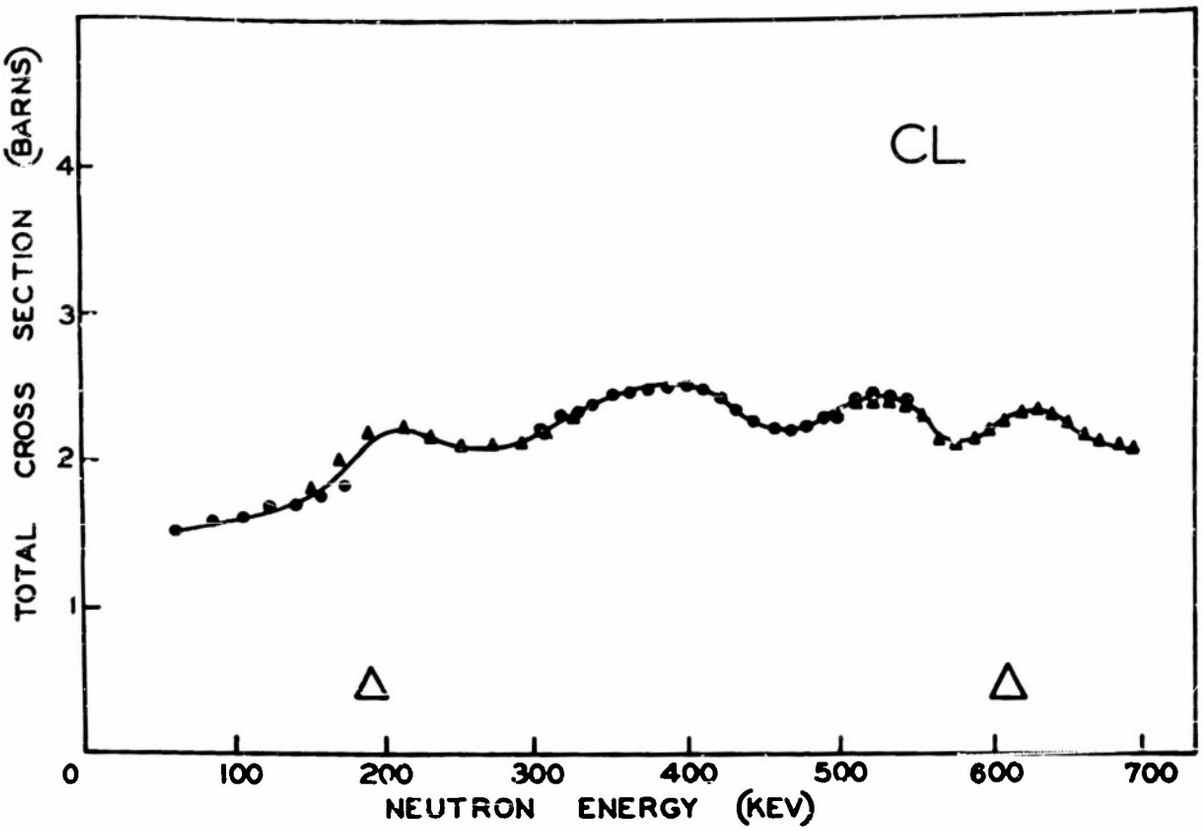


Fig. 14. Total cross section of chlorine for neutrons in the energy range 100 - 700 Kev. The range 100 - 250 Kev was measured in the 60° geometry.

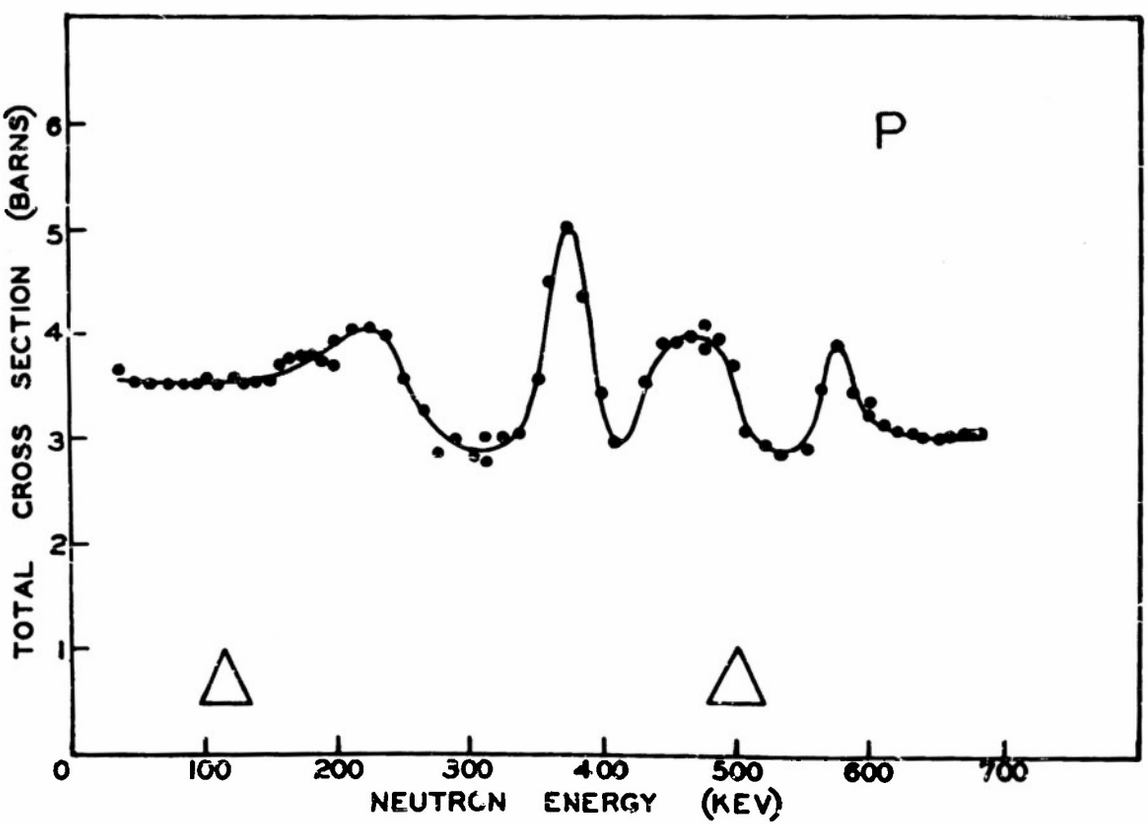


Fig. 15. Total cross section of phosphorous for neutrons in the energy range 100 - 700 Kev. The range 100 - 250 Kev was measured in the 60° geometry.

Appendix

The forward direction yield of the $H^3(p,n)He^3$ reaction from a target of finite thickness as measured by our finite-sized counter (assumed to be a flat circular disk) is given by

$$Y = (N_o n/4\pi) \iint \eta(\theta)\sigma(E) \, (d\Omega\phi_1/d\Omega_\theta + d\Omega\phi_2/d\Omega_\theta) \, d\Omega_\theta \, dx,$$

where N_o is the number of protons striking the target per second, n is the number of tritium nuclei per cubic centimeter, θ is the laboratory angle measured from the proton beam direction, ϕ_1 and ϕ_2 are the two center of mass angles from which emergent neutrons contribute to the laboratory solid angle $d\Omega_\theta$ and $\eta(\theta)$ is the zonal efficiency of the detector. The differential cross section in laboratory co-ordinates has been calculated with the assumption that the differential cross section in the center of mass co-ordinates is a constant. The total cross section, $\sigma(E)$ is then only a function of the energy of the proton E in the layer, dx, of the target.

For convenience in integration, a parameter

$$k = (M_T M_R / M_B M_O)^{1/2} (1 + E_o/E)^{1/2}$$

is introduced where M_T, M_R, M_B and M_O are the masses of the target, residual, bombarding and outgoing particles respectively.

E_o is the threshold energy of the reaction in laboratory co-ordinates. The total cross section of the reaction is assumed to vary as $(E - E_o)^{1/2}$ near threshold and since the exact variation above threshold is not known, it is chosen for convenience in integrating to be such that $\sigma dk \sim k^2 dk$. The zonal efficiency of the counter $\eta(\theta)$ is also assumed to be a constant.

Using the dynamics of the $H^3(p,n)He^3$ reaction, the value of $d\Omega_\phi/d\Omega_\theta$ may be found as a function of k and θ. The integration then may be carried out with the result that

$$Y = (N_o nA/3a)\ K_1^2 \quad \text{for} \quad 0 < K_1 < \text{Sin}\ \theta_o\ .$$

$$Y = (N_o nA/3a)\left[K_1^3 - \text{Cos}\ \theta_o\ (K_1^2 - \text{Sin}^2\ \theta_o)^{3/2} \right]$$

$$\text{for Sin}\ \theta_o < K_1 < (M_R M_T / M_P M_o)^{1/2} \left[1 - E_o / (E_o + at) \right]^{1/2},$$

$$Y = (N_o nA/3a)\left[K_1^3 - K_2^3 - \text{Cos}\ \theta_o\ (K_1^2 - \text{Sin}^2\ \theta_o)^{3/2} \right] \text{ for } 0 < K_2 < \text{Sin}\ \theta_o$$

$$Y = (N_o nA/3a)\left[K_1^3 - K_2^3 - \text{Cos}\ \theta_o\ (K_1^2 - \text{Sin}^2\ \theta_o)^{3/2} + \text{Cos}\ \theta_o \right.$$

$$\left. (K_2^2 - \text{Sin}^2\ \theta_o)^{3/2} \right] \quad \text{for } K_2 > \text{Sin}\ \theta_o \quad \text{but } K_1 \leq 1.$$

In the formulas A is an unknown constant depending on the efficiency of the counter and other constants of the reaction, $\underline{a}$ is the energy loss per cm for the proton beam in the target, θ_c is the half angle subtended by the counter (7.50°) and $\underline{t}$ is the thickness of the target in cm. k_1 is the valus of $\underline{k}$ at the front edge of the target and k_2 is the value of $\underline{k}$ at the back edge of the target, each for an incident proton beam of energy E_B.

III. INSTRUMENTATION AND FUTURE MEASUREMENTS.

The neutrons employed in the measurements of this report were generated by deuteron bombardment of deuterium in the smaller Bartol Van de Graaff generator. In the fall of 1951, this smaller generator was transferred from its previous location to the new off-campus nuclear research center of the Bartol Research Foundation. Much of the spring of 1952 was consumed in bettering the performance of the generator. For example, the bombarding beam of magnetically analyzed deuterons was increased from 0.5 to 1.0 microampere to twenty microamperes facilitating infinitely the production of neutrons for measurements such as those described in Sections I and II of this report.

A Cockroft-Walton set which has been previously described (Reference 3, Section I), is being transferred to a building of its own. This building is being constructed with exclusive use of the private funds of the Bartol Foundation. Neutrons have been successfully produced in this generator, but since it was located in close proximity to the small generator, simultaneous operation of the two accelerators became impossible.

With a view to applying scintillation counter methods to detection of neutrons and gamma rays involved in scattering experiments, two complete detection units are being built.

Each consists of photomultiplier, linear amplifier, single channel pulse height discriminator, and scaling circuit. A coincidence analyzer will also be employed for noting coincidences between neutrons and gamma rays.

Using the 20-cm geometry of Figure 5, Section I, chromium has been irradiated by 4-Mev neutrons. Iron has been irradiated again in a new geometry which will be described in a later report. These exposures have been just completed at the time of writing this manuscript and the associated photographic plates have not been analyzed. It was planned also to irradiate Bi, C, and Fe in the 20-cm geometry. However, since the neutron flux is so great for 22 microamperes of million volt deuterons, the tolerance dosage was experienced in a very short time by the operating crew during the iron-chromium bombardments. It has therefore become necessary to postpone temporarily further irradiations.

It will be recalled that some time ago the large Van de Graaff generator had been built up to one-third of its final height and tested as regards voltage, beam production, and operation. The success of these tests justified the next step, the extension of the generator to its full height. This extension has been carried out and electrostatic voltages in excess of 5 MV have been obtained.

The full length of the accelerating tube has been installed, together with the ion source. Several tests relative to the ion

beam are under way. In this connection, electrostatic deflector plates and the suppressor have been added just below the accelerating tube proper. The purpose of the former is to align the beam and that of the latter to suppress back electrons.

The analyzing magnet is now in operating, although a few refinements are still to be made. Essentially all the energy controlling mechanism has been completed; the elements which have not been completed await the beam tests mentioned above. It is expected that, barring unforeseen circumstances, the generator will be operating with a focused beam and at a voltage in excess of 5 million volts in about a month.

The above progress report on the generator has been included because it is intended that this machine shall be used in connection with the neutron scattering work, permitting neutron beams of much higher energy and greater intensity than those so far available to us.

SEMI ANNUAL REPORT

of the Work of the

BARTOL RESEARCH FOUNDATION

OF THE FRANKLIN INSTITUTE

(February 1, 1953 -- June 30, 1953)

Performed Under Contract Nonr 436(00)

with the

OFFICE OF NAVAL RESEARCH

TABLE OF CONTENTS

I. Inelastic Scattering.

A. Neutrons

B. Gamma rays

II. Total Cross Sections; Angular Distribution of Elastic Scattering; Inelastic Cross Sections.

PERSONNEL

Physicists: (Part-time or full-time)

D. W. Kent

C. E. Mandeville

F. R. Metzger

M. A. Rothman

S. C. Snowdon

W. D. Whitehead

Technicians: (Half-time)

R. W. Gunnett

Report submitted July 30, 1955

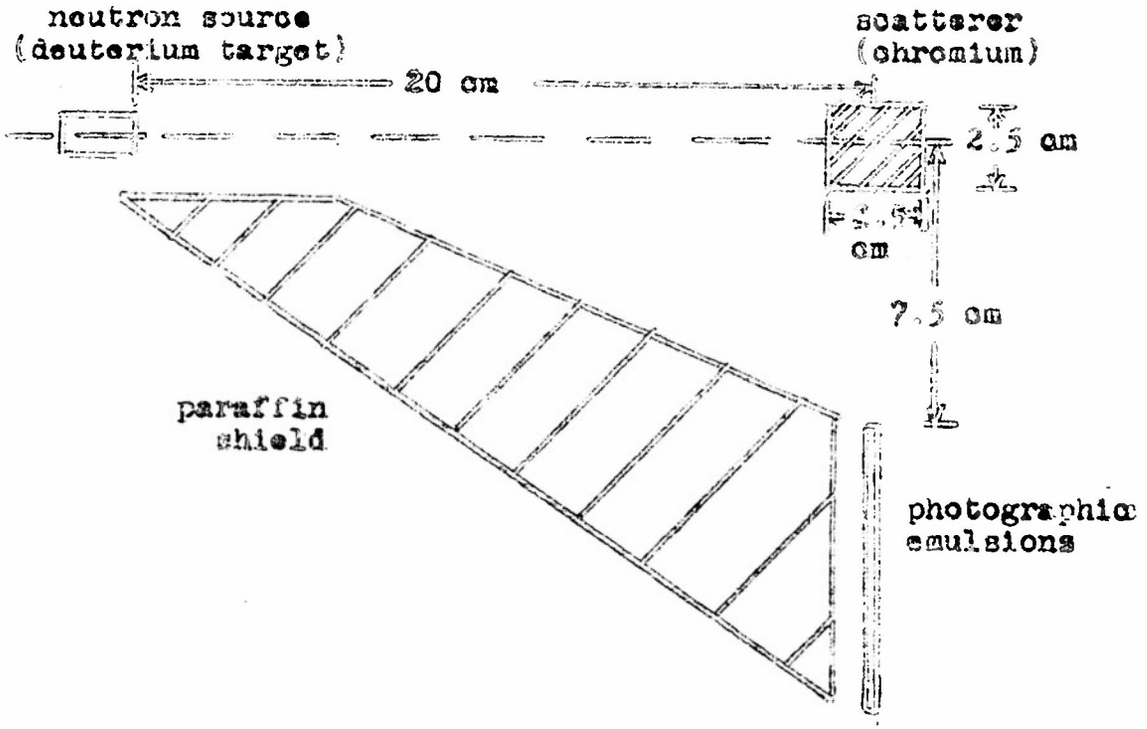
C. E. Mandeville

C. E. Mandeville, Physicist

I. INELASTIC SCATTERING.

MEASUREMENT OF NEUTRON ENERGIES

In the foregoing semi-annual report, results were presented concerning neutron-scattering from iron. A survey of various geometries was carried out with the idea of obtaining one which provided good resolution and at the same time was relatively simple. One of the geometries which appeared promising was that of the 20-cm "paraffin wedge". This arrangement is depicted in Figure 1. As a trial scatterer, a cylinder of chromium was employed. Fast scattered neutrons were detected at an angle of 90° with the incident neutrons. A background run was taken with no scatterer present. The accumulated background was subtracted from the data obtained when the scatterer was present. The background data as well as those with scatterer present were normalized to take properly into account the incident neutron flux and the plate-area scanned. The resulting spectrum is shown in Figure 2 where it is clear that three resolved groups of neutrons are present. The group of greatest energy is the elastically-scattered one. The two groups of neutrons at lower energies result from the inelastic scattering process. They would correspond to formation of Cr^{52} in excited states at $\sim$1.43 and $\sim$ 1.93 Mev. The broken line is the energy distribution of recoil protons corrected for variation with energy of the n-p scattering cross section and acceptance probability.



GEOMETRY FOR DETECTION OF NEUTRONS SCATTERED FROM CHROMIUM

Figure 1

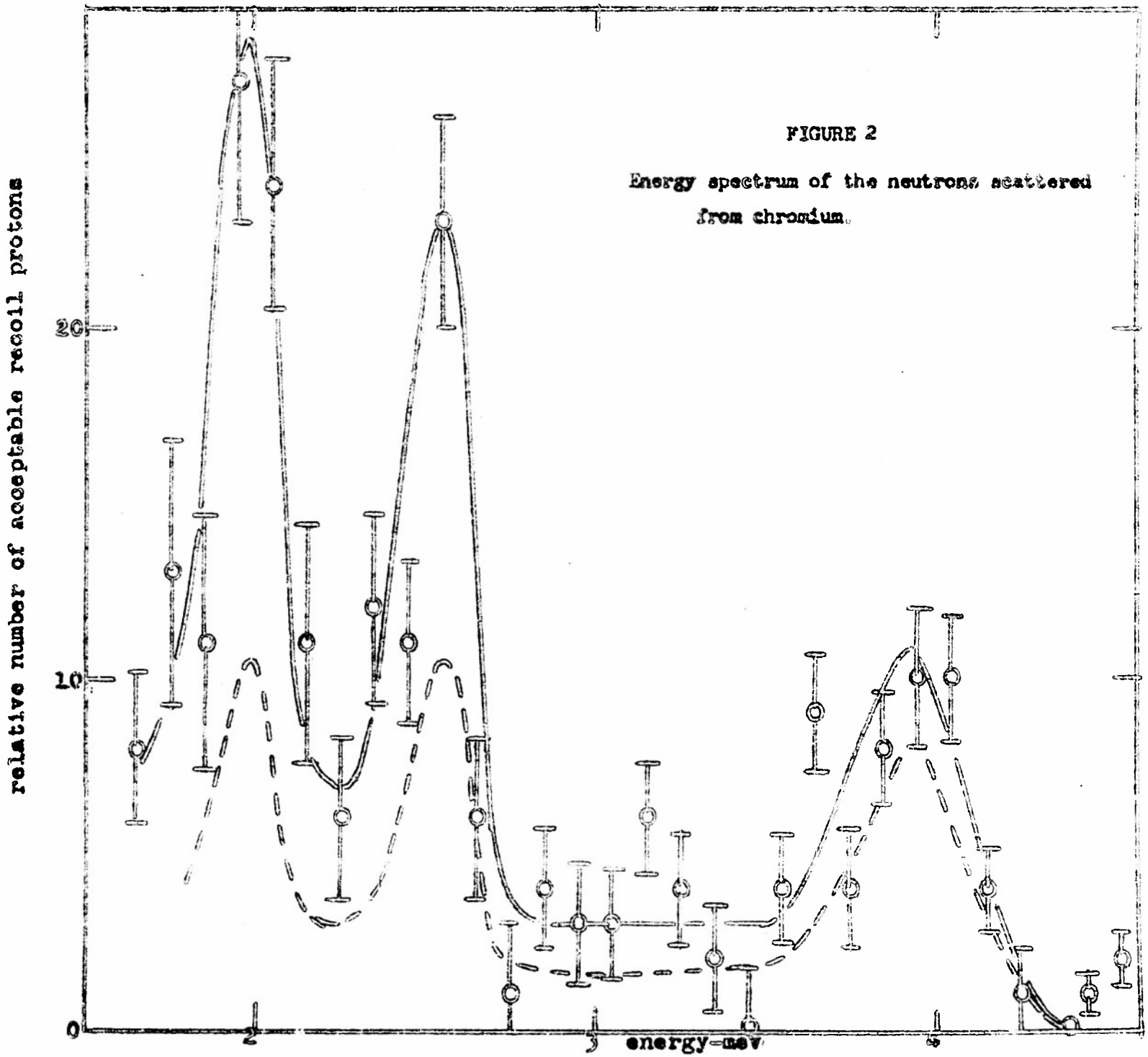


FIGURE 2

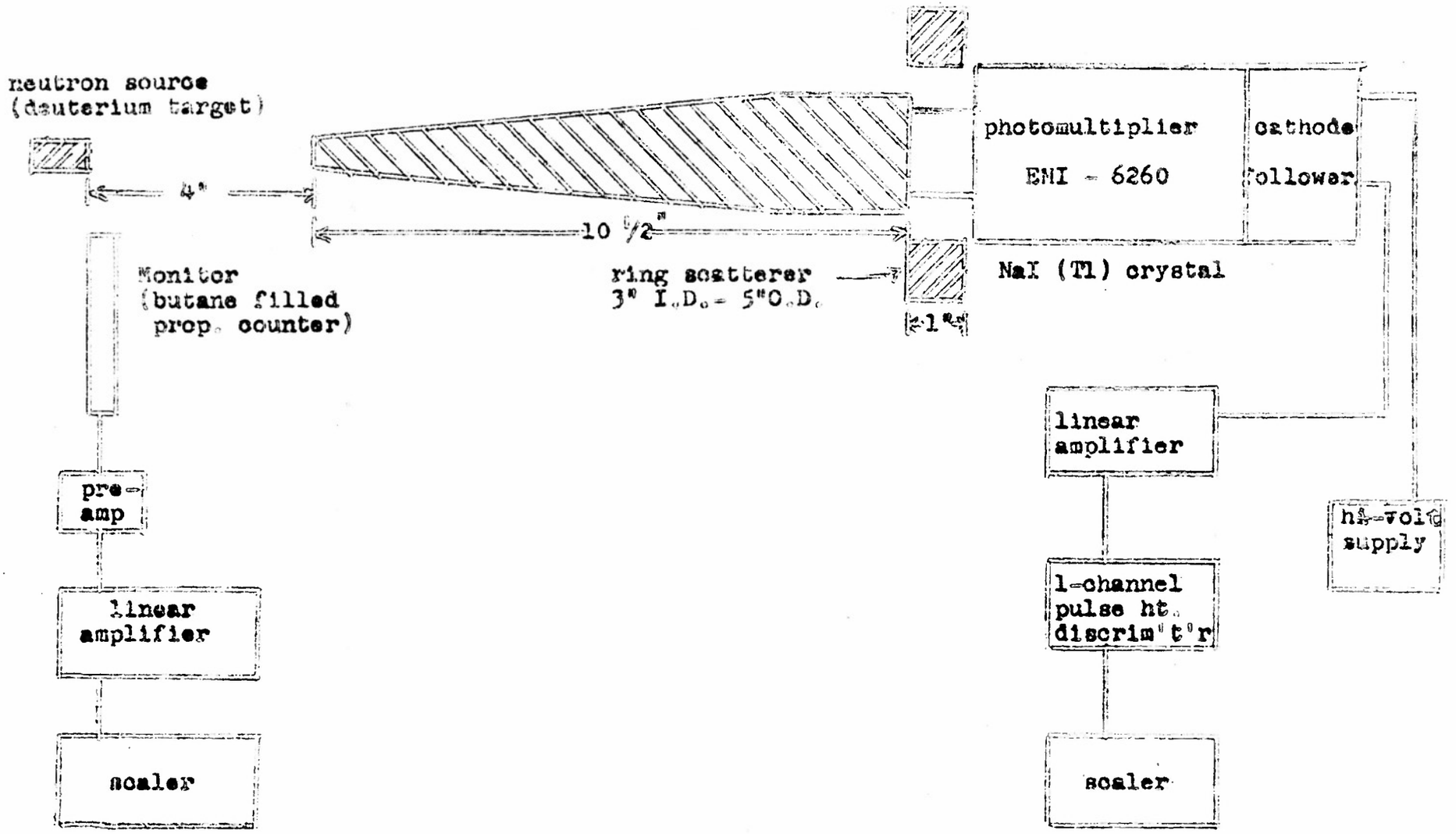
Energy spectrum of the neutrons scattered from chromium.

The gamma rays from neutron scattering in chromium and their relation to the neutron spectrum will be discussed in a later section of this report.

GAMMA-RAY MEASUREMENTS

A geometry for detecting gamma rays excited in the inelastic scattering process is given in Figure 3. In this arrangement, neutrons are produced in the D-D reaction at the target of the Van de Graaff statitron and proceed to the scattering ring of material about the crystal of NaI-Tl. There they are detected, and the pulse-height distribution is observed in a single channel pulse-height discriminator.

The procedure adopted was to measure the background in the scintillation detector and then measure the total counting rate, background and contribution from the scatterer included. The background was measured in each interval of two volts, the dummy scatterer being a graphite ring. Since the first excited level of C^{12} is at 4.43 Mev, the carbon ring contributed no gamma ray arising from any inelastic scattering effects. It was not considered correct to take the measured counting rate with no scatterer present at all as the background, because the scattering ring deflects neutrons into the crystal giving rise to capture gamma rays and to radioactivity, the 25-minute iodine. The high energy beta-ray spectrum of this radioisotope contributes materially to the background count.



GEOMETRY AND CIRCUITRY OF SCINTILLATION COUNTING EXPERIMENT

FIGURE 3

In Figure 4 is the pulse-height distribution of the gamma rays resulting from the scattering of 3.9 Mev gamma rays by chromium along with the background obtained with the carbon ring replacing the metallic scatterer. It should perhaps be remarked that no measurements of any kind were commenced until after the Van de Graaff had been producing neutrons for more than an hour to bring to approximate equilibrium the 25-minute activity. In Figure 5, similar curves are presented for graphite and lead.

In Figures 6, 7, 8, and 9 are pulse-height distributions with background subtracted of gamma rays emitted in the inelastic scattering process by iron, bismuth, chromium, and lead. The energies and relative intensities of the gamma rays are summarized in Table I.

TABLE I.

Element	Gamma Rays (Energies, Mev)	Relative Intensities
Iron	0.85 2.15	680 260
bismuth	0.90 1.63 2.66	540 1000 600
lead	0.84 1.55 2.66	400 650 450
chromium	1.43	= = =

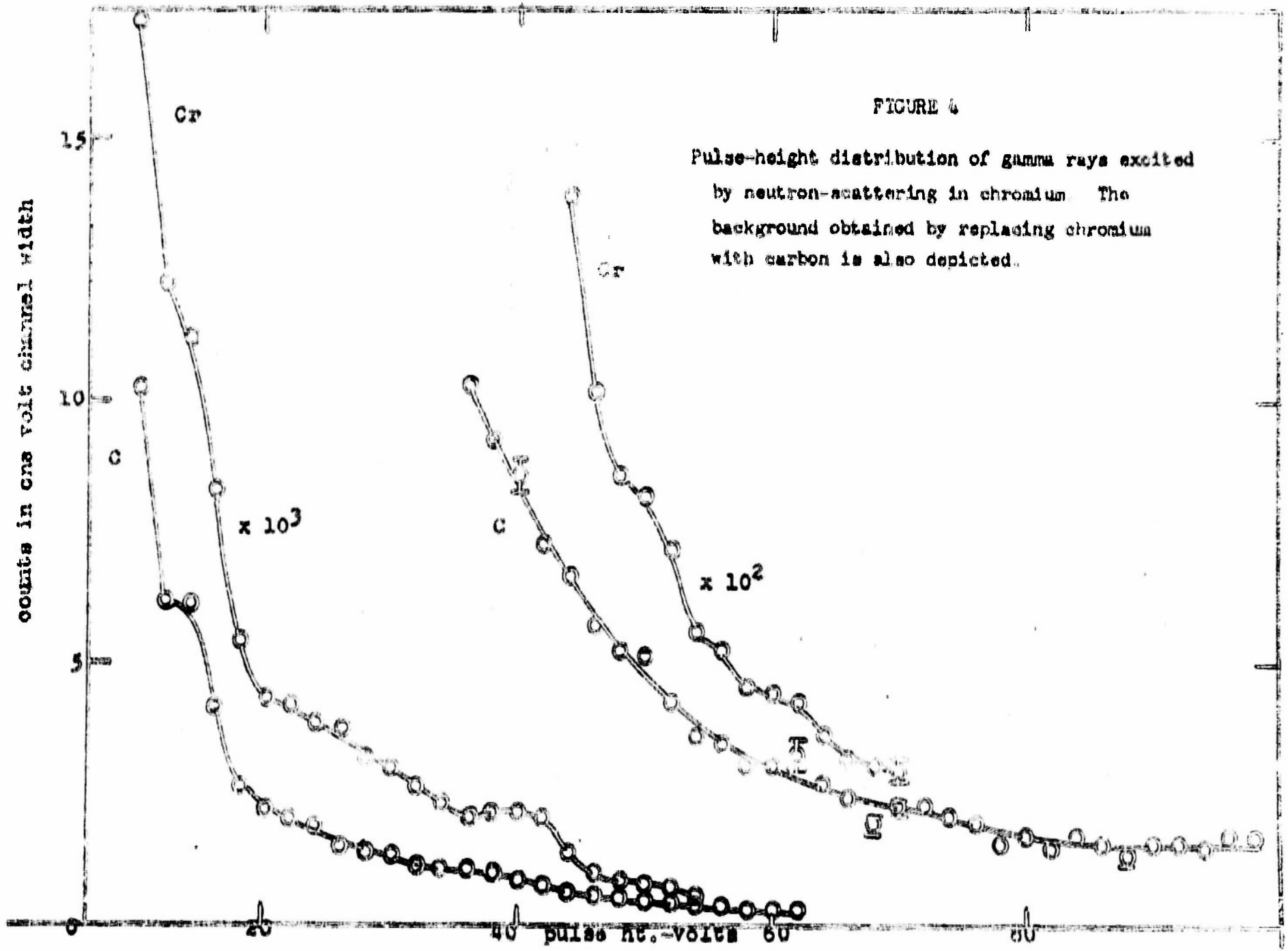


FIGURE 4

Pulse-height distribution of gamma rays excited by neutron-scattering in chromium. The background obtained by replacing chromium with carbon is also depicted.

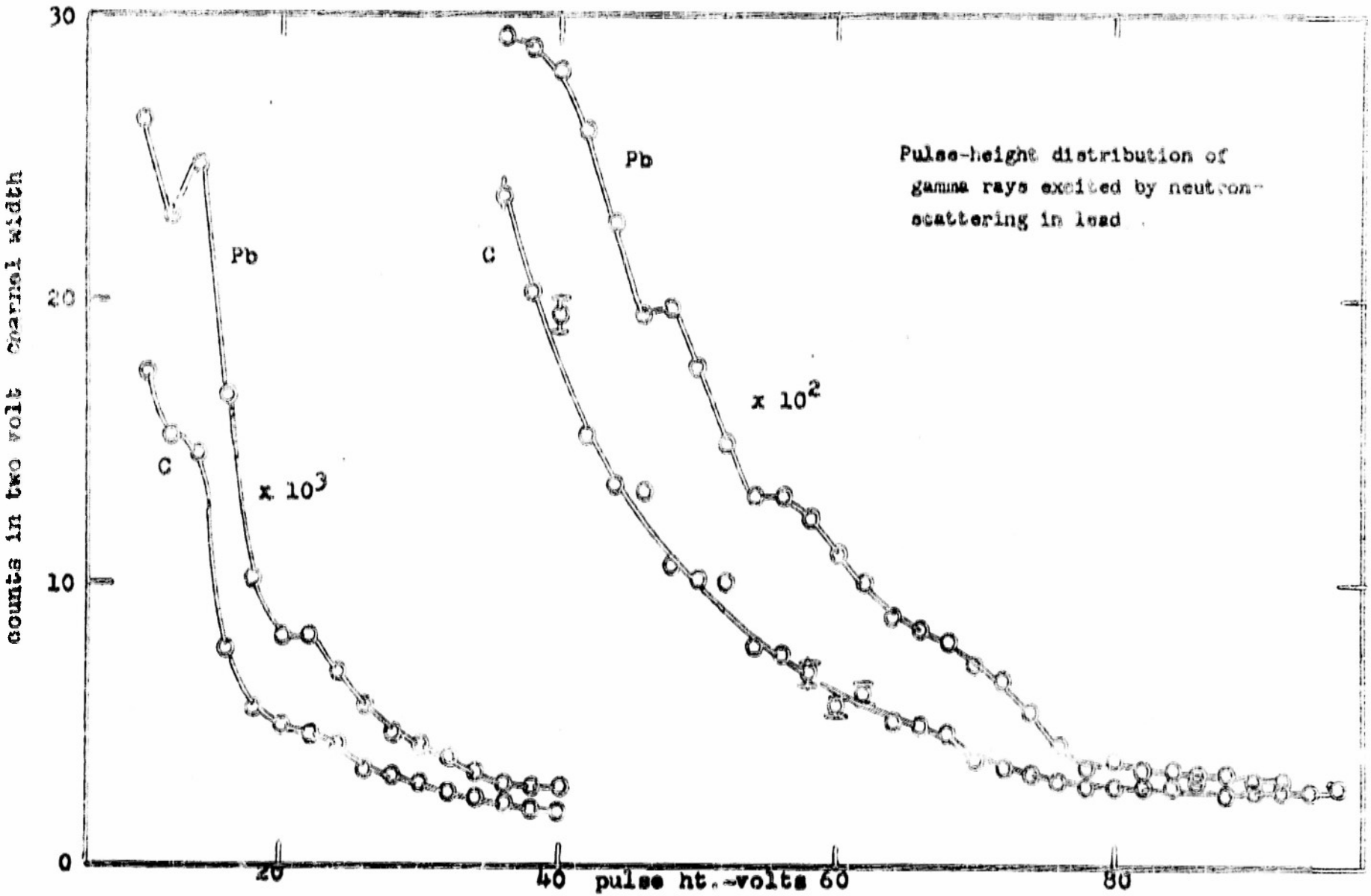
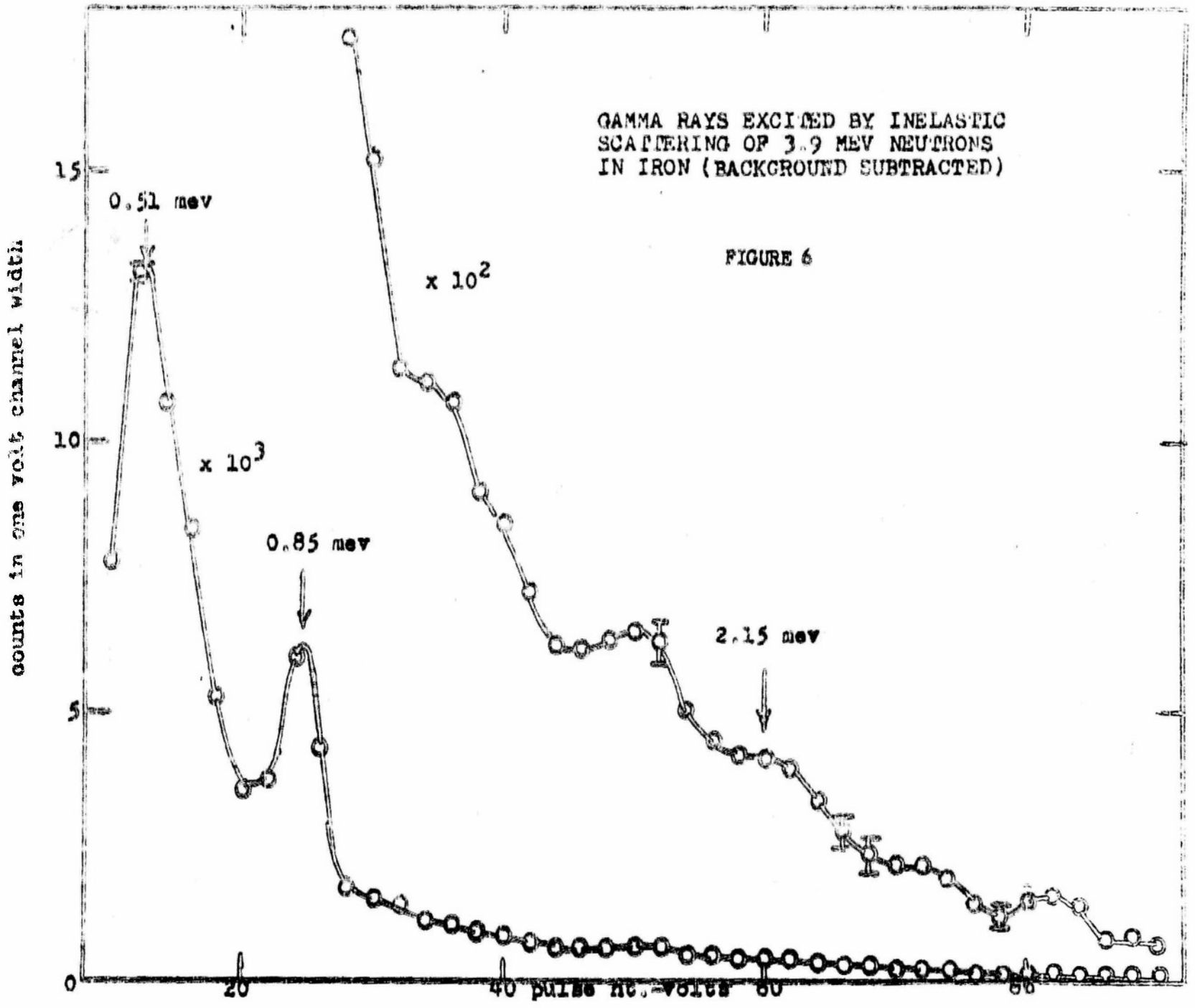

Pulse-height distribution of gamma rays excited by neutron-scattering in lead
counts in two volt channel width
pulse ht.-volts
Pb
C
x 10³
x 10²
0
10
20
30
20
40
60
80

FIGURE 5


GAMMA RAYS EXCITED BY INELASTIC SCATTERING OF 3.9 MEV NEUTRONS IN IRON (BACKGROUND SUBTRACTED)
FIGURE 6
counts in one volt channel width
15
10
5
0
0.51 mev
x 10^3
x 10^2
0.85 mev
2.15 mev
20
40
pulse ht.-volts
60

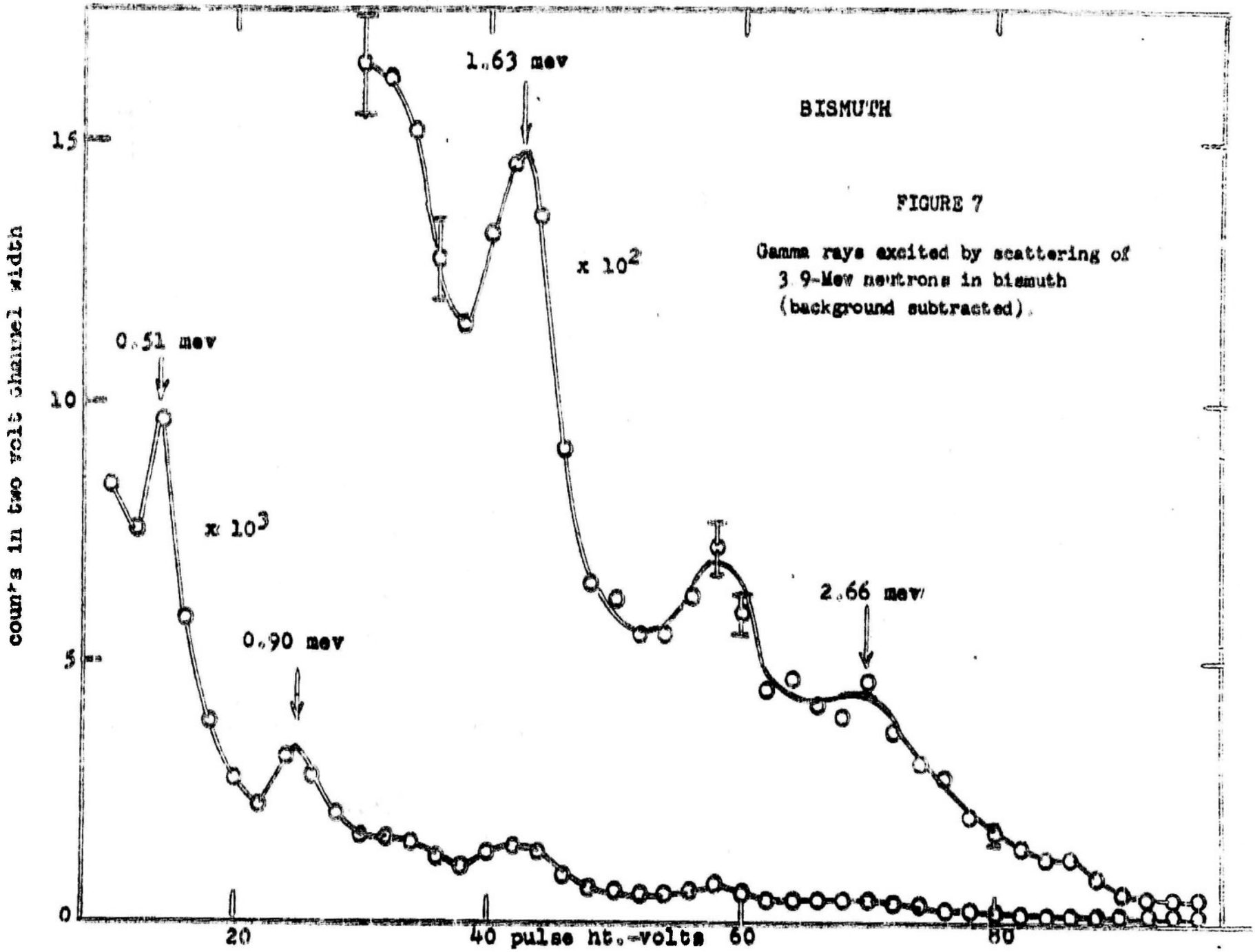


FIGURE 7

Gamma rays excited by scattering of 3.9-Mev neutrons in bismuth (background subtracted).

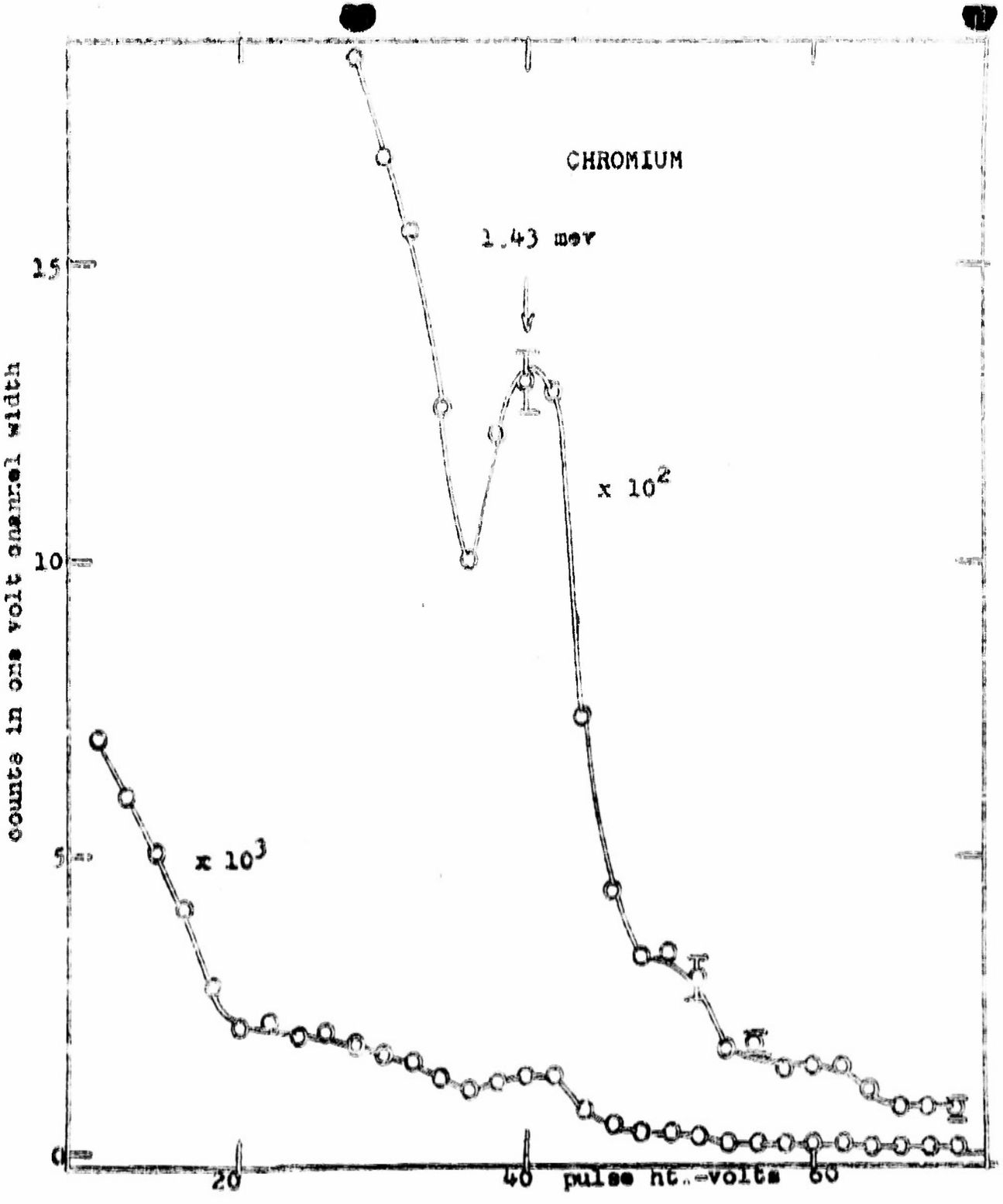


FIGURE 8

Gamma rays excited by scattering of 3.9-Mev neutrons in chromium (background subtracted).

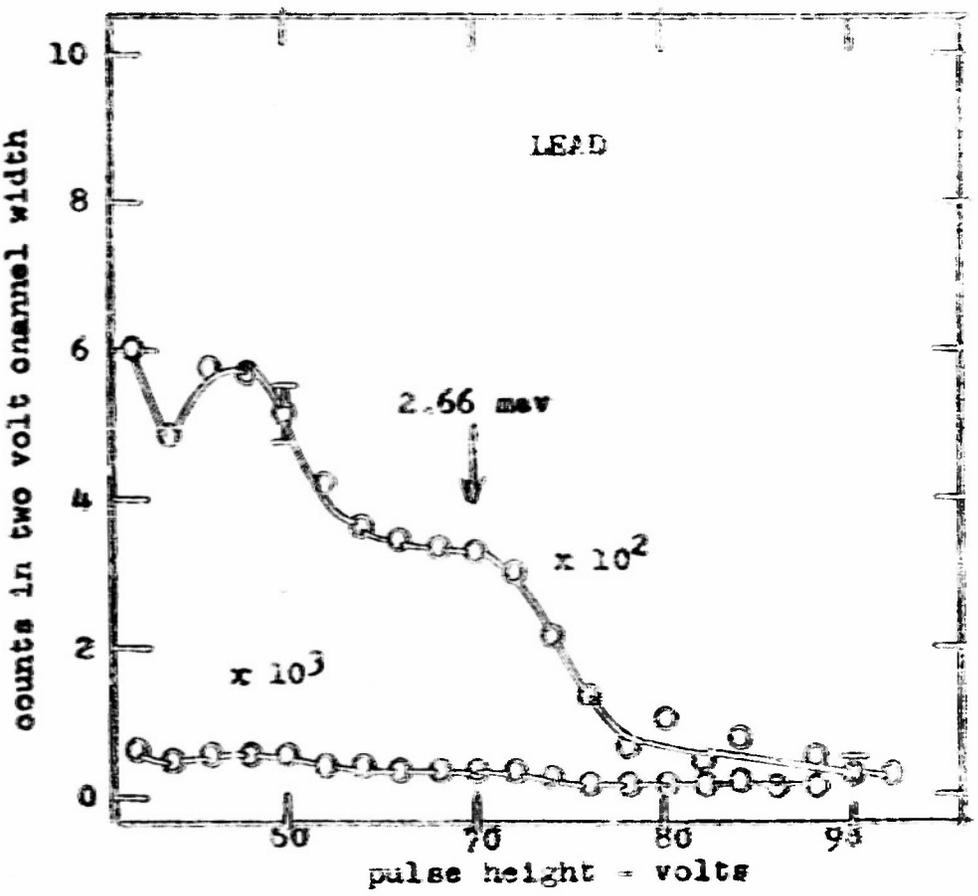


FIGURE 9

Gamma rays excited by scattering of 3.9-Kev neutrons in lead (background subtracted). This curve is obtained by treating the high energy region of Figure 5. Because of certain experimental uncertainties, the region of lower energy was not analyzed in detail for lead.

The relative intensities of the gamma rays are per atom of element present per unit of neutron flux. Thus, the intensities can be compared among themselves, irrespective of element. For example, the ratio of the intensity of the 2.66 Mev gamma ray of lead to that of the 0.85 Mev gamma ray of iron is 450:680, if equal numbers of lead and iron atoms are irradiated by fast neutrons of energy 3.9-Mev. In arriving at the relative intensities of Table I, it was necessary to attempt to take into account the attenuation of neutrons and gamma rays in the ring scatterers. Several approximations are involved; so it is thought that the results are accurate only to a factor of 2 or 3.

The method of analysis of the gamma-ray spectra should now be considered. In Figure 10 is shown the gamma-ray spectrum of Na^{24}. This curve is readily interpretable. The photoelectric peak of the 2.76 Mev gamma ray is present, followed by escape peaks at 2.25 Mev and 1.74 Mev which are superposed upon the Compton distribution. The photoelectric peak of the 1.38 Mev radiation also appears and somewhat lower in energy is the associated Compton edge. The spectrum of Na^{24} was observed with the radioactive source within the lead scattering ring in the geometry of Figure 3, outside the ring, and directly in front of the scintillation-counting crystal. The three spectra did not differ materially among themselves. They all resembled Figure 10 which was taken with the source of Na^{24} in front of the crystal. The value of this curve in making an analysis is immediately

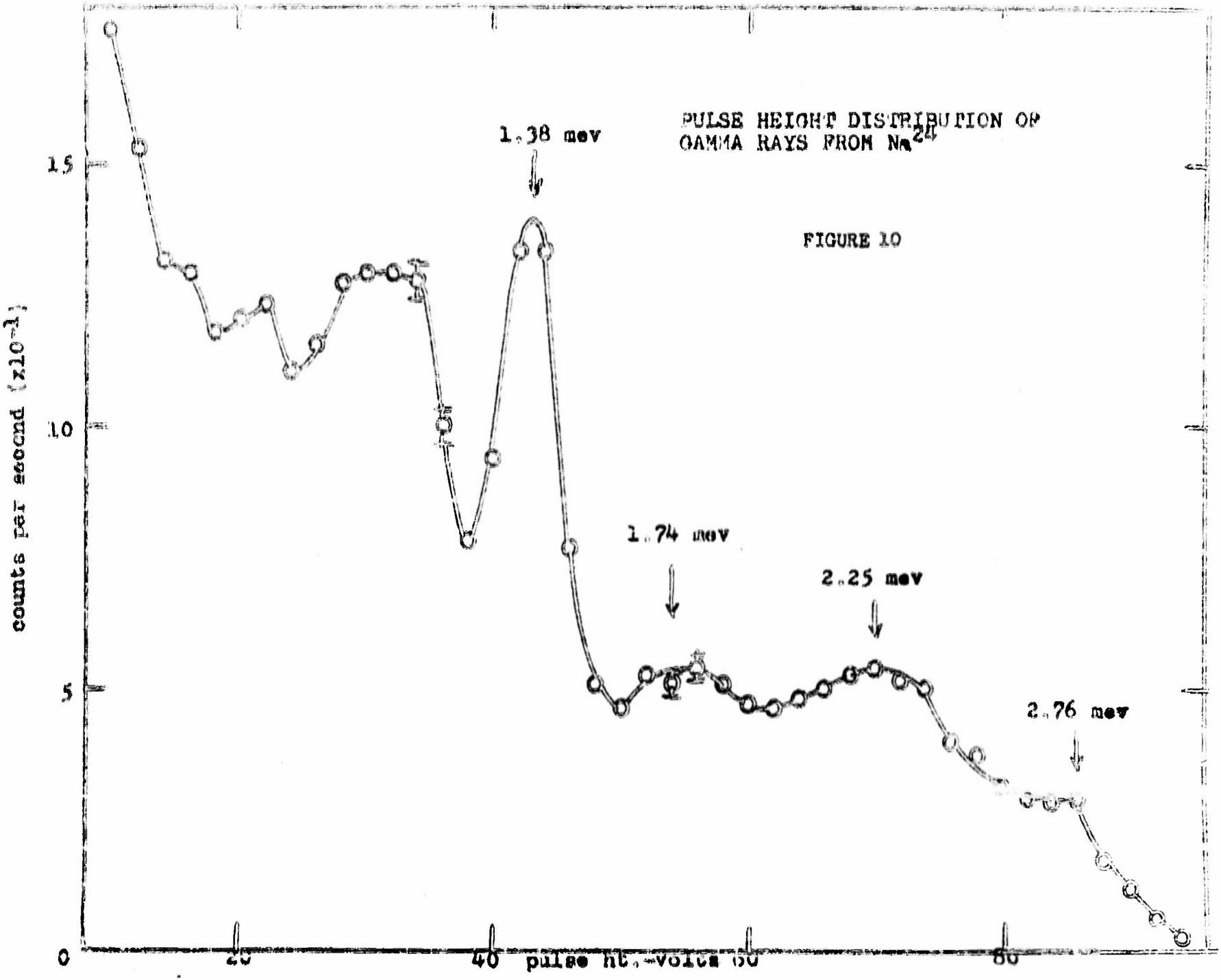

PULSE HEIGHT DISTRIBUTION OF GAMMA RAYS FROM Na^{24}
1.38 mev
1.74 mev
2.25 mev
2.76 mev
counts per second (x10⁻¹)
15
10
5
0
20
40
pulse ht.-volts
60

FIGURE 10

evident. For example, the photoelectric peak and first escape peak of the 2.66 Mev gamma ray are clearly recognizable in Figure 9 on comparing them with the photo-peak and first escape-peak of the 2.76 Mev gamma ray of Na^{24}. Similar comparisons show that a 2.66 Mev gamma ray is excited in bismuth as shown in Figure 7. However, the high energy edge of the photo-peak does not drop off rapidly. Instead, it drops slowly, suggesting the presence of gamma radiation of higher energy. An indication of a photo-peak appears at ~3.26 Mev. The gamma-ray spectrum of iron, given in Figure 6, exhibits peaks which are conservatively interpreted as two gamma rays having respectively energies of 0.85 Mev and 2.15 Mev. The peak lower in energy and adjacent to the photo-peak at 2.15 Mev is at present interpreted as an escape peak. Gamma rays of energies greater than 2.15 Mev are clearly present but are not specifically identified in energy. The bulk of the gamma radiation of chromium is evidently concentrated in a gamma ray at 1.43 Mev as shown in Figure 8. Gamma rays of higher energy are also present. The gamma ray of energy 1.43 Mev is thought to be emitted in Cr^{52}, and the gamma rays of higher energy are thought to be emitted from other isotopes of chromium. The relative isotopic abundance of Cr^{52} is 82 per cent. The gamma rays of higher energy are thought not to be emitted from Cr^{52}, because the spin values of its energy levels make cross-over transitions of energies greater than 1.43 Mev very improbable. In Figures 6, 7, and 9, the spectra for iron,

bismuth, and lead, it is to be noted that an intensive gamma ray appears at 0.51 Mev. This is, of course, the annihilation radiation resulting from pair production by the high energy gamma rays within the ring scatterers themselves.

Returning to the photographic plate spectrum of Figure 2, it should be noted that although the 1.43 Mev gamma ray corresponds properly to the energy difference between the elastic group and the more energetic inelastic one, no gamma ray was detected corresponding to the energy difference between the two inelastic groups. The precise explanation for this discrepancy between the gamma ray and neutron measurements may have either of two forms:

1) The least energetic group of neutrons in the spectrum of Figure 2 may result from scattering of neutrons from the paraffin wedge into the chromium scatterer and thence to the photographic plates. The background run should have been taken with a carbon cylinder in place of the chromium cylinder. Instead, the background was simply collected with the chromium scatterer removed and nothing taking its place.

2) The gamma-ray spectrum of chromium rises steadily below 0.7 Mev. The counting rate is not immediately interpretable. The pile-up of counts in the region

of low energy may be related to scattered gamma radiation having its origin in various parts of the Van de Graaff statitron and obscuring the sought for gamma ray corresponding to the energy difference between the two inelastic groups of neutrons.

It is hoped that these several difficulties will be resolved in the near future.

II. TOTAL CROSS SECTIONS; ANGULAR DISTRIBUTION OF ELASTIC SCATTERING; INELASTIC CROSS SECTIONS.

Introduction

Measurements of the angular distribution of fast neutrons scattered from a large number of elements have been reported previously by Kikuchi and Aoki et al.[1], and Amaldi et al.[2] in which the main features of the distribution could be explained as the diffraction effects due to the scattering of neutron waves by spherical particles. More recently Remund and Ricamo[3] have measured angular distribution of 3.7 Mev neutrons scattered from carbon while Walt and Barschall[4], using 1.00 Mev neutrons have reported the angular distributions for a large number of elements. Feshbach, Porter and Weisskopf[5], using a modification of the continuum theory of nuclear reactions, have reproduced the average features of the total neutron cross section versus energy and atomic number as measured by Barschall[6]. Feshbach, Porter, and Weisskopf[7] have also computed the angular distributions of elastically-scattered neutrons using this same modification of the continuum theory and the general features agree rather well with the measurements of Walt and Barschall[4]. Our measurements on aluminum, iron and lead, using 3.7 Mev neutrons, were undertaken with the thought that the angular distribution in this energy range would be of value in view of the present theoretical considerations.

Experimental

Figure 1 shows the experimental arrangement that was used to measure the angular distribution of neutrons scattered from

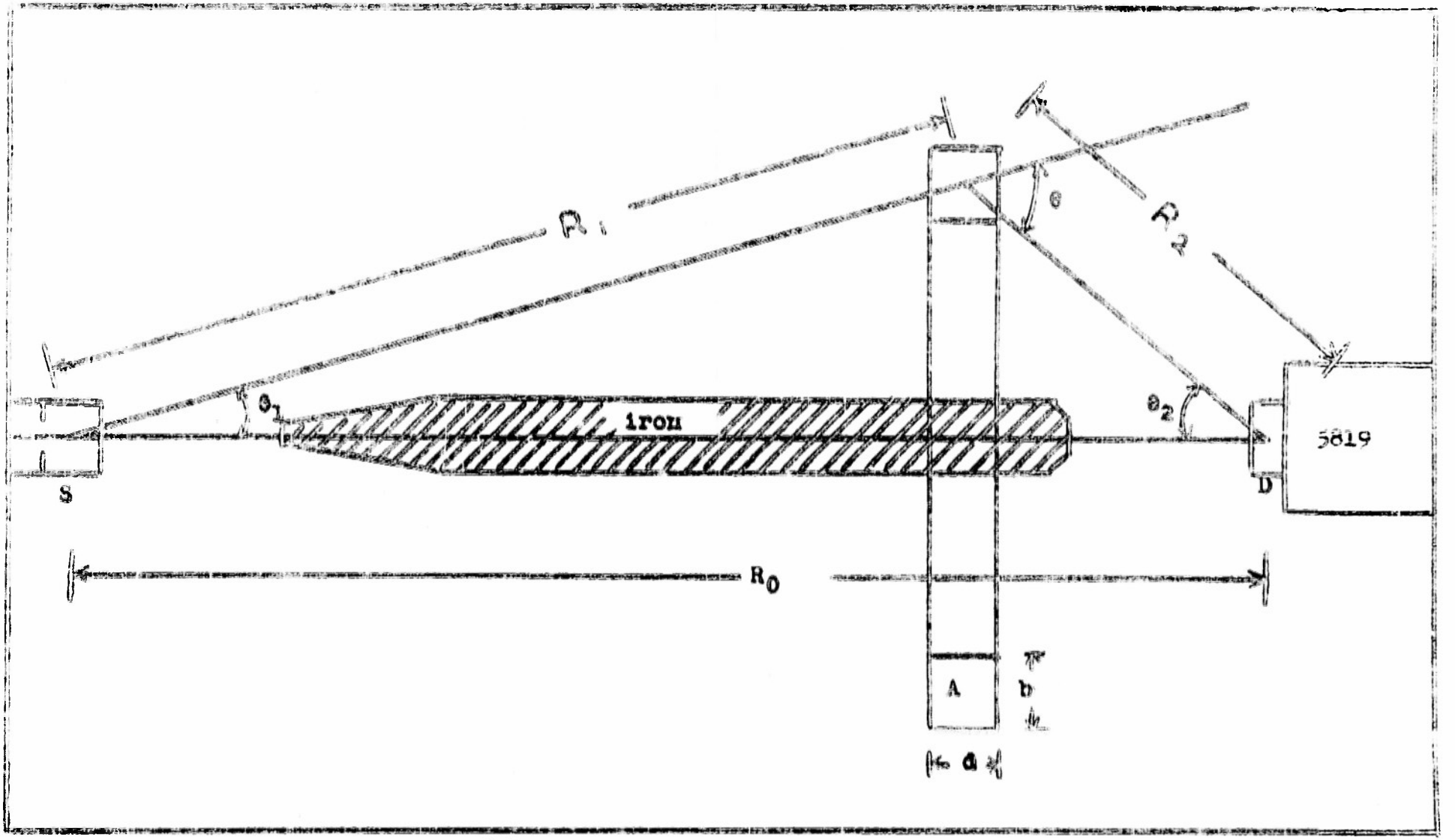


FIGURE 1. Ring geometry for scatterer, (S), deuterium gas at one-half atmosphere pressure to give neutrons of about 3.7 Mev; (D) Lucite-zinc sulphide scintillation detector; (A) ring scatterer of rectangular cross section.

aluminum, iron and lead. The source of neutrons is a chamber of deuterium gas at 0.5 atmosphere and 2.0 cm in depth bombarded with about 10 microamperes of 1.0 Mev deuterons which after passing through the nickel foil and gas have a mean energy of about 0.65 Mev. These neutrons are detected by a pressure molded Lucite-zinc sulphide button[8] mounted directly on the face of an RCA 5819 photomultiplier. The direct beam is cut out by a suitably tapered 10 inch long, 1 1/8 inch diameter iron cylinder. The scatterer was chosen to have the shape of a ring in order to increase as much as possible the number of scattered neutrons. The scattering angle Θ is varied by moving the scattering rings laterally, and by using rings of various sizes. For angles between 52° and 140° degrees, 8 inch O.D. rings were used with a mean source-detector distance R_o of 40 cm. For Θ between 24 degrees and 52 degrees, 6 O.D. inch rings were used with R_o equal to 60 cm. For the point at 13°, 4" O.D. rings were used with R_o equal to 72 cm.

In order to discuss the measurements that must be made to arrive at the differential scattering cross section, it is convenient to define several quantities. For a given number of neutrons emitted by the neutron source, let N_S be the number of neutrons recorded by the detector with the scatterer and direct beam attenuator in place. Let N_B be the number of neutrons detected with the scatterer removed and let N_D be the number of neutrons recorded with the scatterer and attenuator removed. The N_S-N_B is the number of scattered neutrons recorded by the detector that originate in the source, and N_D-N_B is the number

of neutrons direct from the source that are recorded by the detector. Let the scattering ratio be defined as

$$S \equiv (R_S - E_B)/(R_D - E_B).$$

Appendix I then shows that the scattering ratio S is related to the apparent differential scattering cross section $\bar{\sigma}(\Theta)$ through the relation

$$S = \left[I(\Theta_1)/I(0)\right] \cdot \left[R_o^2/R_1^2 R_2^2\right] \cdot \bar{\sigma}(\Theta) A(\Theta_2) E(E_n) nV F(\Theta_2) \exp(-\mu nd) \qquad (1)$$

where $I(\Theta_1)$ is the number of neutrons emitted from the source per steradian per unit monitor flux, $A(\Theta_2)$ is the angular sensitivity of the neutron detector normalised to unity at zero angle, $E(E_n)$ is the energy sensitivity of the neutron detector normalised to unity for the energy of the direct beam, nV is the number of scattering nuclei, σ is the total scattering cross section, and $F(\Theta_2)$ is an attenuation factor which is defined more fully in Appendix I.

In general, the scattering ratio S is made up of a sum of terms $S = S_1 + S_2 + \text{etc.}$, where S_1, S_2, etc. refer to the neutrons scattered into the detector by single scattering, double scattering, etc. Thus, $\bar{\sigma}(\Theta)$ is simply a measure of the differential scattering cross section, assuming that all neutrons are singly scattered, since $\bar{\sigma}(\Theta)$ becomes exactly

$\sigma(\theta)$ if S is replaced by S_1. In order to separate the components S_1, S_2, etc., one measures the scattering ratio S for a fixed angle θ as a function of the axial thickness of the ring scatterer d. The value of $\bar{\sigma}(\theta)$ at d = 0 is then the average differential scattering cross section for all scattered neutrons (elastic and inelastic) weighted according to the energy sensitivity of the detector $E(E_n)$. In the ideal case, if the energy sensitivity curve adequately discriminates against the inelastically scattered neutrons, the above value of $\bar{\sigma}(\theta)$ for d = 0 becomes the differential cross section for elastic scattering $\sigma(\theta)$.

In order to measure $\bar{\sigma}(\theta)$ it is necessary to consider the following factors.

1. Energy resolution of incident neutrons. The mean energy of the neutrons incident on the scatterer varies between 3.70 Mev and 3.74 Mev depending on the angle θ_1. The energy spread in the beam due to target thickness and voltage stability of the generator is about 200 Kev.

2. Neutron flux monitor. A proportional counter filled with one atmosphere of butane was placed very close to the target chamber at 90 degrees with respect to the source-detector axis. The discriminator was set to reject those neutrons that were produced from the $C^{12}(d,n)$ reaction in the vicinity of the magnet box. Actually, some difficulty was experienced in obtaining a constant direct beam neutron count per unit monitor count after the target chamber was just filled

with deuterium. The pattern of change, however, was similar in each case and seemed to indicate that some of the deuterium gas was absorbed into the walls of the chamber. After about an hour or two a ratio was obtained that was constant to $\pm$ 5 per cent.

3. Measurement of S. In general, the direct beam count was about 15-100 times the scattered beam count and the attenuated direct beam count varied from 40 per cent to 90 per cent of the scattered beam count, each depending on the size and position of the scatterer.

4. Spacial distribution of neutron source. The $N_D - N_B$ count exhibited within a few per cent an inverse square variation with distance from the target chamber.

5. Angular variation of the neutron flux from the D-D reaction. $I(\theta_1)/I(0)$. This quantity was computed from the data published by Hunter and Richards[9].

6. Measurement of nV. the number of scattering nuclei. Each scatterer was weighed on a suitable balance to about one per cent accuracy.

7. Angular variation in sensitivity of the neutron detector. $A(\theta_2)$. This quantity varied by about 25 per cent over the range of θ_2 used in this experiment. The value of $A(\theta_2)$ was measured to within about 5 per cent by rotating the

detector about an axis through the detector perpendicular to the source-detector axis.

8. Measurement of the total cross section . This was measured by using 1 1/8 inch diameter, 1 inch long cylinders of aluminum, iron and lead. The cross sections obtained for E_n = 3.7 Mev were σ(Al) = 2.55 barns, σ(Fe) = 3.51 barns, and σ(Pb) = 7.60 barns each in agreement with the values obtained by Nereson and Darden[10]. The scattering-in corrections were 0.75, 2.4, and 4.3 per cent, respectively, for Al, Fe and Pb, and were obtained from our measurements of the differential cross section.

9. The attenuation factor, F. This factor varied from unity by as much as 14 per cent depending on the size and shape of the scatterer. This quantity is discussed briefly in Appendix I and a graph of its variation is given in Fig. 2.

10. Geometrical Measurements. Measurements of distance were carried out to about ± 1 millimeter. The consequent calculation of mean angles is thus accurate to about one per cent. However, because of the finite size of the detector (1 inch diameter, 5/8 inch height) and the finite size of the scatterers, the detected neutrons are received over a range of angles of about ± 10 degrees in the worst case near θ = 90 degrees.

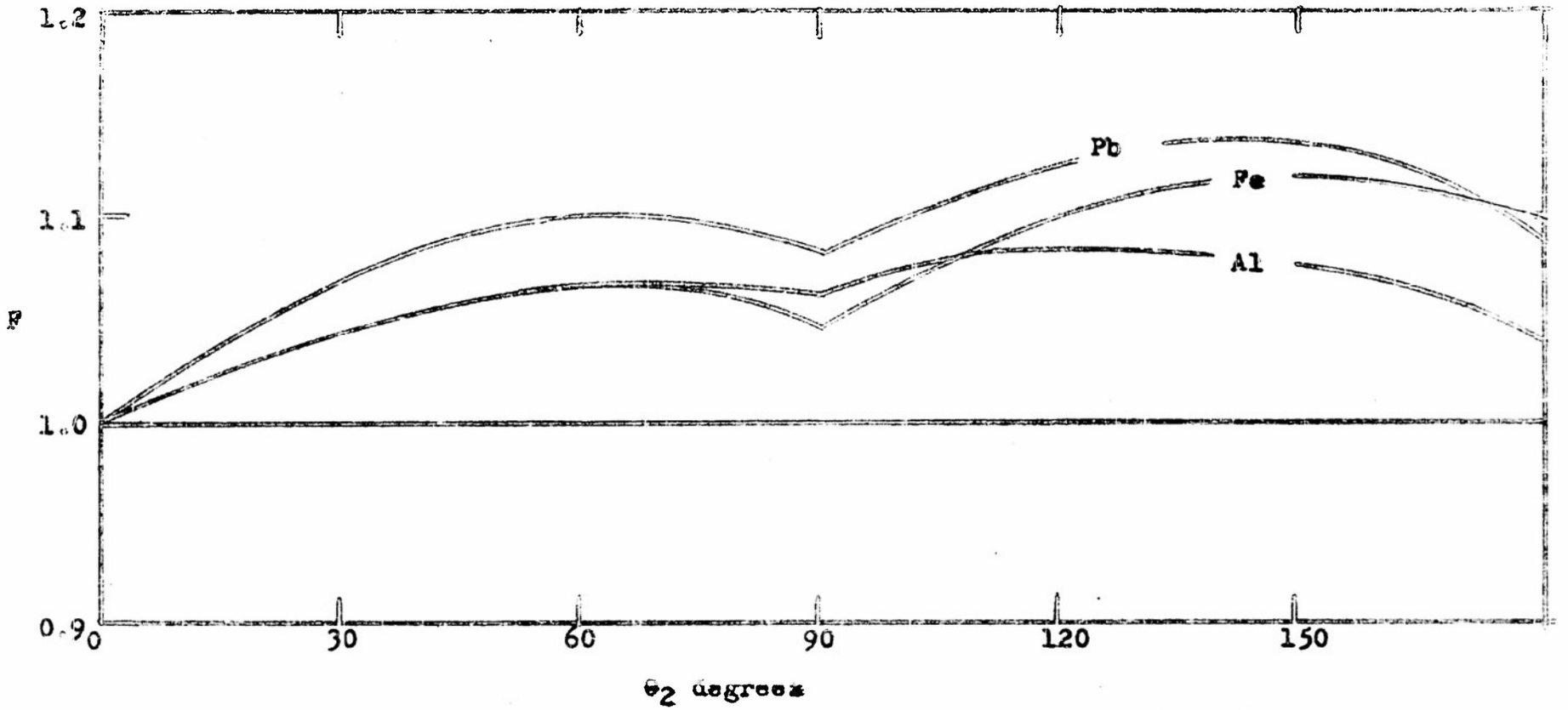


Figure 2 Attenuation factor F. This quantity is defined in Appendix I. F exp(- σnd) essentially measures the attenuation of the direct beam into the scatterer times the attenuation of the scattered beam out of the scatterer. The dimensions are for aluminum, iron and lead: b = 2.54 cm, 2.54 cm and 2.54 cm; d = 3.15 cm, 2.54 cm, and 3.00 cm. The factor F is not shown for the thinner rings used in the experiment.

11. Variation of the sensitivity of the detector with neutron energy. This was measured by comparing our measurement of the angular distribution of neutrons from the D-D reaction with those of Hunter and Richards[9], the discrepancy being ascribed to a non-uniform efficiency in our detector. As may be seen in Fig. 3, the sensitivity only drops off slowly with decreasing neutron energy, decreasing by 40 per cent in 1 Mev. Since it is desired to discriminate against neutrons that have lost more than 200 Kev, this constitutes a serious objection to the use of the Lucite-zinc sulphide detector in this experiment. However, if the inelastically scattered neutrons are more uniformly distributed in angle than the elastically scattered neutrons, then the general features of the differential cross section for elastic scattering will still be evident. In any case the value obtained for $\sigma(\Theta)$ must be such that the total cross section gotten by integrating $\sigma(\Theta)$ is less than the measured total cross section. That this is the case will be shown later.

12. Sensitivity of counter to gamma rays. Neutron detector must not count the gamma rays resulting from the inelastic scattering of neutrons. An ampoule containing 0.1 milligram of radium was placed directly on the Lucite-zinc sulphide detector and gave a negligible counting rate (less than 1 count in 100 seconds).

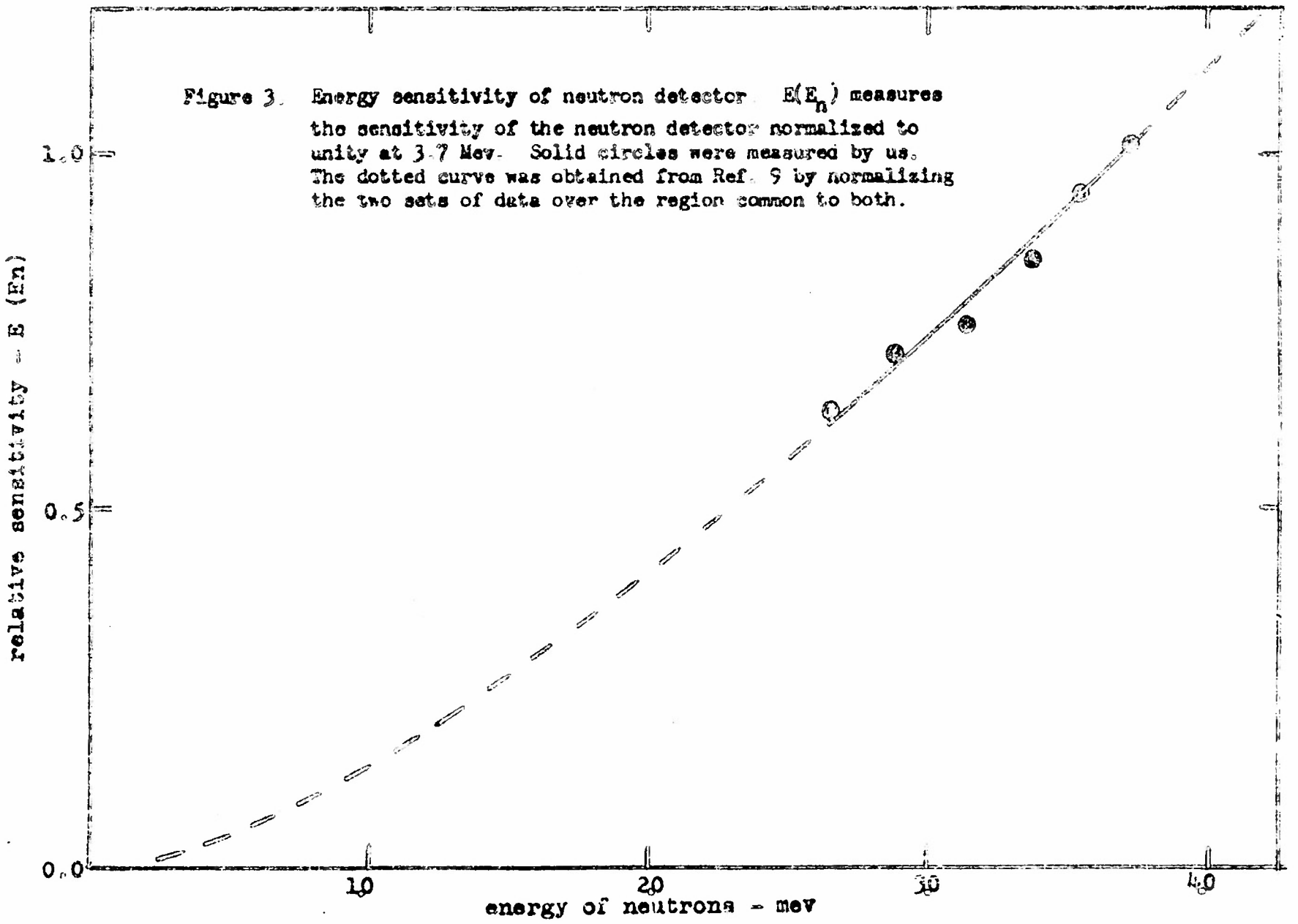


Figure 3. Energy sensitivity of neutron detector $E(E_n)$ measures the sensitivity of the neutron detector normalized to unity at 3.7 Mev. Solid circles were measured by us. The dotted curve was obtained from Ref. 9 by normalizing the two sets of data over the region common to both.

13. Higher order scattering. Appendix II gives an account of the method used in this experiment to allow for double scattering. Essentially it involves placing an upper and lower bound on the possible values of $\bar{\sigma}(\theta)$ for an observed sequence of values of $\bar{\bar{\sigma}}(\theta)$ as a function of the axial thickness of the ring. The first calculation estimates the nature of the variation of $\bar{\bar{\sigma}}(\theta)$ with d/a under the assumption of isotropic scattering. This is given by Eq. (13) which, after comparing with Fig. 4, is seen to reduce to the practical formula

$$\bar{\bar{\sigma}}(\theta) = \bar{\bar{\sigma}}_0(\theta) = .282\, \bar{\bar{\sigma}}'(\theta) \qquad (2)$$

where $\bar{\bar{\sigma}}_0(\theta)$ is the intercept at d/a = 0 of the linear portion of the curve and $\bar{\bar{\sigma}}'(\theta)$ is the slope of the $\bar{\bar{\sigma}}(\theta)$ versus d/a curve in the linear portion.

The second calculation states that if the angular distribution is peaked strongly forward, then one expects that the double scattering contribution will cause $\bar{\bar{\sigma}}(\theta)$ to be a linear function of d or d/a. In this case $\bar{\bar{\sigma}}_0(\theta)$ is the true differential scattering cross section. Both of these extrapolations are presented on the graphs.

If triple scattering is present, then $\bar{\bar{\sigma}}(\theta)$ should be a quadratic function of d or d/a for the case in which there is a strong forward peaking of the scattering. Figure 5 for

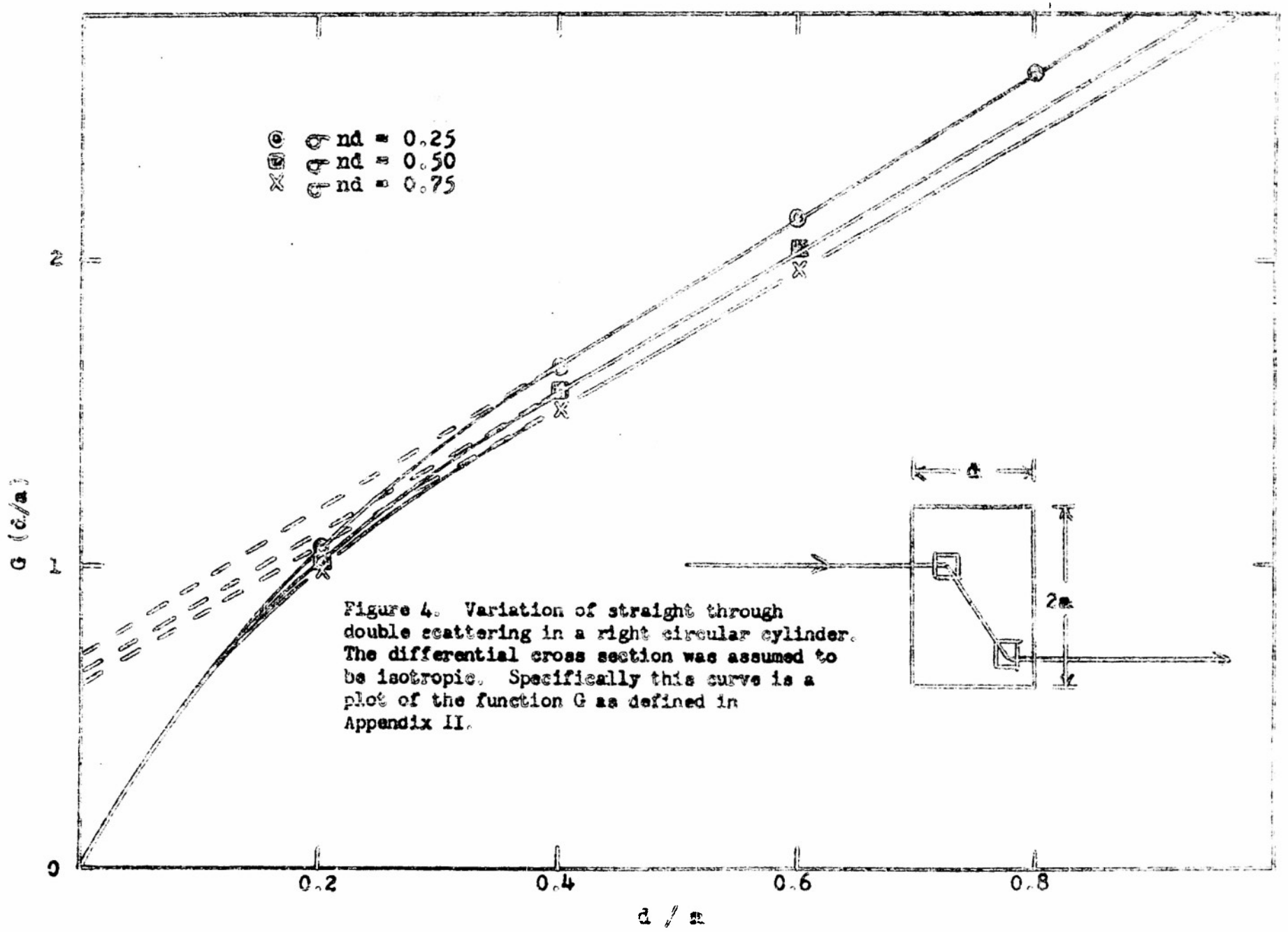


Figure 4. Variation of straight through double scattering in a right circular cylinder. The differential cross section was assumed to be isotropic. Specifically this curve is a plot of the function G as defined in Appendix II.

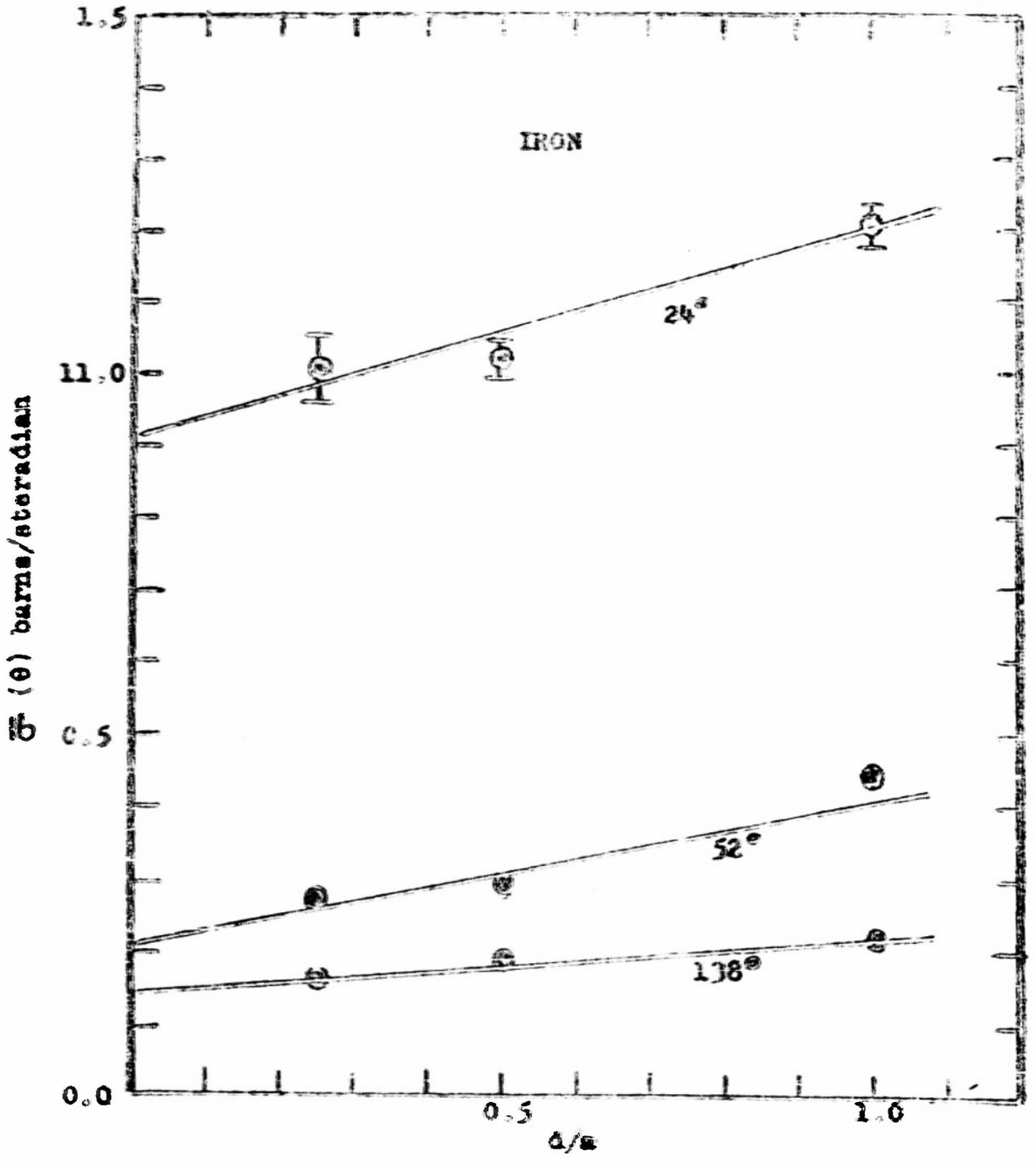


FIGURE 5.

Apparent differential cross section of iron versus thickness of ring scatterer for three different scattering angles. The thickness is measured relative to a quantity a, which we have taken to be equal to the radial width of the ring in order to establish a correspondence between the ring scatterer and the right circular cylinder scatterer.

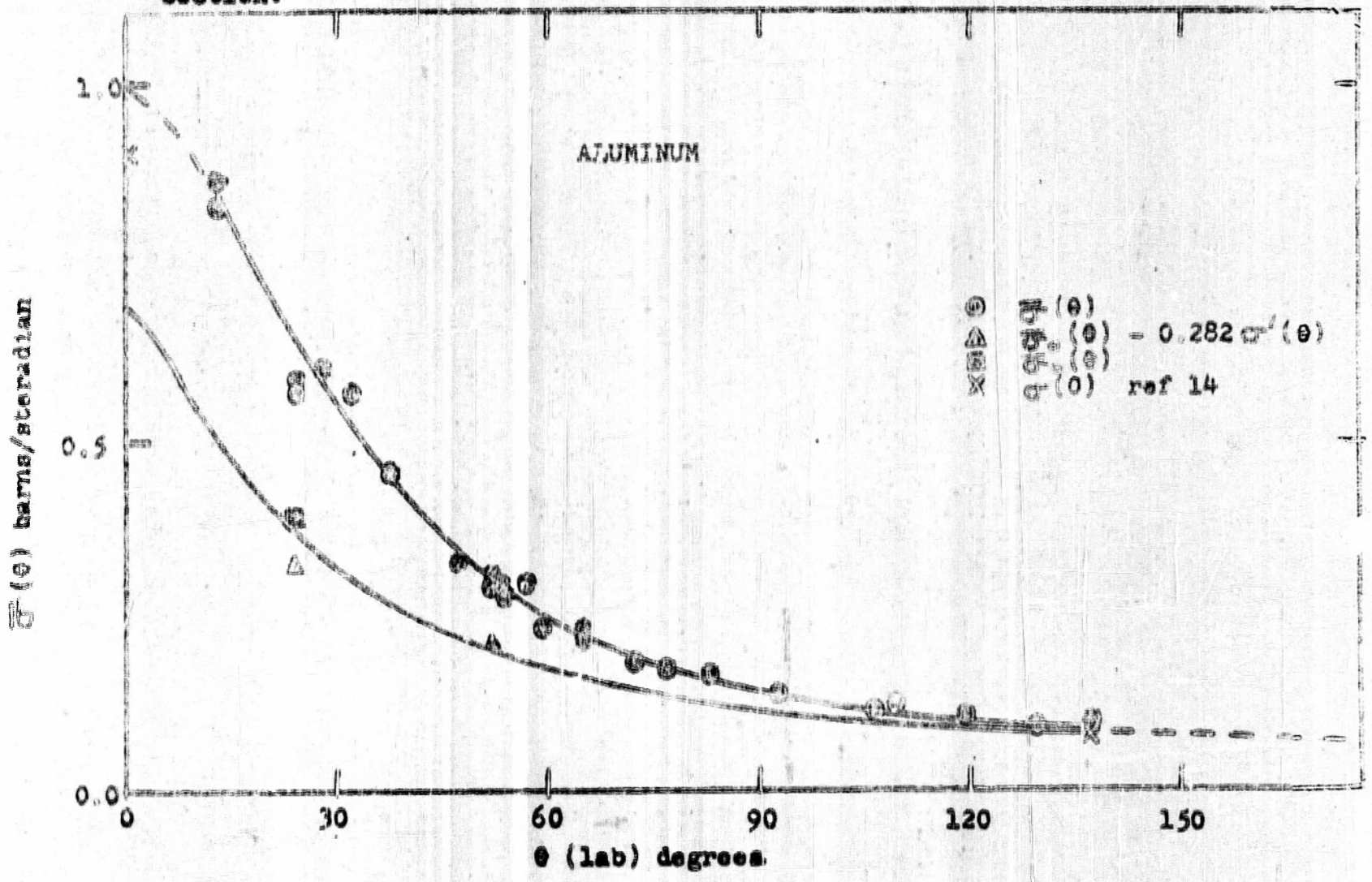
the case of iron shows some indication of the presence of triple scattering, however, the experimental uncertainty is too large to consider this definite. No attempt was made to remove the triple scattering contributions.

A typical run of data was made as follows: (1) direct beam; (2) attenuated beam; (3) scattered beam from one of the rings for all values of the scattering angle; (4) attenuated beam; (5) direct beam. If the two values of the direct beam determination differed by more than 10 per cent, the data were discarded.

DATA

Figures 6, 7, and 8 show the experimental points of the apparent differential cross section for 3.7 Mev neutrons incident on aluminum, iron, and lead as calculated from Eq. (1). Only a limited number of angles were chosen in order to determine the effects of higher order scattering. Figure 5 shows the variation of $\bar{\sigma}(\theta)$ as a function of the ring thickness for the case of iron. In the same manner, similar curves were obtained for lead and aluminum. The extrapolations both for isotropic scattering and forward peaked scattering are shown in Figures 6, 7, and 8 where a curve is drawn through the points thought to be the appropriate differential cross section, $\sigma(\theta)$ for each case. The total cross sections corresponding to $\sigma(\theta)$ have been calculated and are presented together with the measured total cross section in Table I. It will be noted that the integrated differential

FIGURE 6. Angular distribution of 3.7 Mev neutrons scattered from aluminum. $\overline{\sigma}(\theta)$ is apparent differential cross section as defined in the text. $\overline{\sigma}_0(\theta)$ is the differential cross section using a linear extrapolation to remove higher order scatters. $\overline{\sigma}_0(\theta) - .282\,\sigma'(\theta)$ is the differential cross section in which the higher order scatters are removed using the isotropic scattering assumption. $\sigma(0)$ is taken from the Final Report of the Fast Neutron Data Project, NYO-636, in which the nuclear radii were found from our measured values of the total cross section.



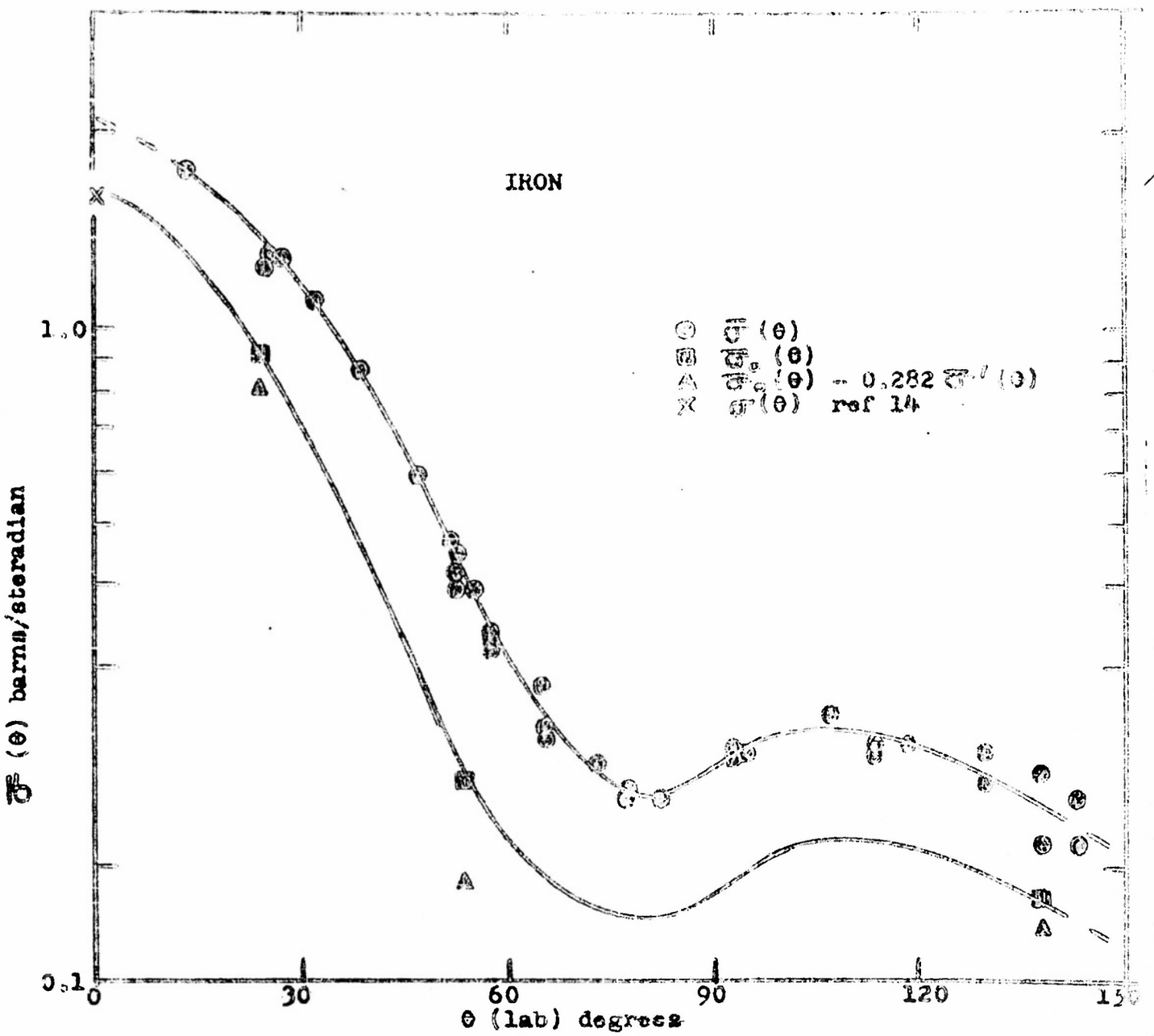


FIGURE 7. Angular distribution of 3.7 Mev neutrons scattered from iron. Other remarks in caption of Fig. 6 apply here also.

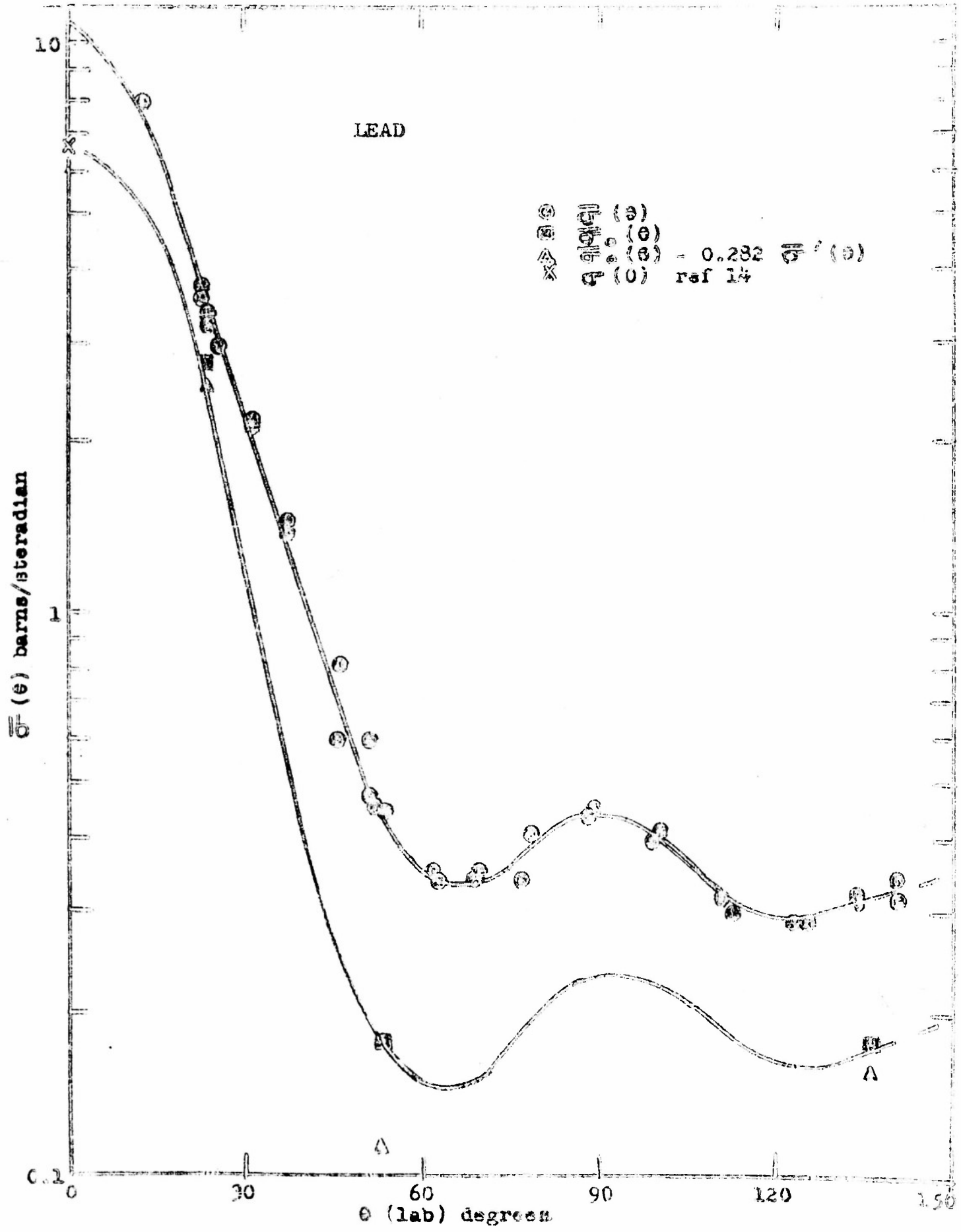


FIGURE 8. Angular distribution of 3.7 Mev neutrons scattered from lead. Other remarks in caption of Fig. 5 apply here also.

TABLE I.

Element	σ_{total} (measured) in barns		$\int \sigma(\Theta) d\Omega_\Theta$ (barns)	σ_I
	This Expt.	Neresen and Darden		
Aluminum	2.55	2.50	1.73	0.82
Iron	3.51	3.55	2.94	0.57
Lead	7.60	7.70	5.17	2.43

Total cross sections. The value of $\int \sigma(\Theta) d\Omega_\Theta$ subject to the reservations in the text is the total elastic cross section.

cross sections in each case is less than the measured total cross section. The total inelastic cross section cannot be obtained as the difference between the two former cross sections since the measurement of the differential cross section did not discriminate adequately against the inelastically scattered neutrons. However, this subtraction can be carried out approximately if one accepts the following rather crude estimate of the inelastic contribution to $\sigma(\epsilon)$: There are seven levels in aluminum that can be excited by 3.7 Mev neutrons[11]. If we assume that the maximum total inelastic cross section is about 50 per cent of the total cross section, and that the seven levels in aluminum are equally excited, then the inelastic neutrons contribute less than 15 per cent to the total cross sections corresponding to $\sigma(\epsilon)$. Similar arguments using the known levels in iron and lead show that the inelastic contribution in these elements is less than 20 per cent.

APPENDIX I. SCATTERING OF NEUTRONS THROUGH RING SCATTERER BY SINGLE SCATTERING.

In general, the scattering rationis made up of a sum of terms $S = S_1 + S_2 + \cdots\cdots$ where S_1, S_2, etc. refer to the neutrons scattered into the detector by single scattering, double scattering, etc. For the single scattering case (Figs. 1 and 9a) we have

$$S_1 = \int_V \left[I(\theta_1)/I(0) \right] \cdot \left[R_o^2/R_1^2 R_2^2 \right] \cdot \sigma(\theta) n \exp\left[-\sigma n(r_1 + r_2) \right] \cdot A(\theta_2) E(E_n) dV \quad (3)$$

The geometry is such that only small errors will be introduced if Eq. (3) is replaced by

$$S_1 = \left[I(\theta_1)/I(0) \right] \cdot \left[R_o^2/R_1^2 R_2^2 \right] \cdot \sigma(\theta) n A(\theta_2) E(E_n) V F(\theta_2) \exp(-\sigma n d) \quad (4)$$

where

$$F = V^{-1} \int_V \exp\left[-\sigma n(r_1 + r_2 - d) \right] dV \quad (5)$$

and the mean angles and distances are used for θ_1, θ_2, R_o, R_1, and R_2. For a fixed size of ring scatterer, the quantity F is a function of θ_1 and θ_2. However, since θ_1 only varies from

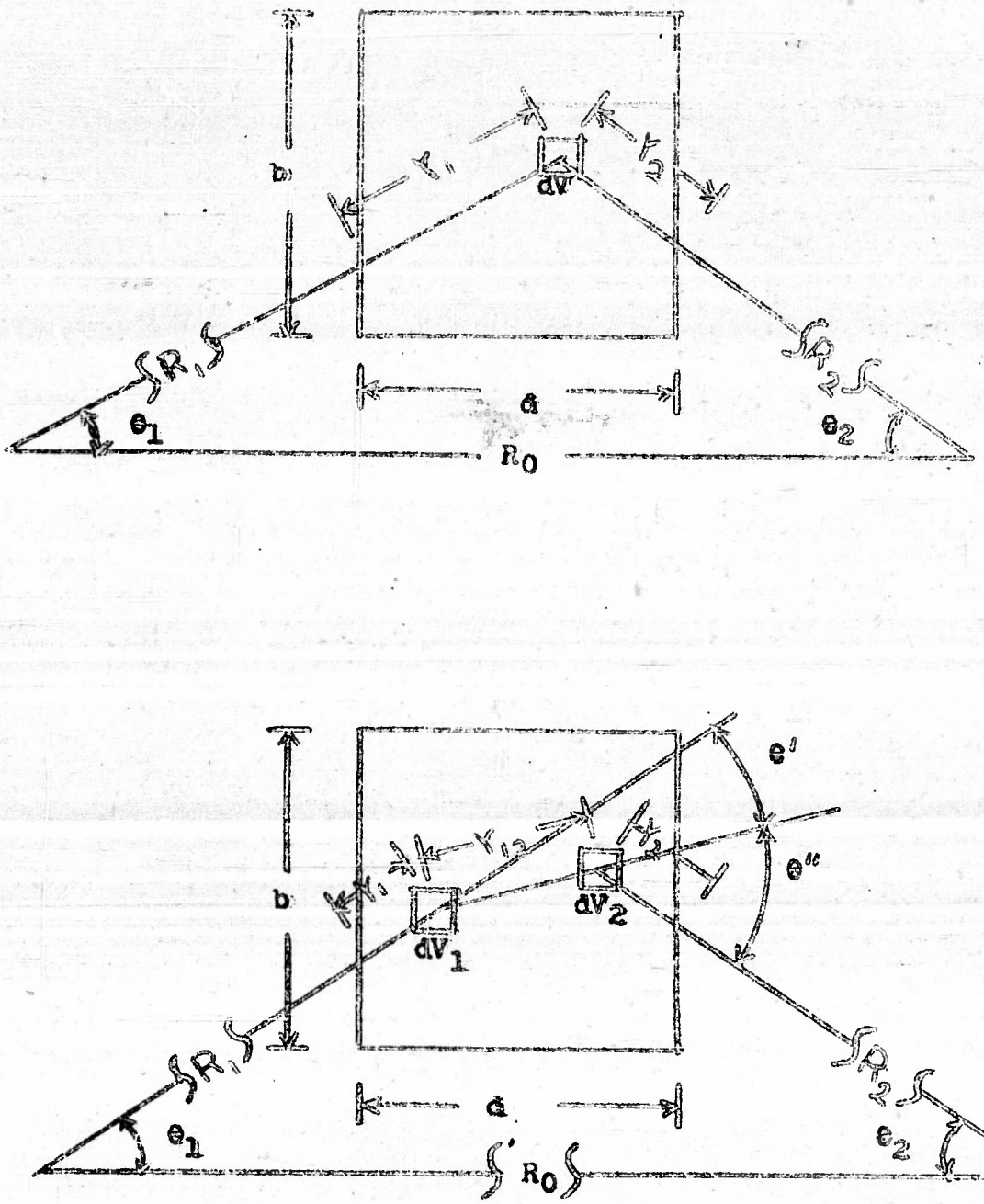


FIGURE 9. DETAIL OF SCATTERING GEOMETRY: (a) single scattering; (b) double scattering.

about 5° to 15°, little error and much simplification is introduced by computing F for $\theta_1 = 0$. For the rectangular cross section of our scatterer, the integral F may be evaluated in terms of elementary functions. The results are displayed in Figure 2.

If only single scattering were present, the quantity S_1 could be replaced by the measured data S and the differential cross section $\sigma(\theta)$ could be calculated. In any case the reduction of the data is facilitated by defining an effective single scattering differential cross section $\bar{\sigma}(\theta)$ such that

$$S = \left[I(\theta_1)/I(0)\right] \cdot \left[R_o^2/R_1^2 R_2^2\right] \cdot \bar{\sigma}(\theta) n A(\theta_2) E(E_n) VF(\theta_2) \exp(-\sigma n d) \qquad (5)$$

APPENDIX II. SCATTERING OF NEUTRONS THROUGH RING SCATTERER BY DOUBLE SCATTERING.

Using the quantities defined in Figures 1 and 9b, the double scattering ratio is seen to be

$$S_2 = \iint_{V_1 V_2} \left[I(\theta_1)/I(0) \right] \cdot \left[R_o^2 / R_1^2 r_{12}^2 R_2^2 \right] \cdot \sigma(\theta_1) \sigma(\theta_{11}) n^2 \exp \left[-\sigma n (r_1 + r_{12} + r_2) \right] A(\theta_2) E(E_n) dV_1 dV_2 \qquad (7)$$

An analytical solution of this integral seems quite involved, if not hopeless, for the geometry of the ring scatterer. In order to get some feeling for the manner in which the double scattering varies with the thickness of the ring, we have chosen to calculate the straight through double scattering from a right circular cylinder assuming isotropic scattering ($\sigma(\theta') = \text{constant}$). In order to simplify this case as much as possible, let the neutron beam, incident on the circular end of the cylinder, be parallel to the cylinder axis, and let the detector sensitivities $A(\theta_2) = E(E_n) = 1$. Also let $r_1 + r_2$ be replaced by an approximate mean value d, the thickness of the cylinder. Equation (7) then reduces to

$$S_2 = \left[\sigma^2 n^2 / 16 \pi^2 R_2^2 \right] \cdot \exp(-\sigma n d) \iint_{V_1 V_2} r_{12}^{-2} \exp(-\sigma n r_{12}) dV_1 dV_2 \qquad (8)$$

If the exponential function is expanded and the first three terms retained, S_2 reduces to the following:

$$S_2 = \left[\sigma^2 n^2 a^4 / 16 R_2^2\right] \cdot \exp(-\sigma n d) \cdot (X - \sigma n d Y + \frac{1}{2}\sigma^2 n^2 a^2 \xi) \qquad (9)$$

where

$$X = -2d^2/a^2 \cdot \ln d/a + 2d^2/a^2 \sin h^{-1} d/2a$$
$$+ \cos h^{-1}(1 + d^2/2a^2) + 2d^2/a^2 - d^4/4a^4 \qquad (10)$$
$$-(1-d^2/2a^2) \cdot \left[(1 + d^2/2a^2)^2 - 1\right]^{1/2}$$

$$Y = 8 \int_0^\infty \left[xd/2a - \exp(-xd/2a) \sin h(xd/2a) \right] J_1(x) \sin x \cdot dx/x^4 \qquad (11)$$

and

$$\frac{1}{2}\xi = d^2/a^2 \qquad (12)$$

The integration of x was facilitated by the use of a theorem in vector analysis[12]. The integration of Y can be effected by recognising that the integral corresponds to the electrostatic energy of a uniform volume distribution of charge[13].

If the single scattering ratio $\bar{\sigma}$, is calculated for the right circular cylinder under the same assumptions, then the effective single scattering cross section is given by

$$\bar{\sigma}/\bar{\sigma} = 1 + (\sigma_T a/4)\, G(d/a) \qquad (13)$$

where

$$G(d/a) = (a/d)(X - \sigma_T a Y + \tfrac{1}{2}\sigma_T^2 a^2 Z) \qquad (14)$$

and is written only as a function of d/a since it varies but slowly with $\sigma_T a$ as may be seen in Figure 4. By considering this mean curve to apply to all cases of interest the function G becomes a function of d/a only.

To apply the calculations of the right circular cylinder to the case of the ring scatterer, we assume that except for multiplying angular functions, the geometrical variation of the single and double scattering ratios is given correctly after associating the radial thickness of the ring scatterer, t, with the radius of the cylinder, a.

If, instead of isotropic scattering, one takes the other extreme of an angular distribution peaked strongly in the forward direction, one finds that the single scattering ratio in the ring scattering varies as d exp $(-\sigma_T d)$ whereas the double scattering ratio varies as d^2 exp $(-\sigma_T d)$; thus leading

to a linear variation of the apparent single scattering cross section with the thickness of the ring.

REFERENCES

1. Kikuchi, Aoki and Wakatuki, Proc. Phys. Math. Soc. Japan 21, 410 (1939); Wakatuki and Kikuchi, Proc. Phys. Math. Soc. Japan 21, 656 (1939); Wakatuki, Proc. Phys. Math. Soc. Japan 22, 430 (1940).

2. Amaldi, Bocciarelli, Cacciapuoti, and Trabacchi, International Conference on Fundamental Particles and Low Temperature, Vol. 1, The Physical Society, London (1947).

3. Remund and Ricamo, Helv. Phys. Acta. 25, 441 (1952).

4. Walt and Barschall, Phys. Rev. 90, 714 (1953).

5. Feshbach, Porter and Weisskopf, Phys. Rev. 90, 166 (1953).

6. H. H. Barschall, Phys. Rev. 86, 431 (1952); Miller, Adair, Bockelman, and Darden, Phys. Rev. 88, 83 (1952).

7. Feshbach, Porter and Weisskopf, Bull. Amer. Phys. Soc. 28, No. 3, 29 (1953).

8. W. F. Hornyak, Rev. Sci. Instru. 23, 264 (1952).

9. The authors are indebted to Dr. Hornyak for supplying them with a Lucite-zinc sulphide molded button.

9. Hunter and Richards, Phys. Rev. 76, 1445 (1949).

10. Meresen and Darden, Phys. Rev. 89, 775 (1953).

11. Nuclear Data, Natl. Bureau of Standards Circular 499 (1950).

12. H. B. Phillips, Vector Analysis (John Wiley and Sons, Inc., New York, 1933). See Chapter III.

13. W. R. Smythe, Static and Dynamic Electricity (McGraw-Hill Book Co., Inc., New York, 1939). See Chapter V.

14. Final Report of the Fast Neutron Data Project, NYO-636.

SEMI ANNUAL REPORT

of the Work of the

BARTOL RESEARCH FOUNDATION

OF THE FRANKLIN INSTITUTE

(July 1, 1953 -- December 31, 1953)

Performed Under Contract Nonr 436(00)

with the

OFFICE OF NAVAL RESEARCH

TABLE OF CONTENTS

I. Inelastic Scattering.

II. Total Cross Sections; Angular Distribution of Elastic Scattering; Inelastic Cross Sections.

III. Low Voltage Accelerator.

IV. Abstract of Study of the Reactions $Ba^{137}(n,n')^{*}\ Ba^{137}$ and $Hg^{199}(n,n')^{*}\ Hg^{199}$.

V. Recent Publications.

VI. Distribution List.

PERSONNEL

Physicists: (Part-time or full-time)

D. W. Kent

C. E. Mandeville

F. R. Metzger

M. A. Rothman

S. C. Snowdon

C. P. Swann *

W. D. Whitehead **

Technicians: (Half-time)

R. W. Gunnett

---

* Mr. Swann has participated in this contract to the extent of coauthorship of the measurements described in Section IV. However, no part of his salary is charged to the contract.

** Terminated.

Report submitted: February 15, 1954

C. E. Mandeville

C. E. Mandeville
Assistant Director

I. INELASTIC SCATTERING.

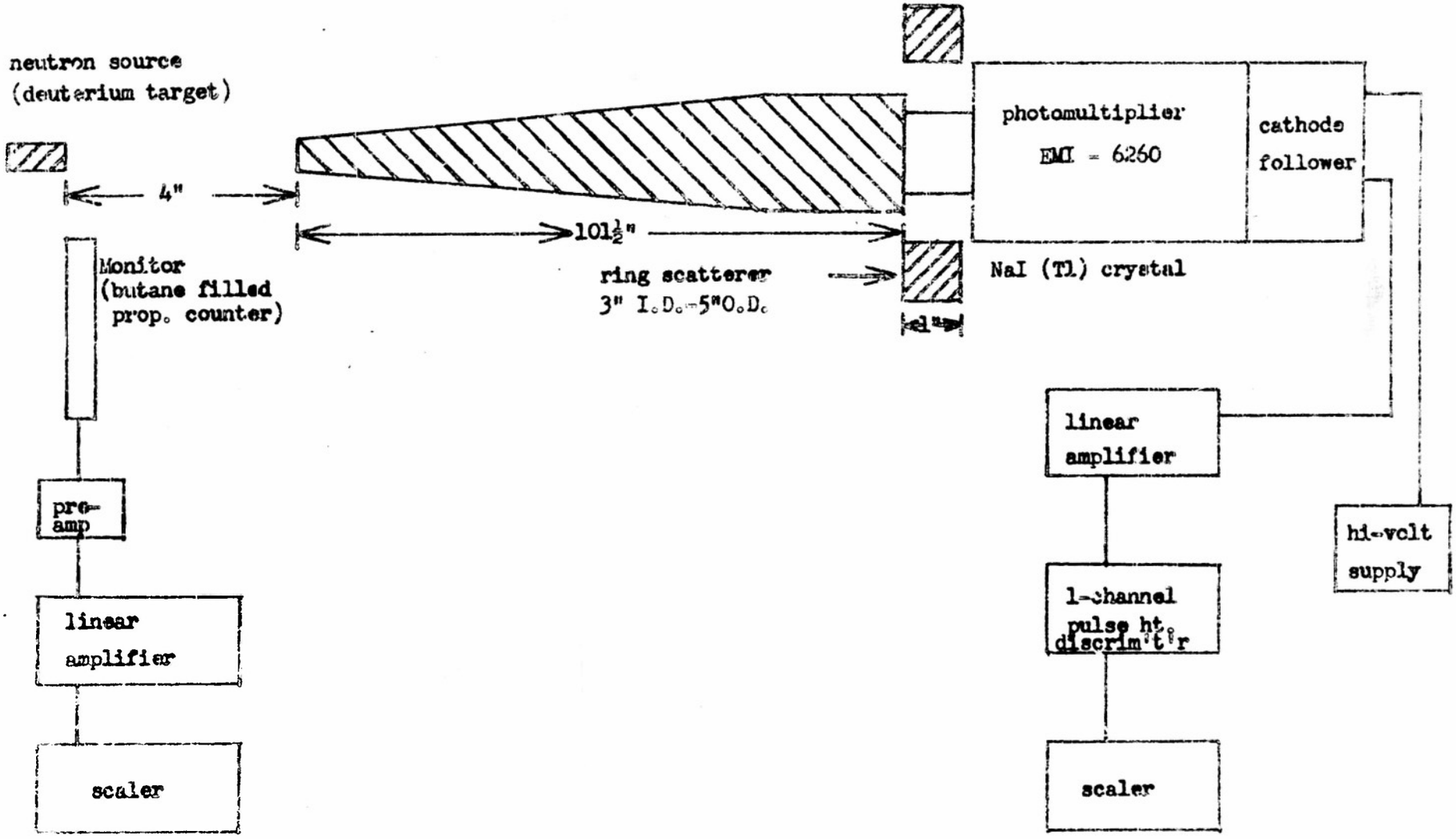
A. Introduction.

In the previous semi-annual report incorrectly dated February 1, 1953 - June 30, 1953 (it should have been designated as January 1, 1953 - June 30, 1953) experiments falling in two different categories were described. The first group of measurements concerned themselves for the most part with a study of gamma rays excited in the nuclei of various elements by the inelastic scattering of neutrons of energy about 3.9 Mev. The remainder of the report dealt with elastic scattering of neutrons of about the same energy in aluminum, iron, and lead. From the elastic scattering data certain aspects of the inelastic scattering process are inferred.

In the six months following the above mentioned report, additional results dealing with the previously discussed measurements have been obtained. The smaller Bartol Van de Graaff generator has served as the neutron source throughout the course of this work.

B. Gamma Rays Excited by Inelastic Scattering of 3.8-Mev Neutrons in Nickel, Copper, Zirconium, and Wolfram.

The geometry employed for detection of the gamma rays is shown in Figure 1. All of the measurements obtained to



GEOMETRY AND CIRCUITRY OF SCINTILLATION COUNTING EXPERIMENT

Figure 1.

date have been taken by means of single channel pulse-height analysis. A twenty-channel multi-channel discriminator will be available in the future to shorten the time to acquire such data.

As in the case of the previous semi-annual report, the background was taken to be that indicated by a carbon scatterer. The background is assumed to arise from neutrons having been elastically scattered into the sodium iodide and there captured to give rise to capture gamma rays which are in turn counted in the crystal. The carbon run is considered to be a "blank", because the first excited state of C^{12} occurs at 4.5 Mev above the ground state so that the neutrons available are not sufficiently energetic to give rise to inelastic scattering. An additional source of background is, of course, the radioactivity of I^{128} (T = 25 min).

A nickel scatterer was constructed of nickel "shot" poured into a thin-walled "doughnut" of tin. When irradiated by 3.8 Mev neutrons, the pulse-height distribution of Figure 2 was obtained. Shown in Figure 2 is the background curve taken with a carbon scatterer present along with the curve for the nickel scatterer. The difference curve is presented in Figure 3 where a photopeak at about 1.36 Mev is clearly present. Although sufficient energy is present for excitation of the 2.52 Mev level in Ni^{60} so that the 1.15 Mev gamma ray might also appear, it is thought that insufficient angular

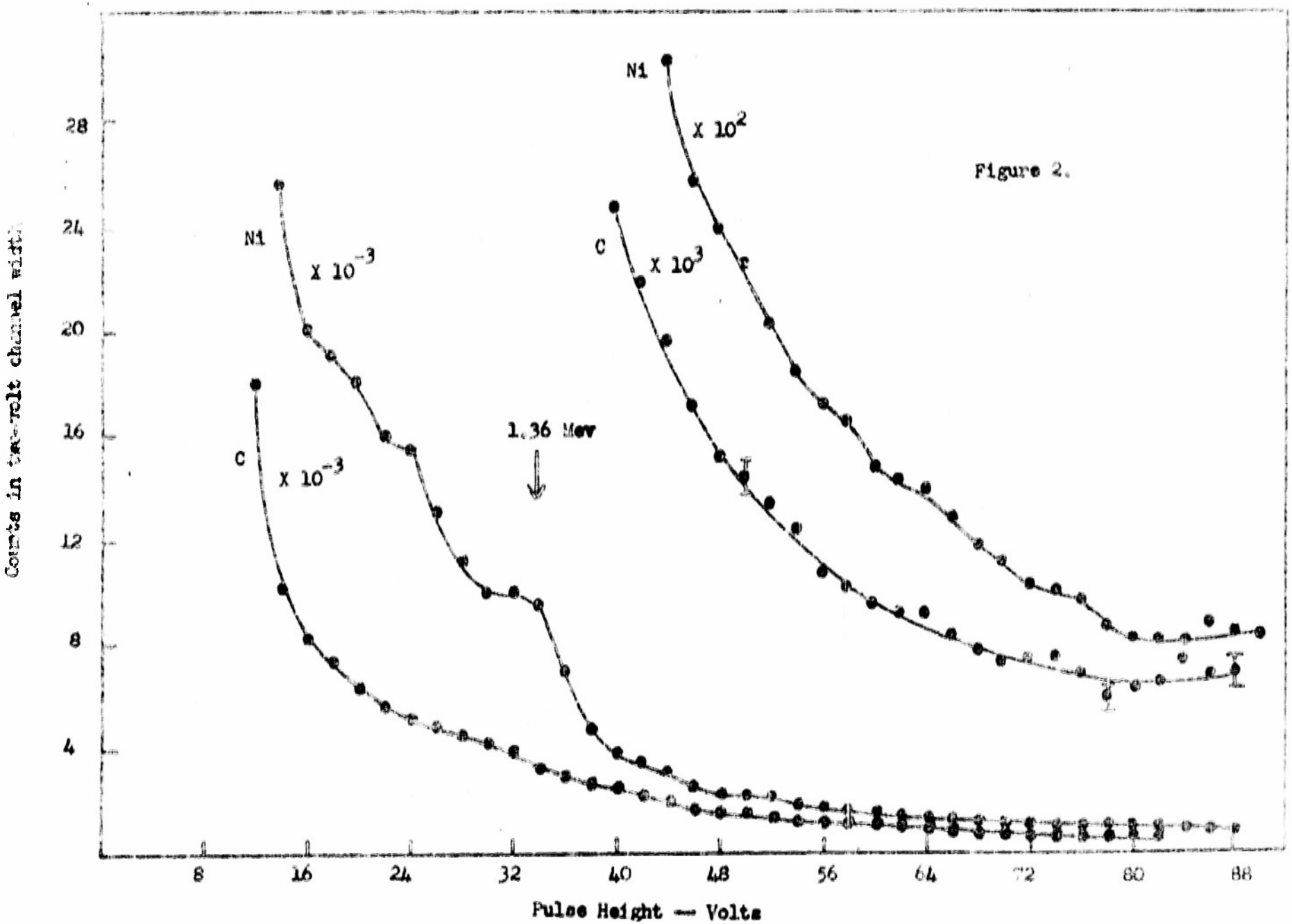
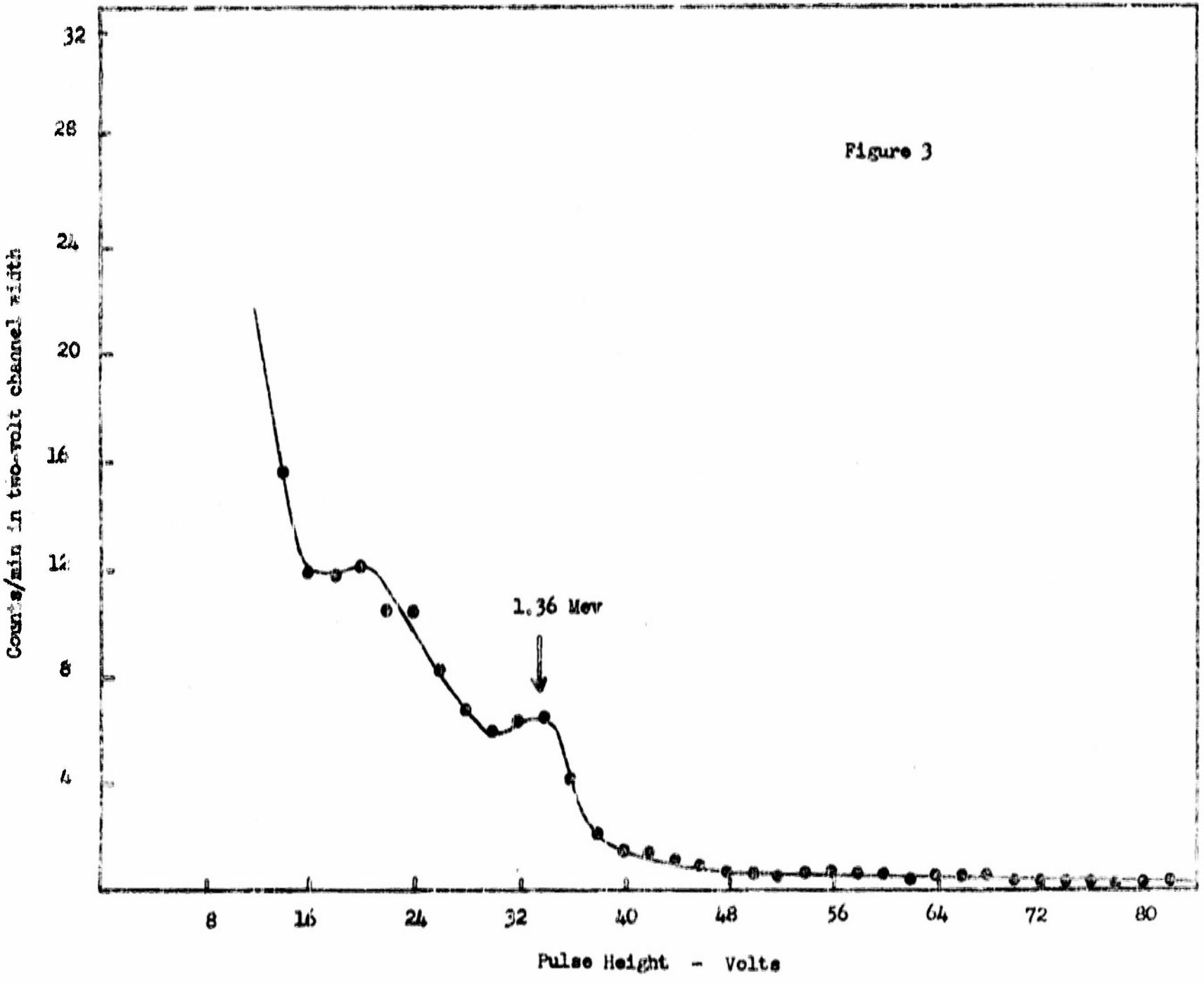

Counts in one-volt channel width
28
24
20
16
12
8
4
Ni
X 10^-3
C
X 10^-3
1.36 Mev
Ni
X 10^-2
C
X 10^-3
8
16
24
32
40
48
56
64
72
80
88
Pulse Height — Volts

Figure 2.

Figure 3


Counts/min in two-volt channel width
32
28
24
20
16
12
8
4
1.36 Mev
8
16
24
32
40
48
56
64
72
80
Pulse Height - Volts

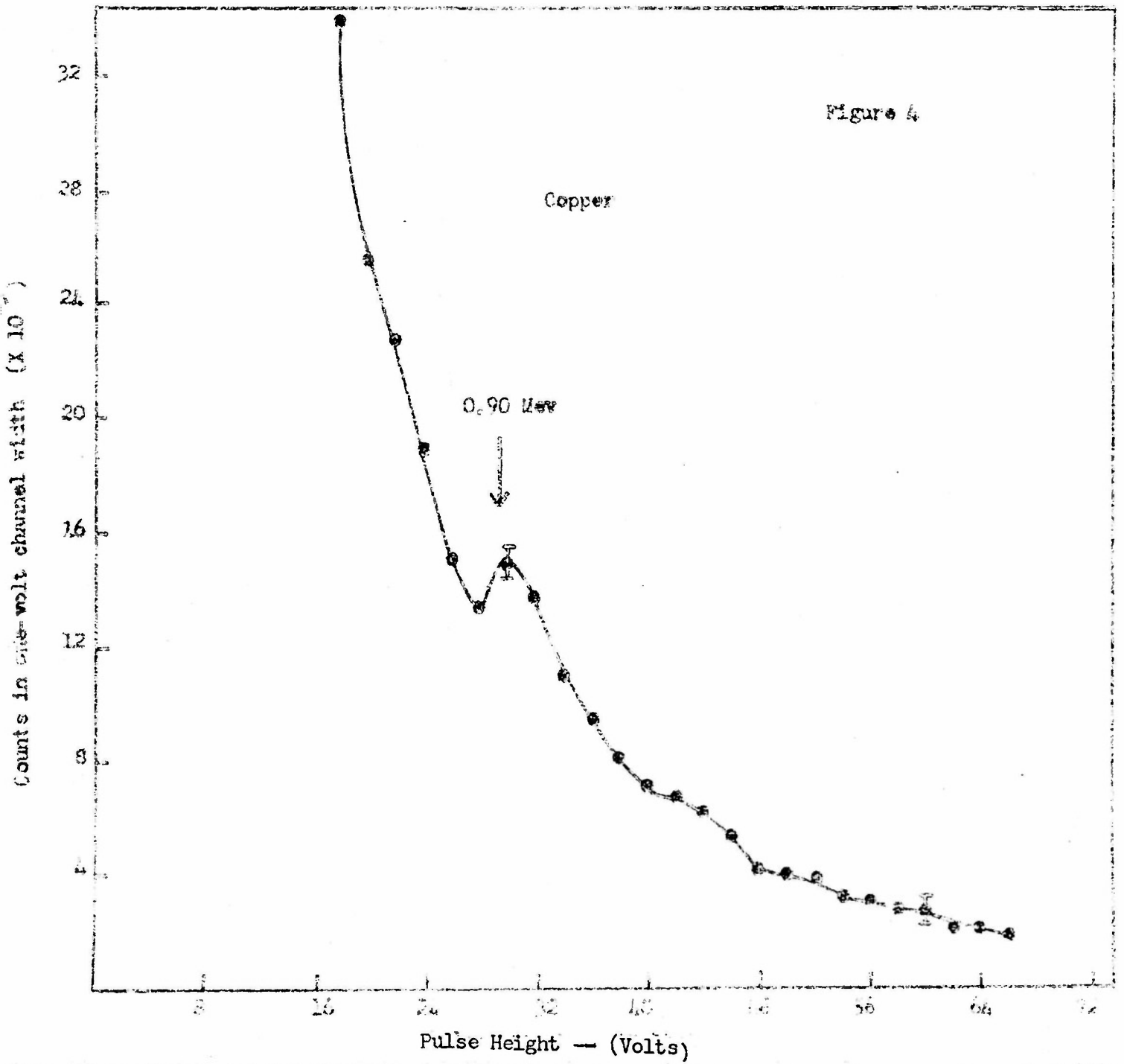
momentum is present in the incident neutron beam to excite the level in any appreciable intensity. The study of the radioactive decay of Co^{60} has shown that the spins of the levels of Ni^{60} follow the pattern of the even-even nuclei, 4 - 2 - 0, so that four units of angular momentum are necessary for excitation of the 2.52 Mev level. The 1.33 Mev gamma ray is of course the second of two gamma rays emitted in cascade in the decay of Co^{60}, the first having an energy of 1.16 Mev. From the shape of the difference curve of Figure 3, it is clear that a gamma ray at about 0.9 Mev may also be present.

The pulse-height distribution (background subtracted) resulting from the scattering of 3.8 Mev neutrons by copper is shown in Figure 4. These data are interpreted as giving evidence of the presence of a gamma ray of energy 0.9 Mev, plus unresolved gamma rays of higher energy.

A zirconium scatterer was irradiated by 3.8 Mev neutrons. The resulting pulse-height distribution is shown in Figure 5. The gamma rays present, have energies of 0.9, 2.2, and possibly 1.15 Mev. A similar spectrum for tungsten is shown in in Figure 6. The resolution is not sufficient to isolate the peaks, but gamma rays appear to be present at about 0.85 and 2.3 Mev.

It is to be noted that the pulse-height distribution curves for Zr was taken with a one-volt channel rather than

Figure 4


Copper
0.90 Mev
32
28
24
20
16
12
8
Counts in one-volt channel width (x 10²)
Pulse Height — (Volts)

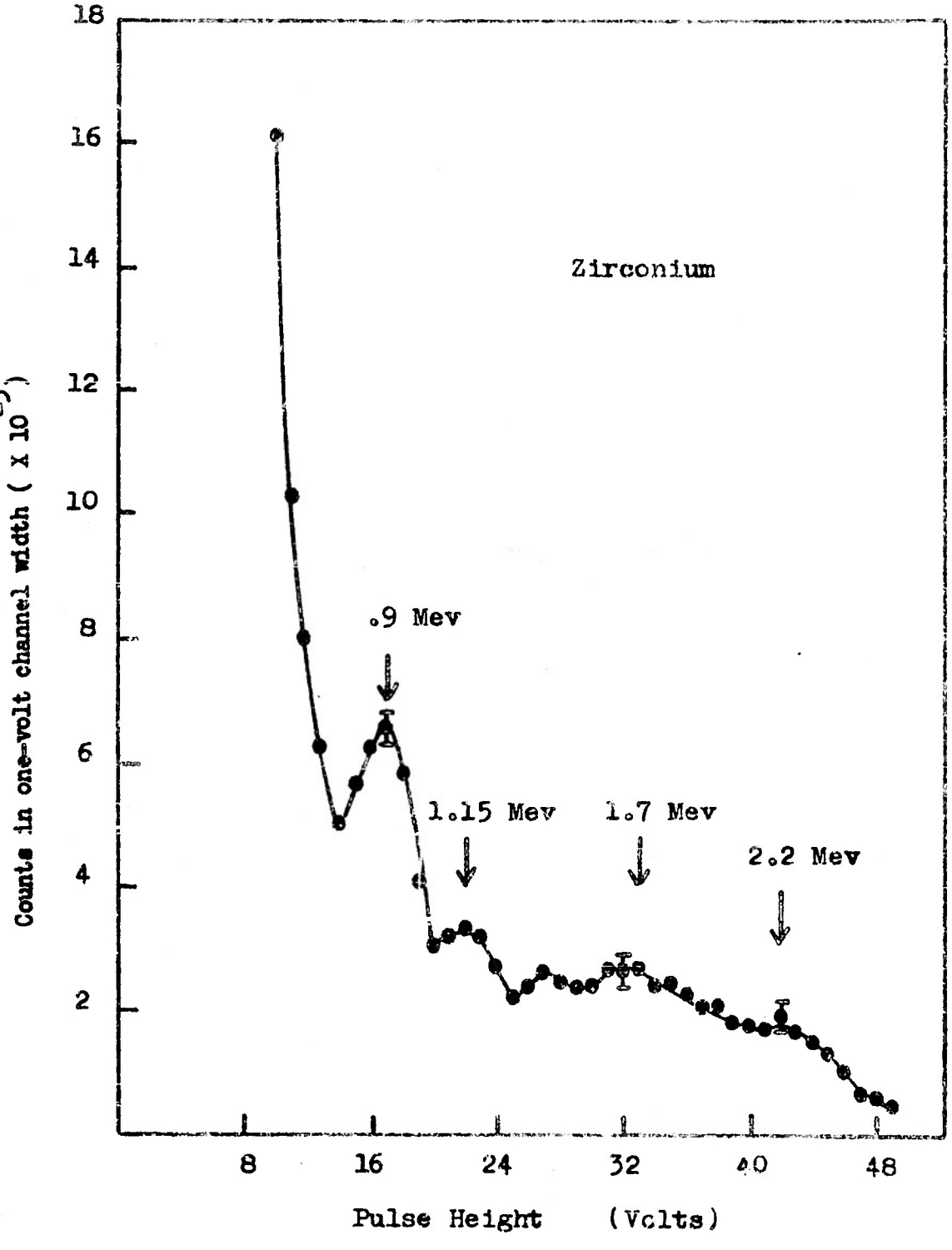
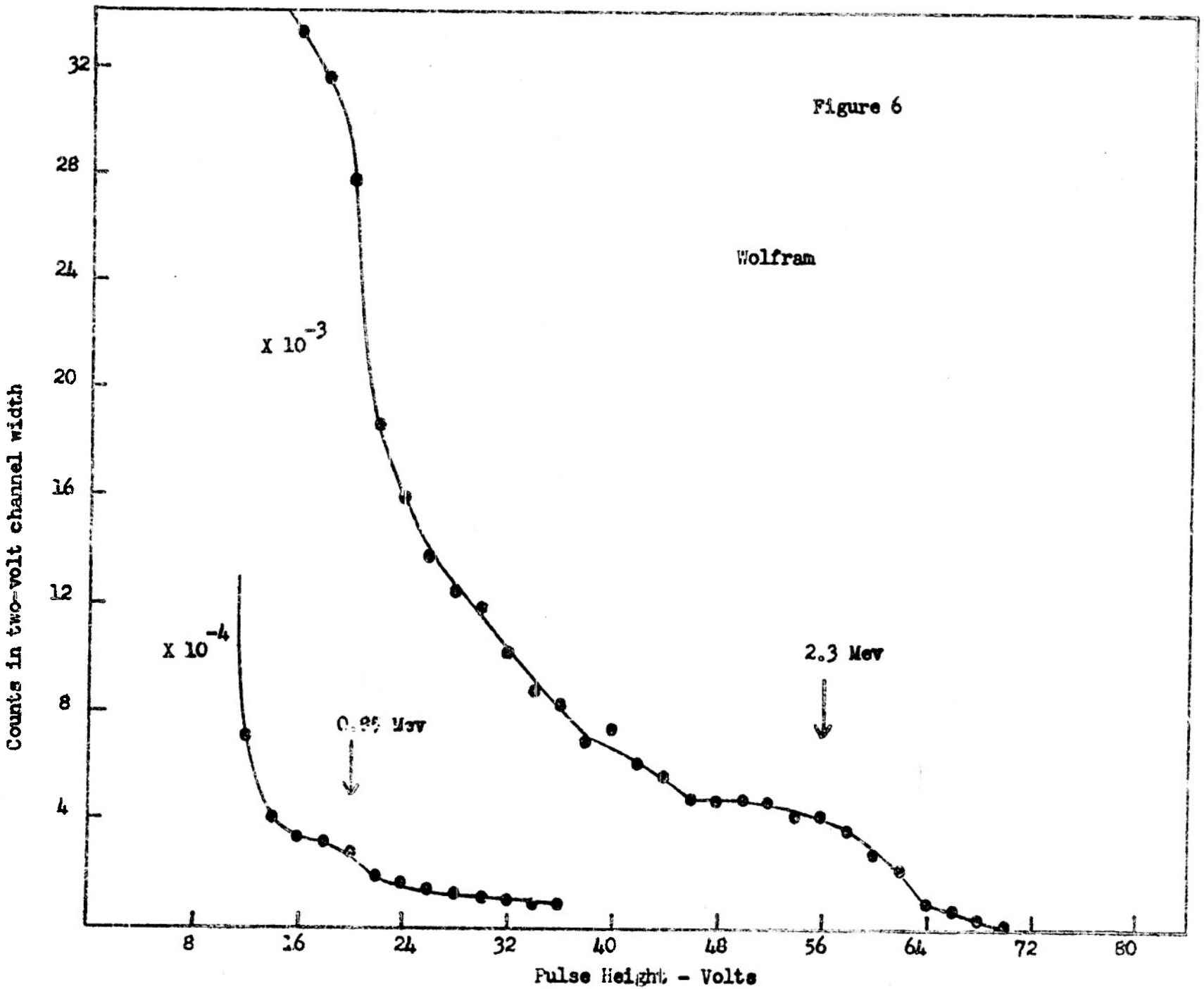

Zirconium
.9 Mev
1.15 Mev
1.7 Mev
2.2 Mev
Counts in one-volt channel width (x 10^{-3})
Pulse Height (Volts)
18
16
14
12
10
8
6
4
2
8
16
24
32
40
48

Figure 5


Figure 6
Wolfram
X 10^-3
X 10^-4
2.3 Mev
0.85 Mev
Counts in two-volt channel width
Pulse Height - Volts
4
8
12
16
20
24
28
32
8
16
24
32
40
48
56
64
72
80

with the usual two-volt width employed in the measurements of the previous report. It was found that the use of the one-volt channel resulted in better energy resolution than was previously obtained. Using the one-volt channel, the pulse-height distribution of the gamma rays of Na^{24} was observed as shown in Figure 7. This spectrum shows considerably better resolution than that obtained in the case of the same spectrum obtained with a two-volt channel width and shown in Figure 10 of the previous report. It is naturally to be expected that the one-volt channel give the better resolution; however, the actual experimental observations show that it is enough better to justify the longer time of observation necessitated by the smaller channel widths.

Figure 7

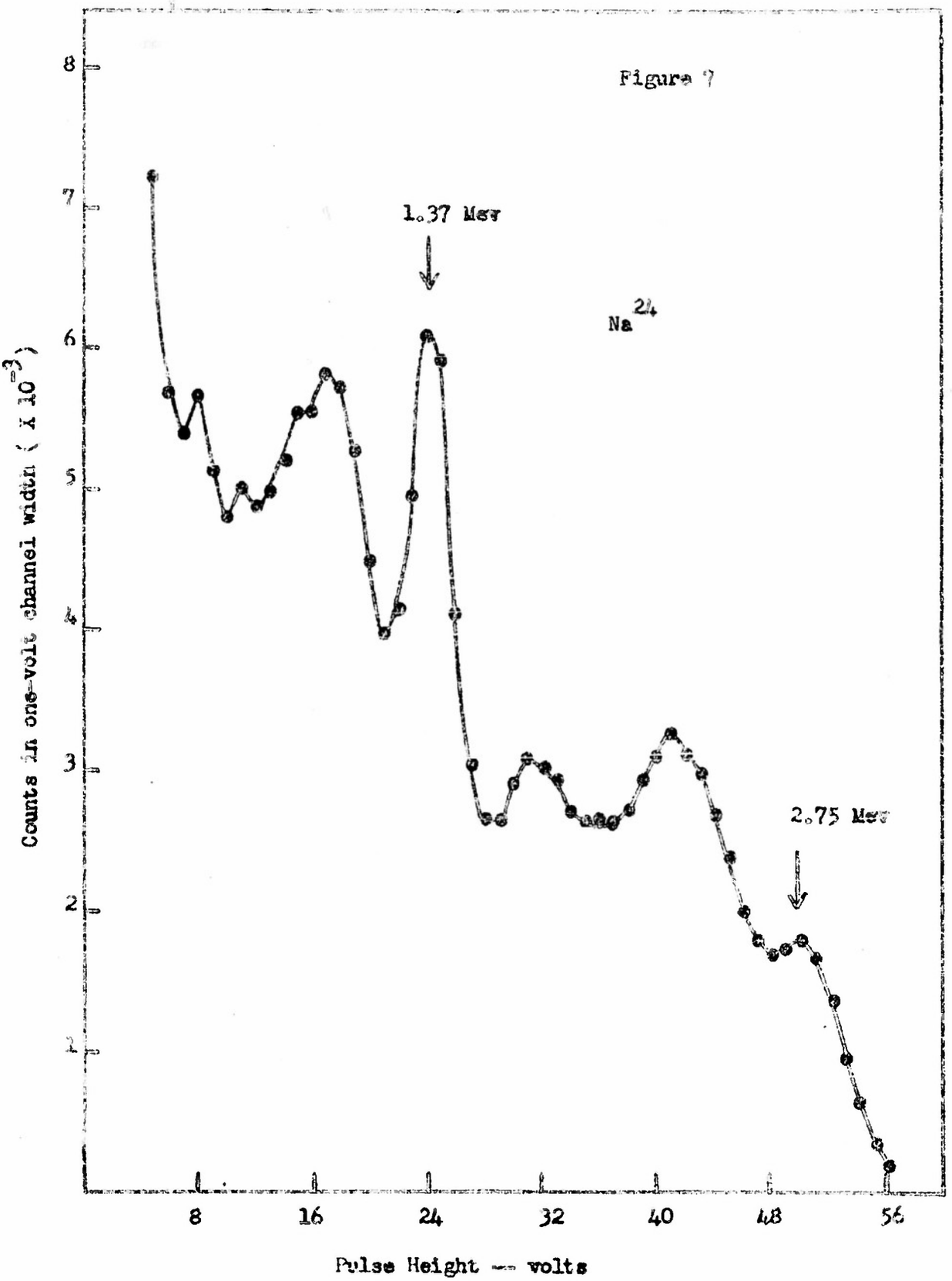

1.37 Mev
Na^{24}
2.75 Mev
Counts in one-volt channel width (x 10^{-3})
8
7
6
5
4
3
2
8
16
24
32
40
48
56
Pulse Height — volts

TABLE I

Gamma Rays Excited by 3.8 Mev. Neutrons	
Element	Energy of Gamma Ray (Mev)
Nickel	0.9 1.36
Copper	0.9
Zirconium	0.9 1.15 (?) 2.2

II. TOTAL CROSS SECTIONS; ANGULAR DISTRIBUTION OF ELASTIC SCATTERING; INELASTIC CROSS SECTIONS.

Introduction

The measurement of the differential cross sections for the scattering of 3.7 Mev neutrons from cadmium, tin, and bismuth represents an extension of similar measurements[1] on aluminum, iron, and lead in order to establish the pattern of variation with atomic weight. In addition, the recent continuum theory of nuclear reactions given by Feshbach, Porter and Weisskopf[2] has been used with a plausible extension to calculate the angular distribution of 3.7 Mev neutrons scattered from nuclei of atomic weight 115 and 209. This should be of value in assessing the possibilities of using the continuum theory in this energy range to give detailed information about neutron scattering.

1) W. D. Whitehead and S. C. Snowdon, Phys. Rev. 92, 114 (1953)

2) Feshbach, Porter and Weisskopf, Phys. Rev. 90, 116 (1953); "Neutron Reactions and the Formation of the Compound Nucleus", U. S. Atomic Energy Commission, NYO 3076, NDA Report 15B-4 (unpublished); "Theory of Average Cross-Sections", M.I.T. Report (unpublished).

Experimental

In general, the arrangement used in this experiment is exactly the same as that used in our previous experiment[1]. Neutrons of about 3.7 Mev were produced by bombarding a deuterium gas chamber with 10 μ.a. of deuterons of 0.65 Mev mean energy. A ring geometry was employed in which the angle of scattering was varied both by using different size rings and by an axial movement of each ring.

The previous experiments demonstrated that corrections of considerable magnitude must be made to allow for the higher order scattering in order to obtain the correct differential cross sections from the apparent differential cross sections observed with a ring of finite thickness. They further demonstrated that, within the experimental accuracy, a linear extrapolation of the apparent differential cross section to zero axial thickness of the scatterer most probably gave the correct differential cross section. The present measurements, therefore, were carried out using only two ring thicknesses. However, unlike the previous experiments in which only a few selected angles were chosen to determine the higher order scattering correction, in these experiments each ring thickness was used at all the angles of measurement. The result gives the apparent differential cross section as a function of angle for each of the two ring thicknesses used. The true differential cross

section now can be found at each angle by a linear extrapolation of the apparent differential cross section to zero ring thickness.

Finally, the neutron flux monitor was changed from that previously used, a butane filled proportional counter, to a Lucite-zinc sulphide scintillator detector[3] identical

---

3) W. F. Hornyak, Rev. Sci. Instr. 23, 264 (1952). The authors are indebted to Dr. Hornyak for supplying them with Lucite-zinc sulphide molded buttons.

---

with that used in detecting the scattered neutrons. In the previous experiments[1] some difficulty was experienced in maintaining a constant $0^{\circ}/90^{\circ}$ neutron flux ratio. Changing the monitor-detector improved this situation somewhat.

Data

Figure 1 shows the experimental points of the apparent differential cross section for the scattering of 3.7 Mev neutrons incident on the 3/8 inch and 1 inch thick rings of cadmium. A point by point linear extrapolation to zero ring thickness gives the true differential cross section $\sigma(\theta)$. Figures 2 and 3 present similar information with regard to tin and bismuth. At every angle the apparent differential cross section for the 1-inch rings is larger

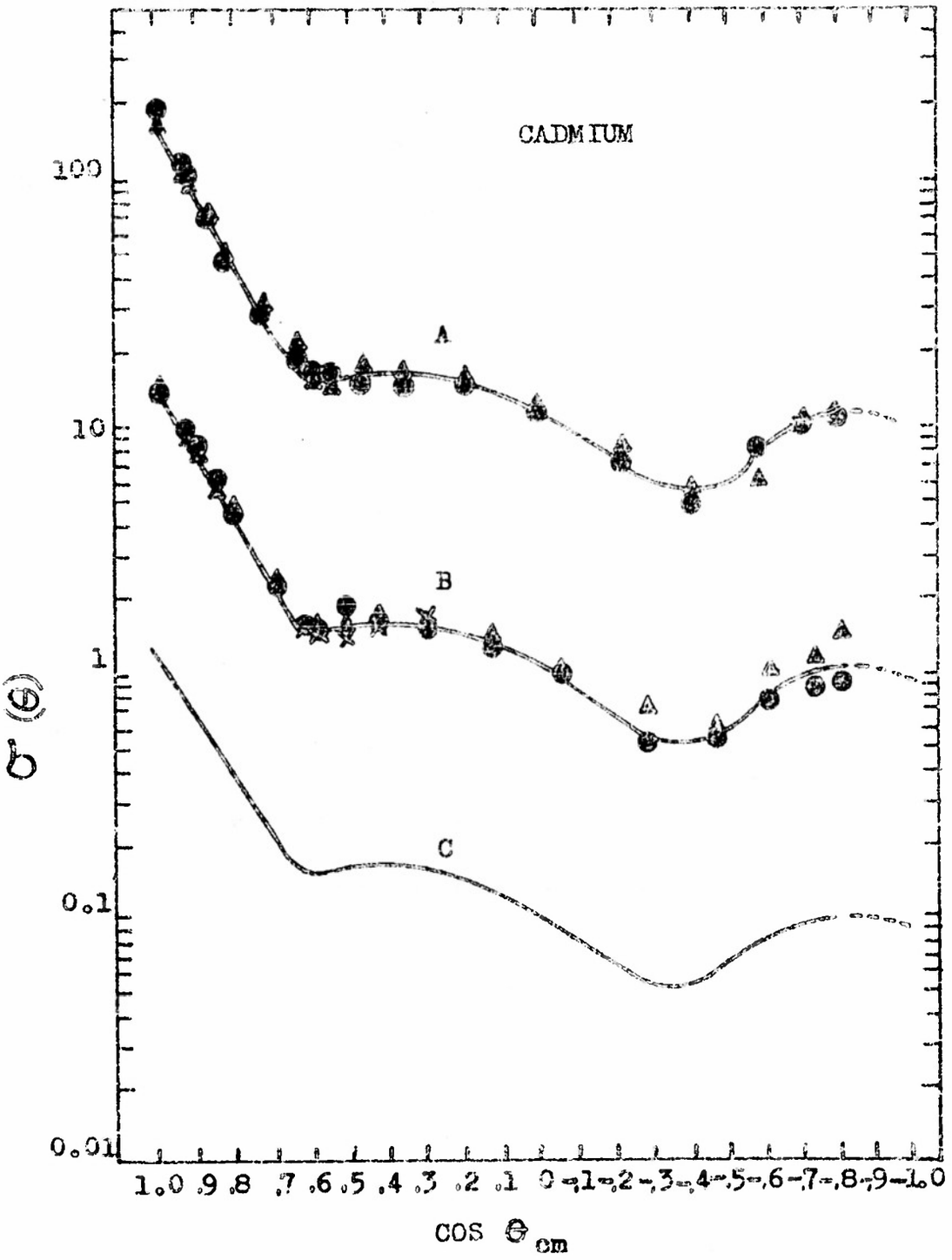

CADMIUM
100
10
1
0.1
0.01
A
B
C
σ (Φ)
1.0 .9 .8 .7 .6 .5 .4 .3 .2 .1 0 -.1 -.2 -.3 -.4 -.5 -.6 -.7 -.8 -.9 -1.0
COS Θ cm

Figure 1

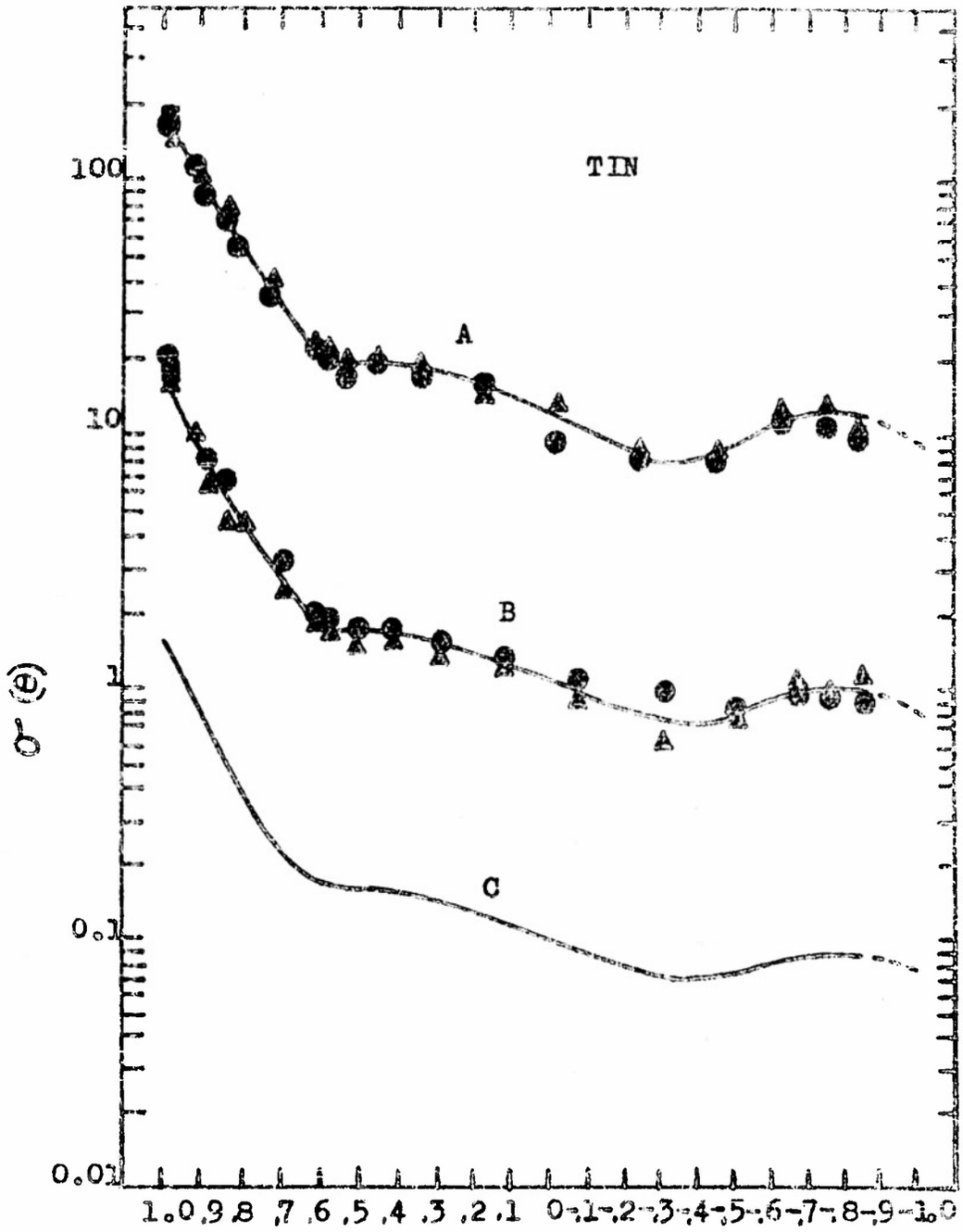


Figure 2

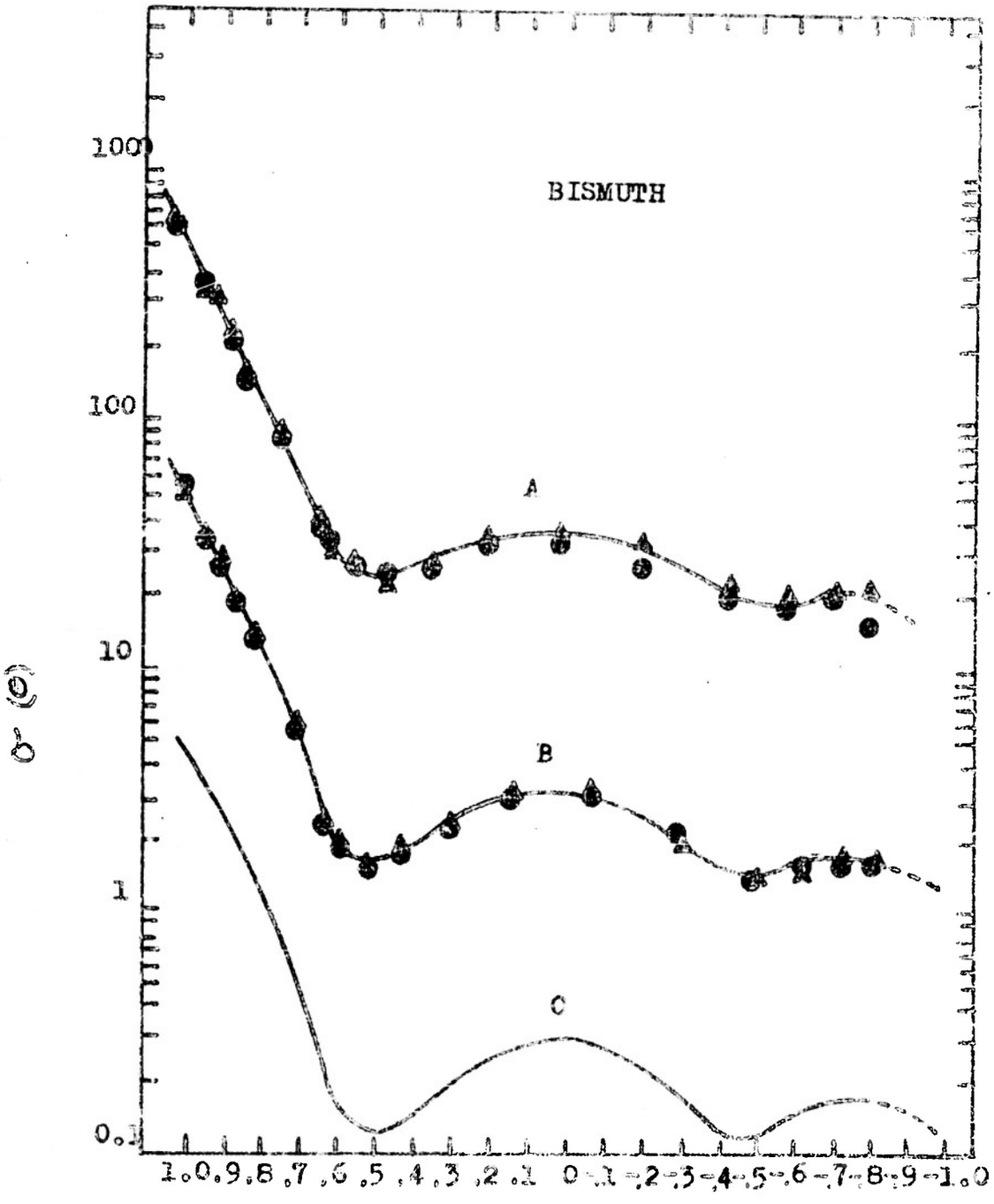


Figure 3

than the apparent differential cross section for the 3/8-inch rings thus demonstrating that at each angle the higher order scattering adds a positive contribution to the apparent differential cross section. The total cross sections corresponding to $\sigma(\theta)$ have been calculated and are presented together with the measured total cross sections in Table 1. The measured total cross sections in each case are about 8-10 per cent higher than those previously measured at an energy close to 3.7 Mev[4].

---

4) "Neutron Cross Sections", U. S. Office of Technical Services, Department of Commerce, AECU-2040 (unpublished); N. Hereson and S. Darden, Phys. Rev. 89, 775 (1953).

However, since both the differential and total cross sections were measured with the same experimental set-up, at worst all measurements are systematically from 8-10 per cent high which is within our over-all uncertainties of about 15 per cent.

As was discussed previously[1], the integrated cross section corresponding to $\sigma(\theta)$ does not accurately measure the total elastic cross section, since the neutron detector does not discriminate adequately against inelastically scattered neutrons. However, to within about 20 per cent, it may be considered to represent this elastic cross section. Subject to this reservation, the difference between the measured total cross section and the integrated

TABLE I.*

Element	σ_{tot} (meas.) in barns			$\int \sigma(\theta) d\Omega$ barns	σ_i (inelastic)
	This exp.	Ref. 4	Theory		
Cadmium	4.5	~ 4.0	5.6	2.5	2.0
Tin	4.6	~ 4.2		2.5	2.1
Bismuth	8.3	7.6	7.7	6.9	1.4

Total cross sections. The value of $\int \sigma(\theta) d\Omega$ subject to the reservations in the text is the total elastic cross section.

* Included in Table I is a column of values giving estimates of the order of magnitude of the inelastic scattering cross section at 3.7 Mev. Because of errors in the measurement of the total and elastic cross sections, the estimates may be incorrect by as much as a factor of two.

cross section corresponding to $\sigma(\theta)$ may be considered to equal the total inelastic cross section. Table I presents a summary of these calculations.

Theory

Since the neutron energy resolution in this experiment is about 200 Kev, the angular distribution of scattered neutrons may be discussed in terms of a theory that averages the differential cross section over an energy interval of this magnitude. Generally, in our energy range there will be many resonance levels within this 200 Kev energy interval, hence we may average the differential cross section over many resonance levels. Feshbach and Weisskopf[5] and

---

5) H. Feshbach and V. F. Weisskopf, Phys. Rev. 76, 1550 (1949); "Final Report of the Fast Neutron Data Project" U. S. Atomic Energy Commission, NYO-636 (unpublished).

Feshbach, Porter and Weisskopf[2] have provided two distinct theories that discuss total neutron cross sections averaged in this manner. The total neutron cross-section measurements of Barschall et al[6]. generally show agreement with the theory

---

6) H. H. Barschall, Phys. Rev. 86, 431 (1952); Miller, Adair, Bockelman, and Darden, Phys. Rev. 88, 83 (1952).

---

of Feshbach, Porter and Weisskopf[2] and are definitely at variance with the theory of Feshbach and Weisskopf[5].

Therefore, we will compare our measurements with the theory of Feshbach, Porter, and Weisskopf suitably formulated to exhibit the angular distribution of neutrons elastically scattered from nuclei.

The theory first will be formulated, assuming that there are no reaction products (i.e. no inelastic scattering, etc.). In general, the differential cross section for elastic scattering is given by[7)]

---

7) J. M. Blatt and V. F. Weisskopf, Theoretical Nuclear Physics (John Wiley and Sons, Inc., New York, 1952) Chapter VIII.

$$\sigma_{sc}(\theta) = \frac{1}{4}\lambda^2 \sum_{\ell}\sum_{m}(2\ell+1)(2m+1)(1-\eta_\ell)(1-\eta_m^*)P_\ell(\cos\theta)P_m(\cos\theta) \qquad (1)$$

where λ is the deBroglie wave length of the neutron, divided by 2π, η_ℓ is the phase constant, and $P_\ell(\cos\theta)$ is the Legendre polynomial. The relation between the phase constant η_ℓ and the corresponding logarithmic derivative f_ℓ if given by[7)]

$$\eta_\ell = \exp(2i\xi_\ell)\cdot\left[(f_\ell - \Delta_\ell + iS_\ell)/(f_\ell - \Delta_\ell - iS_\ell)\right] \qquad (2)$$

where φ_ℓ is the phase determining the potential scattering, and $\Delta_\ell + i s_\ell$ is the logarithmic derivative of the outgoing wave in the entrance channel.

We now average Eq. (1) over an energy interval that includes many resonance levels

$$\sigma_{sc}(\theta) = \frac{1}{4}\lambda^2 \sum_\ell \sum_m (2\ell+1)(2m+1)\left[(1-\bar{\eta}_\ell)(1-\bar{\eta}_m^*) + (\overline{\eta_\ell \eta_m^*} - \bar{\eta}_\ell \bar{\eta}_m^*)\right] P_\ell(\cos\theta) P_m(\cos\theta) \tag{3}$$

where all quantities such as λ, φ_ℓ, s_ℓ, and Δ_ℓ that only vary slowly with the energy are treated as constants. The distribution obtained from the term $(1-\bar{\eta}_\ell)(1-\bar{\eta}_m^*)$ is called the "shape elastic" scattering and the distribution obtained from the term $(\overline{\eta_\ell \eta_m^*} - \bar{\eta}_\ell \bar{\eta}_m^*)$ is called the "compound elastic" scattering[2].

In order to calculate η_ℓ, first it is necessary to choose a model that will provide a logarithmic derivative which includes a description of resonances. Feshbach, Porter and Weisskopf introduce a simplified version of a nuclear reaction. The zero order approximate problem is described by a Hamiltonian

$$H^{(o)} = H_T + H_n \tag{4}$$

where H_T is the Hamiltonian describing the complicated internal motions of the target nucleus and H_n describes the relative motion of the neutron and the target and is given by

$$H_n = \frac{\hbar^2}{2m} \nabla^2 + V(r), \qquad (5)$$

where m is the reduced mass, ∇^2 is the Laplacian in the relative coordinate of the neutron and the target system. V(r) is given by

$$V(r) = -V_0 \text{ for } r < R; \; 0 \text{ for } r > R, \qquad (6)$$

where R is the nuclear radius.

The formation of the compound nucleus is described in the next approximation by adding an interaction operator H' to give for the total Hamiltonian

$$H = H_T + H_n + H' \qquad (7)$$

For a convenient choice of the matrix elements of H' in the basis determined by the eigenfunctions of H_T, the value of the logarithmic derivative may be found. It is shown then that this rather complicated expression for the logarithmic derivative may be approximated by

$$f_\ell = w_{1\ell} + w_{2\ell} \cot z_\ell(\epsilon) \qquad (8)$$

where w_1 and w_2 are slowly varying functions of the energy of the neutron ϵ. The phase $z_\ell(\epsilon)$ is taken as proportional to the energy. If this expression for the logarithmic derivative is inserted into Eq. (2) and averaged over many resonances the result is

$$\bar{\eta}_\ell = \exp(2i\xi_\ell)\cdot\left[(w_{1\ell} - i w_{2\ell} - \Delta_\ell + i s_\ell)\right] \Big/ \left[(w_{1\ell} - i w_{2\ell} - \Delta_\ell - i s_\ell)\right] \qquad (9)$$

Thus, the averaging results in replacing the Cot z_ℓ in Eq. (8) by $-i$. The expressions obtained for $w_{1\ell}$ and $w_{2\ell}$ in the perturbation calculation are such that they may be approximated by the real and imaginary parts of the logarithmic derivative of the following non-Hermitean problem in the relative coordinates of the neutron and the target

$$H = -\frac{\hbar^2}{2m}\nabla^2 + V(r)$$

where

$$V(r) = -V_0(1 + i\xi) \text{ for } r < R;\ 0 \text{ for } r > R \qquad (10)$$

Thus, all quantities in Eq. (3) are provided for except $\overline{\eta_\ell \eta_m^*}$. To obtain this we assume in Eq. (8) that

$z(\epsilon)$ is a linear function of the energy

$$z_\ell = \pi\epsilon/d_\ell + \beta_\ell \qquad (11)$$

where d_ℓ is the average level separation. The product $\eta_\ell \eta_m^*$ is then averaged with respect to ϵ as in the case of η_ℓ. In particular, the result will depend on the unknown parameters β_ℓ. Since we are only interested in statistical results, the average of $\eta_\ell \eta_m$ with respect to ϵ is again averaged with respect to β_ℓ. The result is then

$$\overline{\eta_\ell \eta_n^*} = \bar{\eta}_\ell \bar{\eta}_m^* \quad \text{for } \ell \neq m; \quad | \text{ for } \ell = m \qquad (12)$$

Thus, the average phase constant in Eq. (9) completely defines an angular distribution of the elastic scattering averaged over many resonances. The non-Hermitean problem defined by Eq. (10), which is used to provide an approximate expression for the average phase, may be solved by a method due to Lax and Feshbach[8]. We have used for the

---

8) M. Lax and H. Feshbach, Journ. Acoust. Soc. Amer., 20, 108 (1948); Morse, Lowan, Feshbach and Lax, "Scattering and Radiation from Circular Cylinders and Spheres" (Reprinted by U. S. Navy Department Office of Research and Inventions, Washington, D.C., 1946).

---

potential within the nucleus

$$V = -19(1 + 0.05\ i)\ \text{Mev} \tag{13}$$

and for the nuclear radius

$$R = 1.45 \times 10^{-13}\ A^{1/3}\ (\text{cm}). \tag{14}$$

These values give good agreement with the total cross-section measurements of Barschall[2, 6].

In the preceding theory, it was assumed that no reaction products were present in the decay of the compound nucleus. This restriction may be removed by realizing that the effect of these reaction products upon the entrance channel can be accounted for approximately by introducing an imaginary part to the energy . Thus, Eq. (11) is changed to

$$z_\ell = \frac{\pi}{d_\ell}\left(\epsilon + i\Gamma_r^{(\ell)}/2\right) + \beta_\ell \tag{15}$$

where $\Gamma_r^{(\ell)}$ is the reaction width[2, 9]. When this is

---

9) Feshbach, Peaslee and Weisskopf, Phys. Rev. 71, 145 (1947).

---

done it will be found that Eq. (9) for the average phase $\overline{\eta_\ell}$ is unchanged and that Eq. (12) for the average phase product $\overline{\eta_\ell \eta_m^*}$ is unchanged for $\ell \neq m$ but that for $\ell = m$

$$\overline{\eta_\ell \eta_m^*} = 1 - (\exp 2\pi\Gamma_r^{(\ell)}/d_\ell - 1)(1 - \bar{\eta}_\ell \bar{\eta}_\ell^*) / [\exp 2\pi\Gamma_r^{(\ell)}/d_\ell - \bar{\eta}_\ell \bar{\eta}_\ell^*] \quad (16)$$

Hence, the preceding formulation may be used throughout except for this one change. Table 2 and Figures 4-6 present the chief numerical results of the above theory.

Discussion

A comparison in Figures 4-6 of the experimental differential cross section for the elastic scattering of 3.7 Mev neutrons from cadmium, tin, and bismuth with the theoretical predictions of the continuum model shows that the main features of the experimental curves are reproduced by the theory. In general, the theoretical results give a better fit with bismuth than with cadmium or tin. If one were to use Eq. (16) in the determination of the "compound elastic" scattering, there is no choice of the ratio of reaction width to level separation $\Gamma_r^{(\ell)}/d_\ell$ that would make the fit much better. The addition of "compound elastic" scattering, however, does adjust the "shape elastic" scattering to a distribution that more nearly

TABLE 2.

$R(10^{-13}$ cm)	σ_{se} (barns)	$\overline{\sigma_c}$ (barns)	$\overline{\sigma_{tot}}$ (barns)
7.1 (Cd, Sn)	4.0	1.6	5.6
8.6 (Bi)	6.1	1.6	7.7

σ_{se} is the integrated "shape elastic" cross section. $\overline{\sigma_c}$ is the average cross section for the formation of the compound nucleus. $\overline{\sigma_{tot}}$ is the total neutron cross section. The "compound elastic" cross section plus the average reaction cross section add up to $\overline{\sigma_c}$.

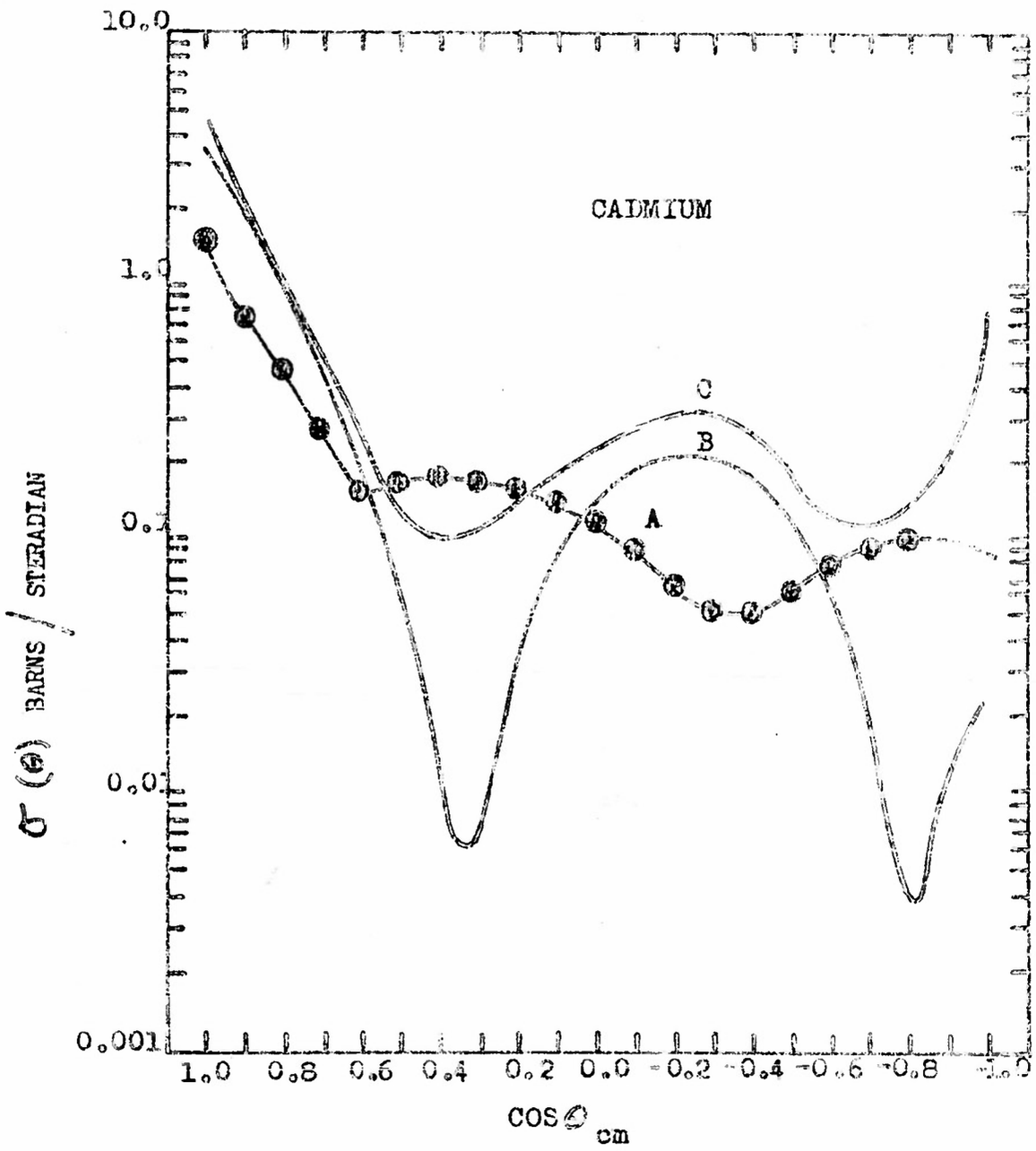

CADMIUM
10.0
1.0
0.1
0.01
0.001
σ (Θ) BARNS / STERADIAN
C
B
A
1.0 0.8 0.6 0.4 0.2 0.0 -0.2 -0.4 -0.6 -0.8 -1.0
COS Θ cm

Figure 4.

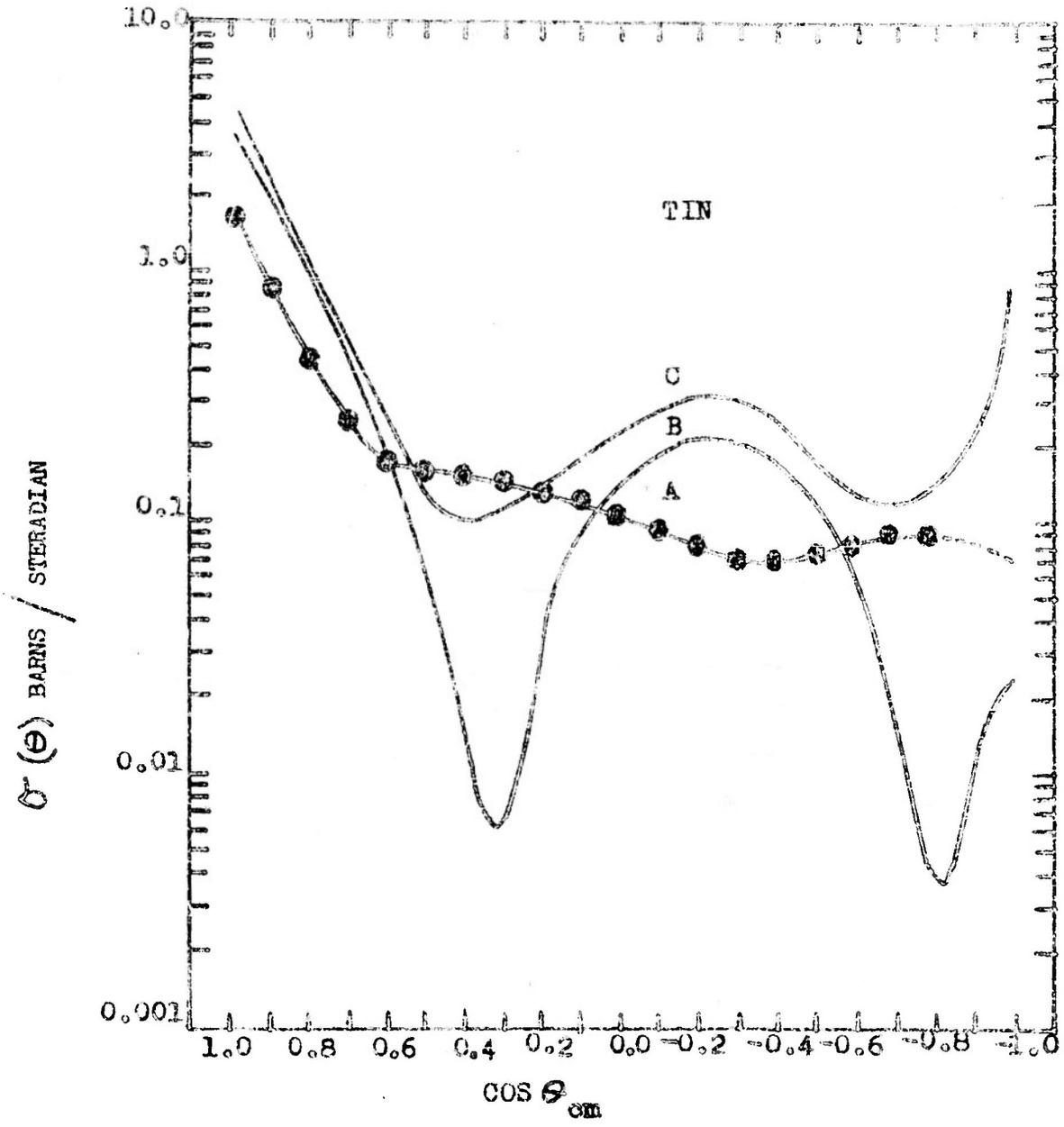

10.0
1.0
0.1
0.01
0.001
TIN
C
B
A
σ (Θ) BARNS / STERADIAN
1.0 0.8 0.6 0.4 0.2 0.0 -0.2 -0.4 -0.6 -0.8 -1.0
COS Θ cm

Figure 5.

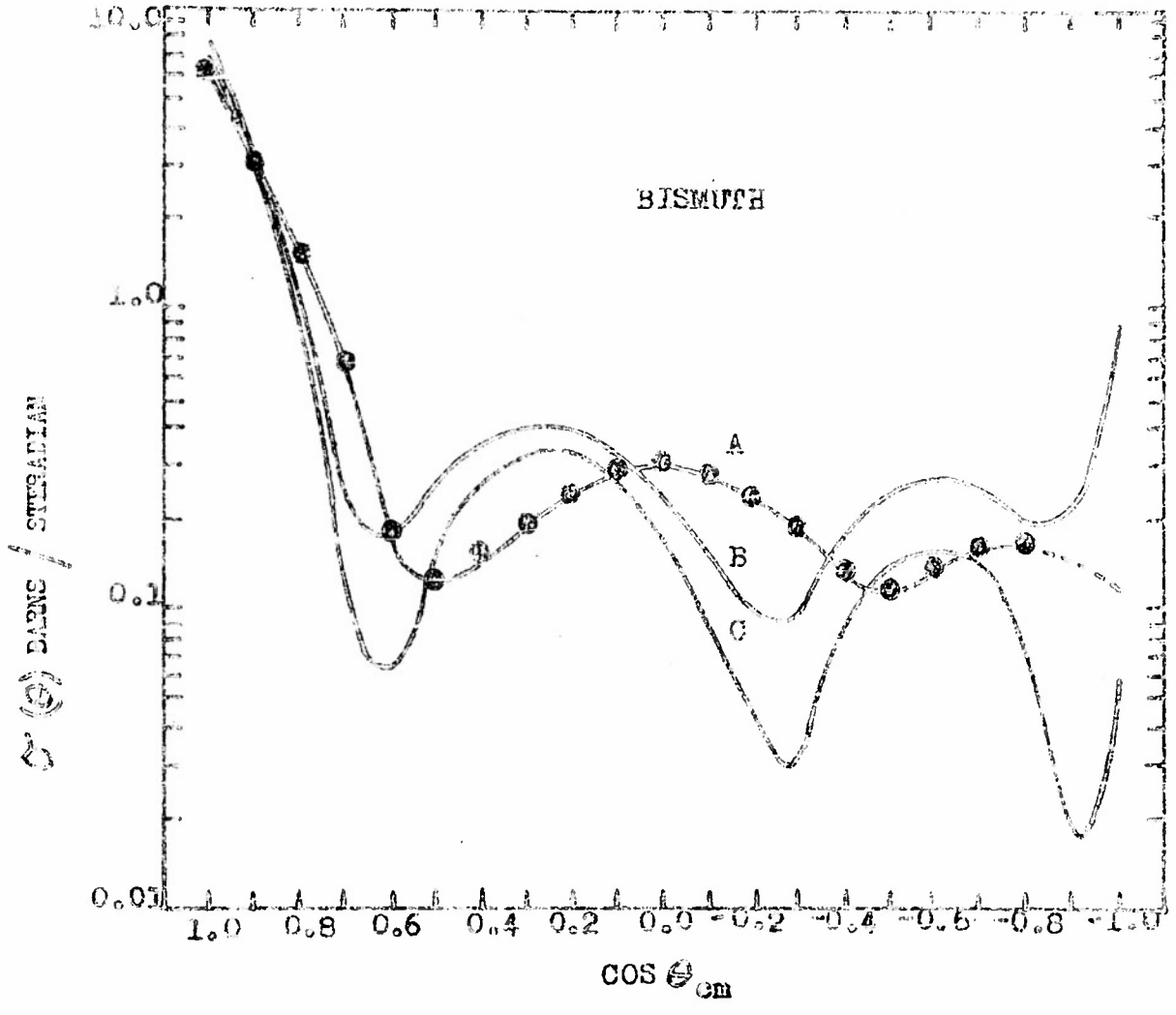

BISMUTH
A
B
C
10.0
1.0
0.1
0.01
1.0 0.8 0.6 0.4 0.2 0.0 -0.2 -0.4 -0.6 -0.8 -1.0
COS θ_{cm}

Figure 6

resembles the experimental curve than does the "shape elastic" scattering alone. In particular, this "compound elastic" scattering shifts the position of the first minima in the "shape elastic" scattering. Since different nuclei have different amounts of "compound elastic" scattering, this may account for the lack of a uniform shift in the position of the first minima in the experimental elastic-scattering distributions as one proceeds from iron to bismuth.

Since the largest discrepancy between theory and experiment occurs in the differential cross section for forward-scattering, $\sigma_{sc}(0)$, it is of interest to consider possible adjustments of $\sigma_{sc}(0)$ in the theory. The minimum theoretical value of $\sigma_{sc}(0)$ is given by a theory that does not include "compound elastic" scattering and has the maximum possible cross section for the formation of the compound nucleus. These conditions are met in the first version of the continuum theory[5]. The values of $\sigma_{sc}(0)$ from this theory agree with the experimental value of $\sigma_{sc}(0)$ in the case of bismuth but are too high in the case of cadmium and tin. In the case of bismuth, however, the subsequent form of $\sigma_{sc}(\theta)$ does not offer any possibility of giving a detailed fit. Therefore, it is not possible to obtain a useful value of $\sigma_{sc}(0)$ that agrees with experiment by adjusting only the value of ζ in Eq. (13) and the value of $\Gamma_r^{(k)}/d_\ell$ in Eq. (16). It can be argued

that the double average used to obtain $\overline{\eta_\ell \eta_m^*}$ in Eq. (12), strictly speaking, is not a necessary feature of the continuum theory and that one should insert some function of ℓ for the parameter β_ℓ in Eq. (11). To get some idea of the restriction introduced by this average over β_ℓ, the value of $\eta_\ell \eta_m^*$ was averaged with respect to ϵ with the value of β_ℓ set equal to zero. For bismuth the difference between this method and the double average method was quite small. For cadmium and tin the difference was somewhat larger but still not large enough to alter appreciably the results of the double average method. Hence, it is not likely that significantly better fits between theory and experiment would be obtained if β_ℓ were known as a function of ℓ.

Since the theoretical value of $\sigma'_{sc}(0)$ can be made to agree with experiment by adjusting the nuclear radius, it is of interest to estimate the magnitude of the change necessary to bring about this agreement. The nuclear radius used for bismuth (A = 209 in Eq. (14)) would have to be lowered by about 6 per cent since $\sigma'_{sc}(0)$ varies approximately as the fourth power of the radius. This also would move the first theoretical minima closer to the first experimental minima. Since this change in radius would lower the total cross section by approximately 15 per cent and since the total cross section is in fair agreement with

experiment, it would be necessary to raise the imaginary part of the potential in Eq. (13) by about 15 per cent in order to maintain agreement of the theoretical and experimental total cross section. Furthermore, a lowering of the nuclear radius by about 6 per cent would be in agreement with the measurements of Coon, Graves, and Barschall[10], in which they find

---

10) J. H. Coon, E. R. Graves, and H. H. Barschall, Phys. Rev. 88, 562 (1952).

---

for 14 Mev neutrons and for elements above barium that the nuclear radius as measured by $(\sigma_{tot}/2\pi)^{1/2}$ falls below the value predicted by $R = 1.5 \times 10^{-13} A^{1/3}$ cm.

In order to adjust the theory to the experimental value of $\sigma_{sc}(0)$ for cadmium and tin it would be necessary to lower the nuclear radius chosen ($A = 115$ in Eq. (14)) by about 30 per cent. Corresponding to this, it would be necessary to increase the parameter ζ by a large amount to give a sufficiently large total cross section if, indeed, a large change in ζ is capable of adjusting the total cross section by a correspondingly large amount. This large adjustment of the nuclear radius is not very palatable in view of the general experimental agreement of the nuclear radius with the formula in Eq. (14) for 14 Mev neutrons and for values

of A near 115[10]. It is conceivable that the theory as it stands would give better agreement if it were applied to an ellipsoidal-shaped target nucleus. However, since only 20-25 per cent of the cadmium and tin isotopes have odd neutron numbers and since nuclear eccentricities in the region of A = 115 are only about 6 per cent[11], it is not likely that the use of an

---

11) J. M. Blatt and V. F. Weisskopf, "Theoretical Nuclear Physics" (John Wiley and Sons, Inc., New York, 1952) pp. 29, 776.

---

ellipsoidal-target nucleus can produce the desired change. Hence, we are reduced to the necessity of a modification of the theory as the only means by which a sufficiently large adjustment can be accomplished. Within the general framework of the theory, it might be possible to choose the matrix elements of H' in Eq. (7) to be a function of the relative coordinate, r, or to let the potential in Eq. (6) be a function of the spins of the neutron and the target nucleus[12]. In any case, however, it would be necessary

---

12) N. C. Francis and K. M. Watson, Phys. Rev. 92, 291 (1953).

---

that these changes introduce little effect on the present results in the neighborhood of A = 209.

In summary then, it may be said that the continuum theory may be brought into rather detailed agreement with the measured angular distribution of 3.7 Mev neutrons scattered from bismuth. The theory in the case of cadmium and tin exhibits only the general features of the experimental results and possibly demonstrates a need for a revision of the theory.

Captions for Figures

Figure 1 - Angular distribution of 3.7 Mev neutrons scattered from cadmium. (A) apparent differential cross section using 1" axial thickness ring scatterers. (B) apparent differential cross sections using 3/8" axial thickness ring scatterers. (C) true differential cross sections for elastic scattering obtained by a point-by-point linear extrapolation of curves (A) and (B) to zero thickness scatterer. Ordinates are for curve (C) and are in units of barns/steradian. Curve (B) ordinate should be reduced by a factor of 10. Curve (A) ordinate should be reduced by a factor of 100.

Figure 2 - Angular distribution of 3.7 Mev neutrons scattered from tin. (A) apparent differential cross section using 1" axial thickness ring scatterers. (B) apparent differential cross section using 3/8" axial thickness ring scatterers. (C) true differential cross section for elastic scattering obtained by a point-by-point linear extrapolation of curves (A) and (B) to zero thickness scatterer. Remarks concerning ordinates are the same as in Figure 1.

Captions for Figures (Continued)

Figure 3 - Angular distribution of 3.7 Mev neutrons scattered from bismuth. (A) apparent differential cross section using 1" axial thickness ring scatterers. (B) apparent differential cross section using 3/8" axial thickness ring scatterers. (C) true differential cross section for elastic scattering; obtained by a point-to-point linear extrapolation of curves. (A) and (B) to zero thickness scatterer. Remarks concerning the ordinates are the same as in Figure 1.

Figure 4 - Comparison of the experimental differential cross section for the elastic scattering of 3.7 Mev neutrons from cadmium with the predictions of the continuum model for a nuclear radius of 7.1×10^{-13} cm and a complex potential constant of (-19(1 + 0.05 i) Mev. (A) experimental results from Figure 1(C). (B) "Shape elastic" differential cross section. (C) "Compound elastic" plus "shape elastic" differential cross section using Eq. (12) to determine the "Compound elastic" scattering. Solid triangle is $\sigma_{sc}(0)$ from first version of the continuum theory.

Figure 5 - Comparison of the experimental differential cross section for the elastic scattering of 3.7 Mev neutrons from tin with the predictions of the continuum model

for a nuclear radius of 7.1×10^{-13} cm and a complex potential constant of $-19(1 + 0.05\ i)$ Mev. (A) experimental results from Figure 2(C). (B) "shape elastic" differential cross section. (C) "compound elastic" plus "shape elastic" differential cross section using Eq. (12) to determine the "compound elastic" scattering. Solid triangle is $\sigma_{sc}(0)$ from first version of the continuum theory.

Figure 6 - Comparison of the experimental differential cross section for the elastic scattering of 3.7 Mev neutrons from bismuth with the predictions of the continuum model for a nuclear radius of 8.6×10^{-13} cm and a complex potential constant of $-19(1 + 0.05\ i)$ Mev. (A) experimental results from Figure 3(C). (C) "shape elastic" differential cross section. (B) "compound elastic" plus "shape elastic" differential cross section using Eq. (12) to determine the "compound elastic" scattering. Solid triangle is $\sigma_{sc}(0)$ from first version of the continuum theory.

III. LOW VOLTAGE ACCELERATOR

In a previous report there is described a bench test ion source assembly used to study operating characteristics of the Bartol radiofrequency ion source. As part of the projected program concerning scattering studies on neutrons it was decided to convert this test bench into a positive ion accelerator which would operate at voltages up to 100 Kv. The chief advantage of this type of accelerator for neutron studies is the provision of a beam current several times greater than those obtained from the Van de Graaff generator and having sufficient energy to yield a reasonable flux of neutrons from the exothermic reactions, $H^2(d,n)He^3$ and $H^3(d,n)He^4$.

It was decided to incorporate an ion source developed at Oak Ridge which differs from the source used in the Van de Graaff generators in that it provides considerably larger beam currents. An ion source of this type was obtained from Oak Ridge and installed in the accelerator last fall.

It became apparent at that time that the completion of the large generator and continual use of the smaller generator would prohibit satisfactory operation of a third accelerator in the same room, and accordingly plans were

made to renovate a garage on the Bartol property for purposes of housing the low-voltage accelerator. In April the building was completed and the accelerator moved to the second floor. During the spring and summer several structural changes were made to provide more convenient and stable operation. In particular, provision was made for extension of the tube through the floor into the middle of the room below in order to reduce as far as practicable the problems associated with scattering of the neutrons from floor and walls.

After several initial difficulties with the vacuum system and adjustments on the ion source a beam of 120 μa has been focused on a target 1 1/2" in diameter at a distance of 10 feet from the source. A liquid air-cooled system was installed in order to freeze D_2O onto the metal target for producing neutrons from the $H^2(d,n)He^3$ reaction.

IV. INELASTIC SCATTERING OF NEUTRONS BY Ba^{137} and Hg^{199} ∕

C. P. Swann and F. R. Metzger

Bartol Research Foundation of The Franklin Institute, Swarthmore, Pa.

Abstract

The production by inelastic scattering of neutrons of the 527 kev isomeric level of Hg^{199} and of the 661 kev isomeric level of Ba^{137} have been studied. Neutrons were produced by bombarding a 50 kev lithium target with protons accelerated in the large Bartol Van de Graaff. The cross section for the production of the 13/2+ level of Hg^{199} increases sharply at 620 ± 10 kev mean neutron energy indicating a level at about 90 kev above the metastable state. Below 620 kev the observed activity decreases with increasing neutron energy and is attributed mainly to fast neutron capture by Hg^{198}. At 620 kev the cross section corresponds to about one mb. Several other breaks indicate higher excited states in Hg^{199}. The 11/2- level of Ba^{137} has been excited with mean neutron energies as low as 670 ± 10 kev indicating direct formation of the metastable state. The experimental cross section at 150 kev above the threshold is about 5 mb which is an order of magnitude smaller than the theoretical estimate based on the compound nucleus model.[1)]

∕ Supported in part by the U. S. Atomic Energy Commission and in part by the joint program of the U.S. Office of Naval Research and the U. S.Atomic Energy Commission.

1) W. Hauser and H. Feshbach, Phys. Rev. 87, 366 (1952).

V. RECENT PUBLICATIONS

Recently published works carried out under this Contract are:

"Nuclear Emulsion Method for Energy Measurement of Inelastically Scattered Neutrons", by S. C. Snowdon, M. A. Rothman, D. W. Kent, Jr., and W. D. Whitehead, Rev. of Scientific Instr., Vol. 24, No. 9, 876-877, September, 1953.

"Angular Distribution of Neutrons Scattered from Aluminum, Iron, and Lead", by W. D. Whitehead and S. C. Snowdon, Phys. Rev., Vol. 92, No. 1, 114-119, October 1, 1953.

Reprinted from THE REVIEW OF SCIENTIFIC INSTRUMENTS, Vol. 24, No. 9, 876–877, September, 1953
Printed in U. S. A.

Nuclear Emulsion Method for Energy Measurement of Inelastically Scattered Neutrons*

S. C. SNOWDON, M. A. ROTHMAN, D. W. KENT, JR., AND W. D. WHITEHEAD
Bartol Research Foundation of The Franklin Institute, Swarthmore, Pennsylvania

(Received April 1, 1953)

NUCLEAR emulsions have been used for some time in what may be called a point source of neutron geometry (point geometry) to record the energy spectrum of neutrons produced in nuclear reactions. The same method applied to the observation of inelastically-scattered neutrons has two defects: (a) the source of bombarding particles is relatively weak because these particles first must be produced by a nuclear reaction in order to get monoenergetic neutrons; (b) the bombarding neutrons as well as the scattered neutrons give proton recoils in the emulsion. The purpose of this letter is to present a method of overcoming these defects. Since the low intensity of flux incident on the scatterer cannot be increased appreciably, one can only hope to arrange the scatterer geometry so that many scattering points give similar contributions to the proton recoil spectrum. In order to prevent the direct neutron flux from producing a proton recoil spectrum comparable with that from the scatterer, it is necessary that the plane of the emulsion be placed at right angles to the incident flux. Both of these conditions are met if the scattering material is placed in an axially symmetric ring (ring geometry), and the photographic emulsion is located on the axis with its plane in the central plane of the ring (Fig. 1).

In order to utilize the ring geometry, the customary acceptance criteria[1] must be changed to the following single criterion: all proton recoil tracks are acceptable if their angle of dip with respect to the plane of the emulsion is less than δ_0. In our case $\delta_0=12°$. The feasibility of the ring geometry will have been ascertained if a calculation is made of the recoil proton spectrum from the following sources of scattered neutrons: (1) the ring (signal); (2) all elements in the emulsion (noise); and (3) the boundaries of the room (noise).

It should be noted that the noise of type (2) may be reduced by interposing some scattering material on the axis between the neutron source and the emulsion. Also, there will be a proton spectrum in the emulsion because of the $N^{14}(n, p)$ reaction ($Q=0.627$ Mev).[2] This spectrum may easily be distinguished from the scattering spectrum, first because it will have a line spectrum, and secondly, because of the positive Q value, the peak will occur at an energy appreciably higher than that of the scattered neutron spectra.

In order to investigate points (1) and (2), it will be assumed that the scattering takes place isotropically. This is not justified in view of the continuum theory of nuclear reactions,[3] but the deviation will reduce the signal and the noise in a similar manner. Figure 2 gives the results of the calculation of points (1) and (2) in reference to the geometry of Fig. 1 for a 14-microampere-hour bombardment of D–D neutrons from a half-atmosphere source of deuterium gas. The neutron energy in the forward-direction was taken to be 4.0 Mev. This gives about 3.75 Mev for the energy of the neutrons scattered from the ring into the emulsion. The background curve is a superposition of proton recoil spectra derived from the attenuated neutron flux scattered from the silver, bromine, oxygen, nitrogen, and carbon that are present in a 330-micron pellicle assumed to have the composition of an NTA emulsion.[4] The actual spectra will be modified because of the following effects: spread in energy of the neutrons from the source; length of track projected onto the plane of the emulsion; range straggling in the emulsion. None of these effects are expected to destroy the general appearance of peaks.

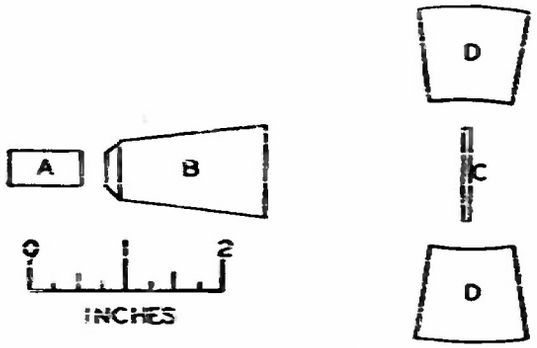


FIG. 1. Ring geometry for scatterer: (A) deuterium gas at one-half atmosphere pressure to give neutrons of 4 Mev from the D–D reaction; (B) copper shield that attenuates the direct neutron flux on the emulsion by 1/e; (C) 330-micron NTA pellicle of about one inch diameter; (D) ring scatterer 6 inch i.d., 9 inch o.d., 12° half-angle from center of emulsion.

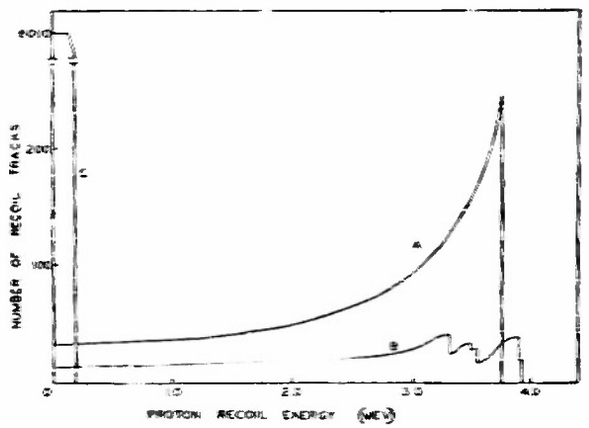


FIG. 2. Proton recoil spectra: (A) Signal spectrum of neutrons elastically scattered from iron for a 14-microampere-hour bombardment where the ordinate represents the number of acceptable recoil tracks in each 500-kev interval in 0.0053 cc of the emulsion; (B) noise spectrum; and (C) the direct beam spectrum under the same conditions.

An investigation of point (3) shows that the proton recoil spectrum between 4 Mev and 1–2 Mev is negligible. This estimate is based on a measurement of the shadow cone background neutron flux as a function of neutron energy in our previous total scattering cross-section measurements.[5]

The signal-to-noise ratio for elastic scattering is seen to be large enough to make the experiment feasible. The inelastic scattering should be comparable with the elastic scattering and hence should be detected by this method. Preliminary measurements using an iron ring scatterer and 4-Mev neutrons show both the elastic and an inelastic group of neutrons separated by about 0.8 Mev in accordance with the expected excited level[6] in Fe^{56}.

* Assisted by the joint program of the U. S. Office of Naval Research and the U. S. Atomic Energy Commission.

[1] H. T. Richards, Phys. Rev. 59, 796 (1941).
[2] F. Ajzenberg and T. Lauritsen, Revs. Modern Phys. 24, 321 (1952).
[3] Final Report of the Fast Neutron Data Project NYO-636.
[4] A. Beiser, Revs. Modern Phys. 24, 273 (1952).
[5] S. C. Snowdon and W. D. Whitehead, Phys. Rev. 90, 615 (1953).
[6] Nuclear Data, Natl. Bur. Standards (U. S.) Circular 499 (1950).

Reprinted from THE PHYSICAL REVIEW, Vol. 92, No. 1, 114-119, October 1, 1953
Printed in U. S. A.

Angular Distribution of Neutrons Scattered from Aluminum, Iron, and Lead*

W. D. WHITEHEAD AND S. C. SNOWDON
Bartol Research Foundation of the Franklin Institute, Swarthmore, Pennsylvania

(Received May 29, 1953)

The differential cross sections for the scattering of 3.7-Mev neutrons from aluminum, iron, and lead have been measured in a ring geometry using a molded Lucite-zinc sulfide button as a detector. The measurements were taken over an angular range of 127 degrees between 13 degrees and 140 degrees with an angular resolution better than ±10 degrees. Effects due to higher-order scattering in the scatterer were removed by extrapolation.

INTRODUCTION

MEASUREMENTS of the angular distribution of fast neutrons scattered from a large number of elements have been reported previously by Kikuchi *et al.*,[1] and Amaldi *et al.*[2] in which the main features of the distribution could be explained as the diffraction effects due to the scattering of neutron waves by spherical particles. More recently Remund and Ricamo[3] have measured angular distribution of 3.7-Mev neutrons scattered from carbon while Walt and Barschall,[4] using 1.00-Mev neutrons have reported the angular distributions for a large number of elements. Feshbach, Porter, and Weisskopf,[5] using a modification of the continuum theory of nuclear reactions, have reproduced the average features of the total neutron cross section as energy and atomic number as measured by Barschall.[6] Feshbach, Porter, and Weisskopf[7] have also computed the angular distributions of elastically scattered neutrons using this same modification of the continuum theory and the general features agree rather well with the measurements of Walt and Barschall.[4] Our measurements on aluminum, iron and lead, using 3.7-Mev neutrons, were undertaken with the thought that the angular distribution in this energy range would be of value in view of the present theoretical considerations.

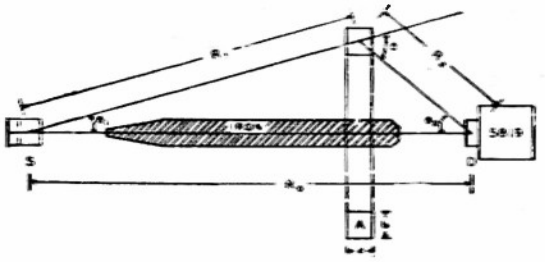


FIG. 1. Ring geometry for scatterer (S), deuterium gas at one-half atmosphere pressure to give neutrons of about 3.7 Mev; (D) Lucite-zinc sulfide scintillation detector; (A) ring scatterer of rectangular cross section.

EXPERIMENTAL

Figure 1 shows the experimental arrangement that was used to measure the angular distribution of neutrons scattered from aluminum, iron, and lead. The source of neutrons is a chamber of deuterium gas at 0.5 atmosphere and 2.0 cm in depth bombarded with about 10 microamperes of 1.0-Mev deuterons which, after passing through the nickel foil and gas, have a mean energy of about 0.65 Mev. These neutrons are detected by a pressure molded Lucite-zinc sulfide button[8] mounted directly on the face of an RCA 5819 photomultiplier. The direct beam is cut out by a suitably tapered 10-inch long, 1⅛-inch diameter iron cylinder. The scatterer was chosen to have the shape of a ring in order to increase as much as possible the number of scattered neutrons. The scattering angle θ is varied by moving the scattering rings laterally and by using rings of various sizes. For angles between 52° and 140°, 8-inch o.d. rings were used with a mean source-detector distance R_8 of 40 cm. For θ between 24° and 52°, 6-inch o.d. rings were used with R_6 equal to 60 cm. For the point at 13°, 4-in. o.d. rings were used with R_4 equal to 72 cm.

In order to discuss the measurements that must be made to arrive at the differential scattering cross section, it is convenient to define several quantities. For a given number of neutrons emitted by the neutron source, let N_S be the number of neutrons recorded by the detector with the scatterer and direct beam attenuator in place. Let N_s be the number of neutrons detected with the scatterer removed and let N_D be the number of neutrons recorded with the scatterer and attenuator removed. N_S-N_s is the number of scattered neutrons recorded by the detector that originate in the source, and N_D-N_s is the number of neutrons direct from the source that are recorded by the detector. Let

* Assisted by the joint program of the U. S. Office of Naval Research and the U. S. Atomic Energy Commission.

[1] Kikuchi, Aoki, and Wakatuki, Proc. Phys. Math. Soc. Japan 21, 420 (1939); T. Wakatuki and S. Kikuchi, Proc. Phys. Math. Soc. Japan 21, 656 (1939); T. Wakatuki, Proc. Phys. Math. Soc. Japan 22, 430 (1940).

[2] Amaldi, Bocciarelli, Cacciapuoti, and Trabacchi, International Conference on Fundamental Particles and Low Temperature (The Physical Society, London, 1947), Vol. 1.

[3] A. E. Remund and R. Ricamo, Helv. Phys. Acta 25, 441 (1952).

[4] M. Walt and H. H. Barschall, Phys. Rev. 90, 714 (1953).

[5] Feshbach, Porter, and Weisskopf, Phys. Rev. 90, 166 (1953).

[6] H. H. Barschall, Phys. Rev. 86, 431 (1952); Miller, Adair, Bockelman, and Darden, Phys. Rev. 88, 83 (1952).

[7] Feshbach, Porter, and Weisskopf, Bull. Am. Phys. Soc. 28, No. 3, 29 (1953).

[8] W. F. Hornyak, Rev. Sci. Instr. 23, 264 (1952). The authors are indebted to Dr. Hornyak for supplying them with a Lucite-zinc sulfide molded button.

the scattering ratio be defined as

$$S \equiv (N_S - N_B)/(N_D - N_B).$$

Appendix I then shows that the scattering ratio S is related to the apparent differential scattering cross section $\bar{\sigma}(\theta)$ through the relation

$$S = [I(\theta_1)/I(0)] \cdot [R_2^2/R_1^2 R_2^2] \cdot \bar{\sigma}(\theta) A(\theta_2) E(E_n) nV F(\theta_2) \exp(-\sigma n d), \quad (1)$$

where $I(\theta_1)$ is the number of neutrons emitted from the source per steradian per unit monitor flux, $A(\theta_2)$ is the angular sensitivity of the neutron detector normalized to unity at zero angle, $E(E_n)$ is the energy sensitivity of the neutron detector normalized to unity for the energy of the direct beam, nV is the number of scattering nuclei, σ is the total scattering cross section, and $F(\theta_2)$ is an attenuation factor which is defined more fully in Appendix I.

In general, the scattering ratio S is made up of a sum of terms $S = S_1 + S_2 + \text{etc.}$, where S_1, S_2, etc. refer to the neutrons scattered into the detector by single scattering, double scattering, etc. Thus, $\bar{\sigma}(\theta)$ is simply a measure of the differential scattering cross section, assuming that all neutrons are singly scattered, since $\bar{\sigma}(\theta)$ becomes exactly $\sigma(\theta)$ if S is replaced by S_1. In order to separate the components S_1, S_2, etc., one measures the scattering ratio S for a fixed angle θ as a function of the axial thickness of the ring scatterer d. The value of $\sigma(\theta)$ at $d=0$ is then the average differential scattering cross section for all scattered neutrons (elastic and inelastic) weighted according to the energy-sensitivity of the detector $E(E_n)$. In the ideal case, if the energy-sensitivity curve adequately discriminates against the inelastically scattered neutrons, the above value of $\bar{\sigma}(\theta)$ for $d=0$ becomes the differential cross section for elastic scattering $\sigma(\theta)$.

In order to measure $\bar{\sigma}(\theta)$ it is necessary to consider the following factors.

1. *Energy resolution of incident neutrons.*—The mean energy of the neutrons incident on the scatterer varies between 3.70 Mev and 3.74 Mev depending on the angle θ_1. The energy spread in the beam due to target thickness and voltage stability of the generator is about 200 kev.

2. *Neutron flux monitor.*—A proportional counter filled with one atmosphere of butane was placed very close to the target chamber at 90 degrees with respect to the source-detector axis. The discriminator was set to reject those neutrons that were produced from the $C^{12}(d, n)$ reaction in the vicinity of the magnet box. Actually some difficulty was experienced in obtaining a constant direct-beam neutron count per unit monitor count after the target chamber was just filled with deuterium. The pattern of change, however, was similar in each case and seemed to indicate that some of the deuterium gas was absorbed into the walls of the chamber. After about an hour or two a ratio was obtained that was constant to ±5 percent.

3. *Measurement of S.*—In general the direct beam count was about 15–100 times the scattered beam count and the attenuated direct beam count varied from 40 percent to 90 percent of the scattered beam count, each depending on the size and position of the scatterer.

4. *Spacial distribution of neutron source.*—The $N_D - N_B$ count exhibited within a few percent an inverse square variation with distance from the target chamber.

5. *Angular variation of the neutron flux from the D−D reaction, $I(\theta_1)/I(0)$.*—This quantity was computed from the data published by Hunter and Richards.[9]

6. *Measurement of nV, the number of scattering nuclei.*—Each scatterer was weighed on a suitable balance to about one percent accuracy.

7. *Angular variation in sensitivity of the neutron detector, $A(\theta_2)$.*—This quantity varied by about 25 percent over the range of θ_2 used in this experiment. The value of $A(\theta_2)$ was measured to within about 5 percent by rotating the detector about an axis through the detector perpendicular to the source-detector axis.

8. *Measurement of the total cross section.*—This was measured by using 1½-inch diameter, 1-inch long cylinders of aluminum, iron, and lead. The cross sections obtained for $E_n = 3.7$ Mev were $\sigma(\text{Al}) = 2.55$ barns, $\sigma(\text{Fe}) = 3.51$ barns, and $\sigma(\text{Pb}) = 7.60$ barns each in agreement with the values obtained by Nereson and Darden.[10] The scattering-in corrections were 0.75, 2.4, and 4.3 percent, respectively, for Al, Fe, and Pb, and were obtained from our measurements of the differential cross section.

9. *The attenuation factor F.*—This factor varied from unity by as much as 14 percent depending on the size and shape of the scatterer. This quantity is discussed briefly in Appendix I and a graph of its variation is given in Fig. 2.

10. *Geometrical measurements.*—Measurements of distance were carried out to about ±1 millimeter. The consequent calculation of mean angles is thus accurate to about one percent. However, because of the finite size of the detector (1 inch diameter, ⅝ inch height) and the finite size of the scatterers, the detected neutrons are received over a range of angles of about ±10 degrees in the worst case near $\theta = 90$ degrees.

11. *Variation of the sensitivity of the detector with neutron energy.*—This was measured by comparing our measurement of the angular distribution of neutrons from the D−D reaction with those of Hunter and Richards,[9] the discrepancy being ascribed to a non-uniform efficiency in our detector. As may be seen in Fig. 3, the sensitivity only drops off slowly with decreasing neutron energy, decreasing by 40 percent in 1 Mev. Since it is desired to discriminate against neutrons that have lost more than 200 kev, this consti-

[9] G. T. Hunter and H. T. Richards, Phys. Rev. 76, 1445 (1949).
[10] N. Nereson and S. Darden, Phys. Rev. 89, 775 (1953).

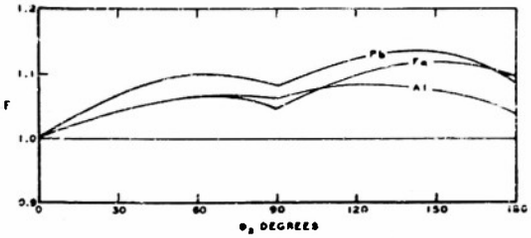


FIG. 2. Attenuation factor F. This quantity is defined in Appendix I. $F\exp(-\sigma nd)$ essentially measures the attenuation of the direct beam into the scatterer times the attenuation of the scattered beam out of the scatterer. The dimensions are for aluminum, iron, and lead: $b=2.54$ cm, 2.54 cm, and 2.54 cm; $d=3.15$ cm, 2.54 cm, and 3.00 cm. The factor F is not shown for the thinner rings used in the experiment.

tutes a serious objection to the use of the Lucite-zinc sulfide detector in this experiment. However, if the inelastically scattered neutrons are more uniformly distributed in angle than the elastically scattered neutrons, then the general features of the differential cross section for elastic scattering will still be evident. In any case the value obtained for $\sigma(\theta)$ must be such that the total cross section achieved by integrating $\sigma(\theta)$ is less than the measured total cross section. That this is the case will be shown later.

12. *Sensitivity of counter to gamma rays.*—Neutron detector must not count the gamma rays resulting from the inelastic scattering of neutrons. An ampoule containing 0.1 milligram of radium was placed directly on the Lucite-zinc sulfide detector and gave a negligible counting rate (less than 1 count in 100 seconds).

13. *Higher-order scattering.*—Appendix II gives an account of the method used in this experiment to allow for double scattering. Essentially it involves placing an upper and lower bound on the possible values of $\sigma(\theta)$ for an observed sequence of values of $\bar{\sigma}(\theta)$ as a function of the axial thickness of the ring. The first calculation estimates the nature of the variation of $\bar{\sigma}(\theta)$ with d/a under the assumption of isotropic scattering. This is given by Eq. (13) which, after comparing with Fig. 4, is

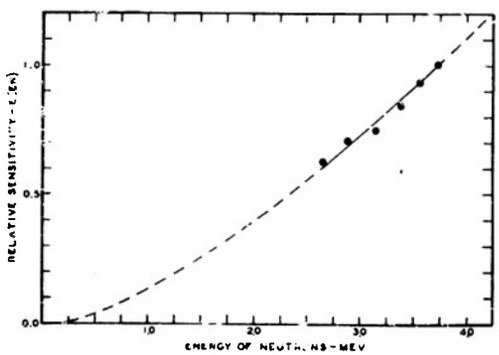


FIG. 3. Energy sensitivity of neutron detector. $E(E_n)$ measures the sensitivity of the neutron detector normalized to unity at 3.7 Mev. Solid circles were measured by us. The dotted curve was obtained from reference 9 by normalizing the two sets of data over the region common to both.

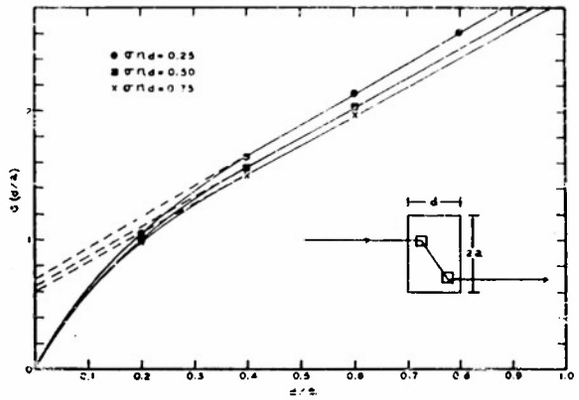


FIG. 4. Variation of straight-through double scattering in a right circular cylinder. The differential cross section was assumed to be isotropic. Specifically this curve is a plot of the function G as defined in Appendix II.

seen to reduce to the practical formula

$$\bar{\sigma}(\theta)=\bar{\sigma}_0(\theta)-0.282\bar{\sigma}'(\theta), \qquad (2)$$

where $\bar{\sigma}_0(\theta)$ is the intercept at $d/a=0$ of the linear portion of the curve and $\bar{\sigma}'(\theta)$ is the slope of the $\bar{\sigma}(\theta)$ *vs* d/a curve in the linear portion.

The second calculation states that, if the angular distribution is peaked strongly forward, then one expects that the double scattering contribution will cause $\bar{\sigma}(\theta)$ to be a linear function of d or d/a. In this case $\bar{\sigma}_0(\theta)$ is the true differential scattering cross section. Both of these extrapolations are presented on the graphs.

If triple scattering is present, then $\bar{\sigma}(\theta)$ should be a quadratic function of d or d/a for the case in which there is a strong forward peaking of the scattering. Figure 5, for the case of iron, shows some indication of the presence of triple scattering; however, the experimental uncertainty is too large to consider this definite. No attempt was made to remove the triple scattering contributions.

A typical run of data was made as follows: (1) direct beam; (2) attenuated beam; (3) scattered beam from one of the rings for all values of the scattering angle; (4) attenuated beam; (5) direct beam. If the two

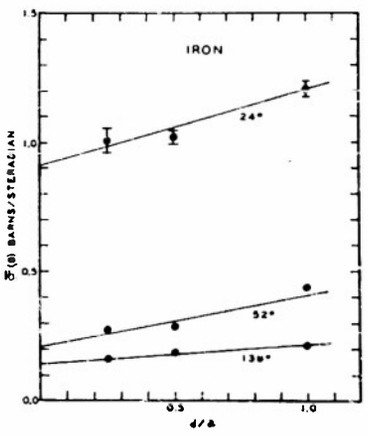


FIG. 5. Apparent differential cross section of iron *vs* thickness of ring scatterer for three different scattering angles. The thickness is measured relative to a quantity a, which we have taken to be equal to the radial width of the ring in order to establish a correspondence between the ring scatterer and the right circular cylinder scatterer.

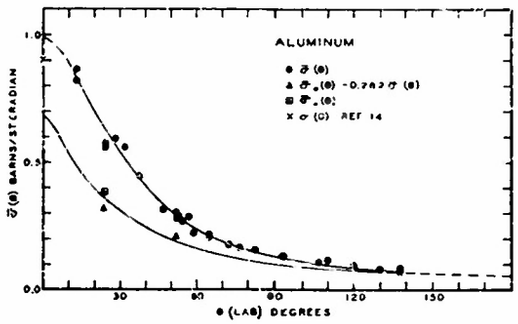


FIG. 6. Angular distribution of 3.7-Mev neutrons scattered from aluminum. $\bar{\sigma}(\theta)$ is apparent differential cross section as defined in the text. $\bar{\sigma}_0(\theta)$ is the differential cross section using a linear extrapolation to remove higher-order scatters. $\bar{\sigma}_0(\theta)-0.282\sigma'(\theta)$ is the differential cross section in which the higher-order scatters are removed using the isotropic scattering assumption. $\sigma(0)$ is taken from the "Final Report of the Fast Neutron Data Project," U. S. Atomic Energy Commission, NYO-636 (unpublished), in which the nuclear radii were found from our measured values of the total cross section.

values of the direct beam determination differed by more than 10 percent, the data were discarded.

DATA

Figures 6–8 show the experimental points of the apparent differential cross section for 3.7-Mev neutrons incident on aluminum, iron, and lead as calculated from Eq. (1). Only a limited number of angles were chosen in order to determine the effects of higher-order scattering. Figure 5 shows the variation of $\bar{\sigma}(\theta)$ as a function of the ring thickness for the case of iron. In the same manner, similar curves were obtained for lead and aluminum. The extrapolations both for isotropic scattering and forward peaked scattering are shown in Figs. 6, 7, and 8 where a curve is drawn through the points thought to be the appropriate differential cross section, $\sigma(\theta)$ for each case. The total cross sections corresponding to $\sigma(\theta)$ have been calculated and are presented together with the previously measured total cross sections[10] in Table I. It will be noted that the

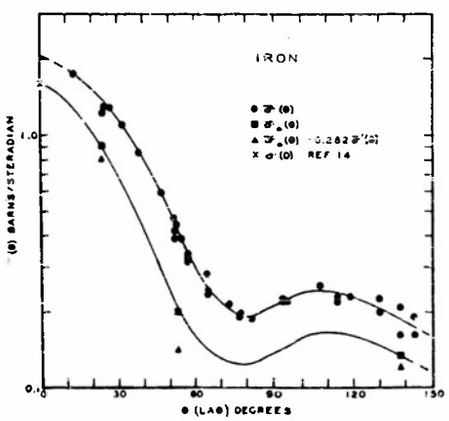


FIG. 7. Angular distribution of 3.7-Mev neutrons scattered from iron. Other remarks in caption of Fig. 6 apply here also.

TABLE I. Total cross sections. Subject to the reservations in the text, the value of $\int\sigma(\theta)d\Omega_\theta$ is the total elastic cross section.

Element	σ_{tot} (meas.) in barns This expt.	Ref. 10	$\int\sigma(\theta)d\Omega_\theta$ (barns)
Aluminum	2.55	2.50	1.73
Iron	3.51	3.55	2.94
Lead	7.60	7.70	5.17

integrated differential cross sections in each case are less than the measured total cross section. The total inelastic cross section cannot be obtained as the difference between the two former cross sections since the measurement of the differential cross section did not discriminate adequately against the inelastically scattered neutrons. However, this subtraction can be carried out approximately if one accepts the following rather crude estimate of the inelastic contribution to $\sigma(\theta)$. There are seven levels in aluminum that can be excited by 3.7-Mev neutrons.[11] If we assume that the maximum total inelastic cross section is about 50 percent of the total cross section and that the seven levels in aluminum are equally excited, then the inelastic neutrons contribute less than 15 percent to the total cross sections corresponding to $\sigma(\theta)$. Similar arguments using the known levels in iron and lead show that the inelastic contribution in these elements is less than 20 percent.

In conclusion, the authors wish to express their appreciation to Dr. W. F. G. Swann, Director of The Bartol Research Foundation, for his sustained interest in this problem.

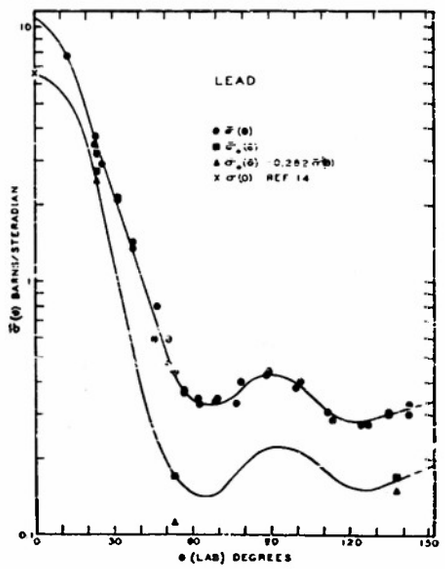


FIG. 8. Angular distribution of 3.7-Mev neutrons scattered from lead. Other remarks in caption of Fig. 6 apply here also.

[11] *Nuclear Data*, Natl. Bureau Standards Circ. 499 (U. S. Government Printing Office, Washington, D. C., 1950).

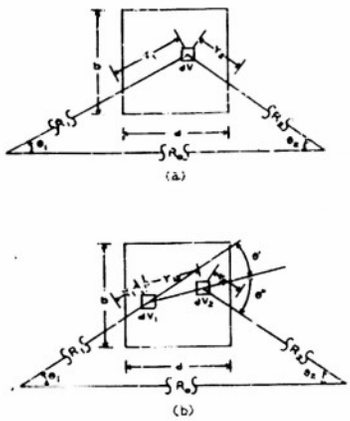


FIG. 9. Detail of scattering geometry: (a) single scattering; (b) double scattering.

APPENDIX I. SCATTERING OF NEUTRONS THROUGH RING SCATTERER BY SINGLE SCATTERING

In general the scattering ratio is made up of a sum of terms $S=S_1+S_2+\cdots$, where S_1, S_2, etc., refer to the neutrons scattered into the detector by single scattering, double scattering, etc. For the single scattering case [Figs. 1 and 9(a)] we have

$$S_1=\int_V [I(\theta_1)/I(0)]\cdot[R_0^2/R_1^2R_2^2]\cdot\sigma(\theta)n \times\exp[-\sigma n(r_1+r_2)]\cdot A(\theta_2)E(E_n)dV. \quad (3)$$

The geometry is such that only small errors will be introduced if Eq. (3) is replaced by

$$S_1=[I(\theta_1)/I(0)]\cdot[R_0^2/R_1^2R_2^2] \cdot\sigma(\theta)nA(\theta_2)E(E_n)VF(\theta_2)\exp(-\sigma nd), \quad (4)$$

where

$$F=V^{-1}\int_V \exp[-\sigma n(r_1+r_2-d)]dV, \quad (5)$$

and the mean angles and distances are used for θ_1, θ_2, R_0, R_1, and R_2. For a fixed size of ring scatterer, the quantity F is a function of θ_1 and θ_2. However, since θ_1 only varies from about 5° to 15°, little error and much simplification is introduced by computing F for $\theta_1=0$. For the rectangular cross section of our scatterer, the integral F may be evaluated in terms of elementary functions. The results are displayed in Fig. 2.

If only single scattering were present, the quantity S_1 could be replaced by the measured data S and the differential cross section $\sigma(\theta)$ could be calculated. In any case the reduction of the data is facilitated by defining an effective single scattering differential cross section $\bar{\sigma}(\theta)$ such that

$$S=[I(\theta_1)/I(0)]\cdot[R_0^2/R_1^2R_2^2] \cdot\bar{\sigma}(\theta)nA(\theta_2)E(E_n)VF(\theta_2)\exp(-\sigma nd). \quad (6)$$

APPENDIX II. SCATTERING OF NEUTRONS THROUGH RING SCATTERER BY DOUBLE SCATTERING

Using the quantities defined in Figs. 1 and 9b, the double scattering ratio is seen to be

$$S_2=\int_{V_1}\int_{V_2}[I(\theta_1)/I(0)]\cdot[R_0^2/R_1^2r_{12}^2R_2^2] \cdot\sigma(\theta')\sigma(\theta'')n^2\exp[-\sigma n(r_1+r_{12}+r_2)] \times A(\theta_2)E(E_n)dV_1dV_2. \quad (7)$$

An analytical solution of this integral seems quite involved, if not hopeless, for the geometry of the ring scatterer. In order to get some feeling for the manner in which the double scattering varies with the thickness of the ring, we have chosen to calculate the straight-through double scattering from a right circular cylinder assuming isotropic scattering [$\sigma(\theta')=\text{const}=\sigma/4\pi$]. In order to simplify this case as much as possible, let the neutron beam, incident on the circular end of the cylinder, be parallel to the cylinder axis, and let the detector sensitivities $A(\theta_2)=E(E_n)=1$. Also let r_1+r_2 be replaced by an approximate mean value d, the thickness of the cylinder. Equation (7) then reduces to

$$S_2\equiv[\sigma^2n^2/16\pi^2R_2^2]\cdot\exp(-\sigma nd) \times\int_{V_1}\int_{V_2} r_{12}^{-2}\exp(-\sigma nr_{12})dV_1dV_2. \quad (8)$$

If the exponential function is expanded and the first three terms retained, S_2 reduces to the following:

$$S_2=[\sigma^2n^2a^4/16R_2^2]\cdot\exp(-\sigma nd) \cdot(X-\sigma naV+\tfrac{1}{2}\sigma^2n^2a^2Z), \quad (9)$$

where

$$X=-2(d^2/a^2)\cdot\ln d/a+2(d^2/a^2)\sinh^{-1}d/2a +\cosh^{-1}(1+d^2/2a^2)+2d^2/a^2-d^4/4a^4 -(1-d^2/2a^2)\cdot[(1+d^2/2a^2)^2-1]^{\frac{1}{2}}, \quad (10)$$

$$Y=8\int_0^\infty[xd/2a-\exp(-xd/2a) \times\sinh(xd/2a)]J_1(x)\sin x\cdot dx/x^4, \quad (11)$$

and

$$Z=d^2/a^2. \quad (12)$$

The integration of X was facilitated by the use of a theorem in vector analysis.[12] The integration of Y can be effected by recognizing that the integral corresponds to the electrostatic energy of a uniform volume distribution of charge.[13]

If the single scattering ratio S is calculated for the right circular cylinder under the same assumptions, then

[12] H. B. Phillips, *Vector Analysis* (John Wiley and Sons, Inc., New York, 1933), Chap. III.

[13] W. R. Smythe, *Static and Dynamic Electricity* (McGraw-Hill Book Company, Inc., New York, 1939), Chap. V.

the effective single scattering cross section is given by

$$\bar{\sigma}/\sigma = 1 + (\sigma n a/4) G(d/a), \tag{13}$$

where

$$G(d/a) = (a/d)(X - \sigma n a Y + \tfrac{1}{2}\sigma^2 n^2 a^2 Z) \tag{14}$$

and is written only as a function of d/a since it varies but slowly with σna, as may be seen in Fig. 4. By considering the mean curve to apply to all cases of interest, the function G becomes a function of d/a only.

To apply the calculations of the right circular cylinder to the case of the ring scatterer, we assume that except for multiplying factors which are angular functions, the geometrical variation of the single and double scattering ratios is given correctly after associating the radial thickness of the ring scatterer b with the radius of the cylinder a.

If, instead of isotropic scattering, one takes the other extreme of an angular distribution peaked strongly in the forward direction, one finds that the single scattering ratio in the ring scattering varies as $d \exp(-\sigma n d)$ whereas the double scattering ratio varies as $d^2 \exp(-\sigma n d)$, thus leading to a linear variation of the apparent single scattering cross section with the thickness of the ring.

Distribution List

Argonne National Laboratory, Attn: A. S. Langsdorf
P. O. Box 5207, Chicago 80, Illinois

Brookhaven National Laboratory, Attn: D. J. Hughes
Upton, Long Island, New York

Prof. H. Newson, Department of Physics, Duke University
Durham, North Carolina

E. I. DuPont de Nemours Co., Attn: C. W. J. Wende
Nemours Building, Wilmington 98, Delaware

Dr. G. E. Owen, Johns Hopkins University
Baltimore 18, Md.

Prof. J. D. Stranathan, Department of Physics
University of Kansas, Lawrence, Kansas

Dr. P. F. Gast, Hanford Works
P. O. Box 550, Richland, Washington

Knolls Atomic Power Laboratory, Attn: T. M. Snyder
P. O. Box 1072, Schenectady, New York

Los Alamos Scientific Laboratory, Attn: R. F. Taschek
P. O. Box 1663, Los Alamos, New Mexico

Dr. W. M. Preston, Laboratory for Nuclear Science and
Engineering, Massachusetts Institute of Technology,
Cambridge 39, Massachusetts

U. S. Atomic Energy Commission, Attn: R. F. Van Wye
Division of Technical Advisers, New York Operations Office
P. O. Box 30, Ansonia Station, New York 23, New York

North American Aviation, Inc., Attn: Chauncey Starr
P. O. Box 309, Downey, California

Oak Ridge National Laboratory, Attn: A. H. Snell
P. O. Box P, Oak Ridge, Tennessee

Prof. T. W. Bonner, Department of Physics
Rice Institute, Houston, Texas

Dr. J. W. Coltman, Research Laboratories
Westinghouse Electric Corporation
East Pittsburgh, Pennsylvania

Westinghouse Electric Corporation, Attn: S. Krasik
Atomic Power Division, Bettis Field, P. O. Box 1468
Pittsburgh 30, Pennsylvania

Prof. R. H. Herb, Department of Physics
University of Wisconsin, Madison 6, Wisconsin

Dr. J. L. McKibben, Los Alamos Scientific Laboratory
P. O. Box 1663, Los Alamos, New Mexico

Dr. R. A. Peck, Jr., Department of Physics
Brown University, Providence 12, Rhode Island

Chief of Naval Research, Attn: Nuclear Physics Branch
Navy Department, Washington 25, D. C.

Director
Office of Naval Research, Chicago Branch Office
844 North Rush Street, Chicago 11, Illinois

Director
Office of Naval Research, San Francisco Branch Office
801 Donahue Street, San Francisco 24, California

Director
Office of Naval Research, New York Branch Office
346 Broadway, New York 13, New York

Director
Office of Naval Research, Pasadena Branch Office
1030 E. Green Street, Pasadena 1, California

Officer in Charge
Office of Naval Research, London Branch Office,
Navy No. 100, Fleet Post Office, New York, New York

Dr. George A. Kolstad, Chief, Physics and Mathematics Branch
Division of Research, U. S. Atomic Energy Commission
Washington 25, D. C.

Superintendent, Nucleonics Division
Naval Research Laboratory, Anacostia, Washington, D. C.

Chief of the Bureau of Ships, Attn: Code 390
Navy Department, Washington 25, D. C.

Chief of the Bureau of Ships, Attn: Code 330
Navy Department, Washington 25, D. C.

Chief of the Bureau of Ordnance, Attn: Rem
Navy Department, Washington 25, D. C.

Chief of the Bureau of Ordnance, Attn: Re9a
Navy Department, Washington 25, D. C.

Chief of the Bureau of Aeronautics,
Attn: Applied Nuclear and General Physics Branch
Navy Department, Washington 25, D. C.

Officer in Charge, Naval Radiological Defense Laboratory
San Francisco Naval Shipyard, San Francisco, California

Chief of Naval Operations, Attn: Op 36
Navy Department, Washington 25, D. C.

Senior Scientific Advisor
Office of the Under Secretary of the Army
Department of the Army, Washington 25, D. C.

Director, Research and Development Division
General Staff
Department of the Army, Washington 25, D. C.

National Bureau of Standards Library
Room 203, Northwest Building, Washington 25, D. C.

Commanding General
Air Research and Development Command, Attn: RDRRP
P. O. Box 1395, Baltimore 3, Md.

Nuclear Development Associates, Inc., Attn: Dr. H. Goldstein
80 Grand Street, White Plains, New York

Dr. V. L. Parsegian
Director, Research Division
U. S. Atomic Energy Commission, New York Operations Office
P. O. Box 30, Ansonia Station, New York 23, New York

Armed Services Technical Information Agency

AD

43910

NOTICE: WHEN GOVERNMENT OR OTHER DRAWINGS, SPECIFICATIONS OR OTHER DATA ARE USED FOR ANY PURPOSE OTHER THAN IN CONNECTION WITH A DEFINITELY RELATED GOVERNMENT PROCUREMENT OPERATION, THE U. S. GOVERNMENT THEREBY INCURS NO RESPONSIBILITY, NOR ANY OBLIGATION WHATSOEVER; AND THE FACT THAT THE GOVERNMENT MAY HAVE FORMULATED, FURNISHED, OR IN ANY WAY SUPPLIED THE SAID DRAWINGS, SPECIFICATIONS, OR OTHER DATA IS NOT TO BE REGARDED BY IMPLICATION OR OTHERWISE AS IN ANY MANNER LICENSING THE HOLDER OR ANY OTHER PERSON OR CORPORATION, OR CONVEYING ANY RIGHTS OR PERMISSION TO MANUFACTURE, USE OR SELL ANY PATENTED INVENTION THAT MAY IN ANY WAY BE RELATED THERETO.

Reproduced by

DOCUMENT SERVICE CENTER

KNOTT BUILDING, DAYTON, 2, OHIO

UNCLASSIFIED